A Study of Alteration and Mineralisation at the Mace Mo-Cu Porphyry, Ireland

Submitted to the University of Dublin, Trinity College

For the fulfilment of the degree Master of Science in Geology

Submitted November 2019

by

Shane Lavery

Declaration

I declare that this thesis has not been submitted as an exercise for a degree at this or any other university and it is entirely my own work.

I agree to deposit this thesis in the University's open access institutional repository or allow the Library to do so on my behalf, subject to Irish Copyright Legislation and Trinity College Library conditions of use and acknowledgement.

I consent to the examiner retaining a copy of the thesis beyond the examining period, should they so wish.

_____

Shane Lavery

Summary

The Mace molybdenum-copper (Mo-Cu) deposit in the west of Ireland has been explored since the early 1960s, but remains poorly understood in terms of classic porphyry style systems. Knowledge of porphyry systems in general has greatly improved in the past few decades, and this knowledge can now be applied to better understand the nature of Mo-Cu mineralisation at Mace. This thesis presents new reflected and transmitted light petrographic descriptions, geostatistical analyses, laboratory analyses including SEM and LA-ICP-MS, and field relations, to define a new paragenetic sequence of events that have affected the Mace deposit.

The deposit is hosted in the Galway Granite, a large and complex body of granitic rocks, outcropping along the northern shore of Galway Bay and extending inland for c.20km. The Galway Granite is a composite batholith; available geochronological data indicate that emplacement occurred between c.423Ma and c.385Ma, with most granites emplaced between c.410 and c.400Ma. Molybdenite from Mace Head has been directly dated using the Re-Os isotope system to 407±1.5Ma. Molybdenum in the deposit occurs as molybdenite, and copper as chalcopyrite, both finely disseminated and concentrated in veins.

Mineralisation is predominantly structurally controlled, with a south-southwest to north-northeast orientation. Mineralised veins can be seen at surface, particularly along the coast, where the rocks are well exposed in outcrop. East-southeast to west-northwest faults have been mapped, which appear to cut and dextrally offset the deposit and associated mineralised zones, indicating that they post-date early mineralisation. It is apparent that this persistent east-southeast to west-northwest structural trend provided a weakness for exploitation by mineralising fluids within a preferential orientation, and subsequently a locus for fault displacement. This is particularly evident in the central ‘Bog Zone’ on the eastern shore of Lough Bunacliffa, which is offset by the Narrow Waters Fault, a major local structural control on mineralisation. The offsets are not significant, being in the order of no more than tens of metres.

Extensional quartz-pyrite veins were co-magmatic, or close to coeval with pluton emplacement, and mark the first vein set in the sequence at Mace. Pyrite in these veins contains elements (e.g. cobalt, nickel, selenium) with clear oscillatory zonation patterns, linking their growth to late magmatic fluid. These extensional veins generally do not contain Mo-Cu mineralisation, but are commonly cross-cut by chalcopyrite- and molybdenite-bearing veins.

Several generations and types of alteration are evident at the Mace deposit, including potassic, propylitic, and phyllic alteration, which as a whole are typical of porphyry deposits. Mineralisation and alteration at Mace are inherently linked. A high Cu:Mo ratio in assay results is thought to be associated with proximity to the source of mineralisation, due to a combination of high chalcopyrite and molybdenite content in mineralised veins in the deposit and disseminated chalcopyrite associated with potassic alteration in the host granite. In general, strong potassic alteration is indicative of proximity to the core of porphyry deposits, therefore a high Cu:Mo ratio may be regarded as a reliable vector of mineralisation. The Cu:Mo ratio decreases from potassic into propylitic alteration zones, due to a decrease in modal proportion of finely disseminated chalcopyrite in the groundmass. At Mace, propylitic alteration is characterised by an epidote-chlorite assemblage, which is usually interpreted as a distal alteration style in porphyry deposits. The identification of propylitic alteration at Mace is, however, complicated by superimposed phyllic alteration seen as sericite replacement of potassium feldspar and associated with remobilisation of molybdenite in large quartz veins and angular quartz vein breccias. Quartz veins and breccias are associated with some of the highest molybdenum assays seen in drilling to date. Phyllic alteration is commonly observed in the upper level of porphyry systems, suggesting the Mace deposit represents the upper-middle level of a porphyry deposit.

A series of dacite dykes intruded the pluton from early in its history through to post-mineralisation, and are not thought to be related to mineralising fluids. Late calcite-fluorite-chlorite veins were intruded post-mineralisation and mark the final hydrothermal event at Mace Head. These veins do not host economic minerals and clearly overprint all other observed vein types. The deposit may contain further concentrations of economic mineralisation at depths below those drilled to date.

Acknowledgements

Sincere thanks to my supervisor Quentin Crowley for all his support and encouragement throughout the past year. Thanks to the technicians, especially Frank and Maura for their help with core and thin sections, and everyone in the CMA and TTEC.

Thanks to Deirdre, Paul, and all at SLR for facilitating, allowing, and helping to fund me while I took a year away from work to do this research project. I especially must thank Nick O'Neill for his help and support not only during this year but in all my time at SLR.

Thanks also to Bradley Jones and MOAG for allowing me to work on their project and use their data and core. I would like to express my gratitude to the Geological Survey of Ireland for funding and supporting this research.

Most importantly, I need to thank Nicola Raftery for her endless encouragement and motivation over this year and since I've known her. Her drive and ambition are inspiring.

Table of Contents

List of Figures

List of Tables

1.0 CHAPTER 1 INTRODUCTION

1.1 Introduction

Porphyry systems are not commonly associated with Irish granites, and the Mace deposit is the only currently known porphyry deposit on the island of Ireland. Porphyry deposits are usually kilometre-scale hydrothermal systems, closely related in space and time to sub-volcanic porphyritic intrusions of intermediate to felsic composition, and producing broadly dispersed alteration and mineralisation (Sillitoe 2010, Sinclair 2007). They are normally high tonnage, low- to medium-grade deposits, and tend to occur in linear belts, mainly associated with Mesozoic and Cenozoic orogenic belts such as in the western US and South America (Sinclair 2007). Porphyry deposits often have complex histories; commonly there is evidence for repeated emplacement of both barren and mineralized porphyry intrusions and overprinting of mineralisation and alteration zones (D'Angelo et al. 2017; e.g. Carten et al. 1988; Ballard et al. 2001; Sillitoe and Mortensen 2010; Deckart et al. 2013, 2014).

Porphyry deposits are the world's most important source for Cu and Mo, with porphyries accounting for up to 60% of Cu production and 96% of total Mo production worldwide (Sinclair 2007). The principal ore mineral containing molybdenum is molybdenite (MoS2). Copper is usually the main economic constituent of porphyry deposits, but molybdenum-dominant porphyries are known in parts of China (e.g. Cong-Ying Li et al. 2012) and in Canada (D'Angelo 2017). Age ranges for porphyry deposits are from Proterozoic such as at the c.1867 Ma Haib deposit in Namibia (Grumbley 2015) through to much younger Miocene and Pleistocene deposits (Sillitoe 2010).

The Mace deposit has been known since before the 1960s, when exploration including drilling and geochemical sampling was undertaken by Anglo United Trust. Sporadic exploration work has been undertaken on the deposit since then, culminating in a resource estimate by RPA Consultants for SLR Consulting on behalf of MOAG Copper Gold Resources Ltd. of between five and fifteen million tonnes, grading between 0.10% Mo and 0.15% Mo, 0.05% Cu and 0.10% Cu, and between 0.5 g/t Ag and 1 g/t Ag. This

thesis describes research examining the petrography, geochemistry and vein paragenesis of the Mace molybdenum-copper deposit.

1.2 Introduction to porphyry systems

While porphyry systems are usually associated with sub-volcanic, porphyritic intrusions of intermediate-felsic composition, other associated mineralisation can include skarn, carbonate-replacement, sediment hosted, and high- to intermediate-sulphidation epithermal mineralisation (Sillitoe 2010). Porphyry systems tend to occur in linear belts and are mainly associated with Mesozoic and Cenozoic orogenic belts such as in the western US and South America, however, rare examples are also found in Precambrian terranes (Sillitoe 2010, Sinclair 2007).

Porphyry deposits represent some of the largest accumulations of metal in the Earth's crust and are the primary source of the world's Cu and Mo, as well as an important source of Au and other metals (Sillitoe 2010). Porphyry systems are closely related to underlying composite plutons, representing the supply chambers for the magmas and fluids that formed the mineralisation (Sillitoe 2010). Porphyry deposits may be formed in subduction related continental and island arc settings or in anorogenic continental settings (Sinclair 2007, Sillitoe 2010). Sillitoe (2010) noted that precursor plutons, which are typically multiphase, of batholithic dimensions, and of dioritic to granitic composition, are often spatially, temporally, and genetically related to porphyry systems, and may act as hosts to a single deposit, as is the case at Mace head in the Galway batholith. Sillitoe's observation that the precursor plutons and porphyry stocks are typical separated by time gaps of 1 to 2 m.y or less matches with recorded age ranges for the Carna Granite (410Ma) and the Mace porphyry deposit (407Ma±1.5) (Feely et al. 2010).

Porphyry deposits are formed by hydrothermal fluids exsolving from intrusive magmatic bodies, which precipitates metals into the surrounding rocks. Addition of mafic melt to the base of a granodioritic to granitic magma chamber adds metals, sulphur and volatiles that are concentrated in an aqueous phase at the roof (cupola) during magma chamber convection (Grumbley 2015; Keith et al. 1997). Increased heat and pressure of

the mafic intrusion causes porphyry dyke propagation from the cupola (Sinclair 2007). Copper and molybdenum are affected by pressure so that they are concentrated in an aqueous phase at lithostatic depths of 3-4km (Williams et al. 1995). The outward movement of these hydrothermal fluids creates distinct alteration zones recognised by the occurrence of specific mineral assemblages (Sillitoe 2010; Cooke et al. 2014). The propylitic alteration zone represents the most distal signature of mineralisation, detectable kilometres away from the main orebody (Cooke et al. 2014), and therefore useful as a target for exploration. In addition to its expression in mineralogy, alteration zoning is also expressed in whole-rock and mineral geochemical trends which can act as vectors towards orebodies (e.g. Norman et al. 1991; Wilkinson et al. 2015).

Hydrothermal alteration associated with porphyry systems can be extensive, displaying zoning on a deposit scale as well as surrounding individual fractures and veins (Sinclair 2007).

In Figure 1-1, the generalised anatomy of a porphyry alteration system illustrates the central potassic alteration zone of primarily biotite-K-feldspar with a marginal zone of propylitic alteration (epidote-chlorite-albite-carbonate) (Sillitoe 2010). The upper parts of the alteration system may form a broad zonal pattern from potassic alteration through chlorite-sericite, sericite, and argillic alteration to the propylitic alteration zone, or irregularly superimposed on earlier alteration types (Sinclair 2007).

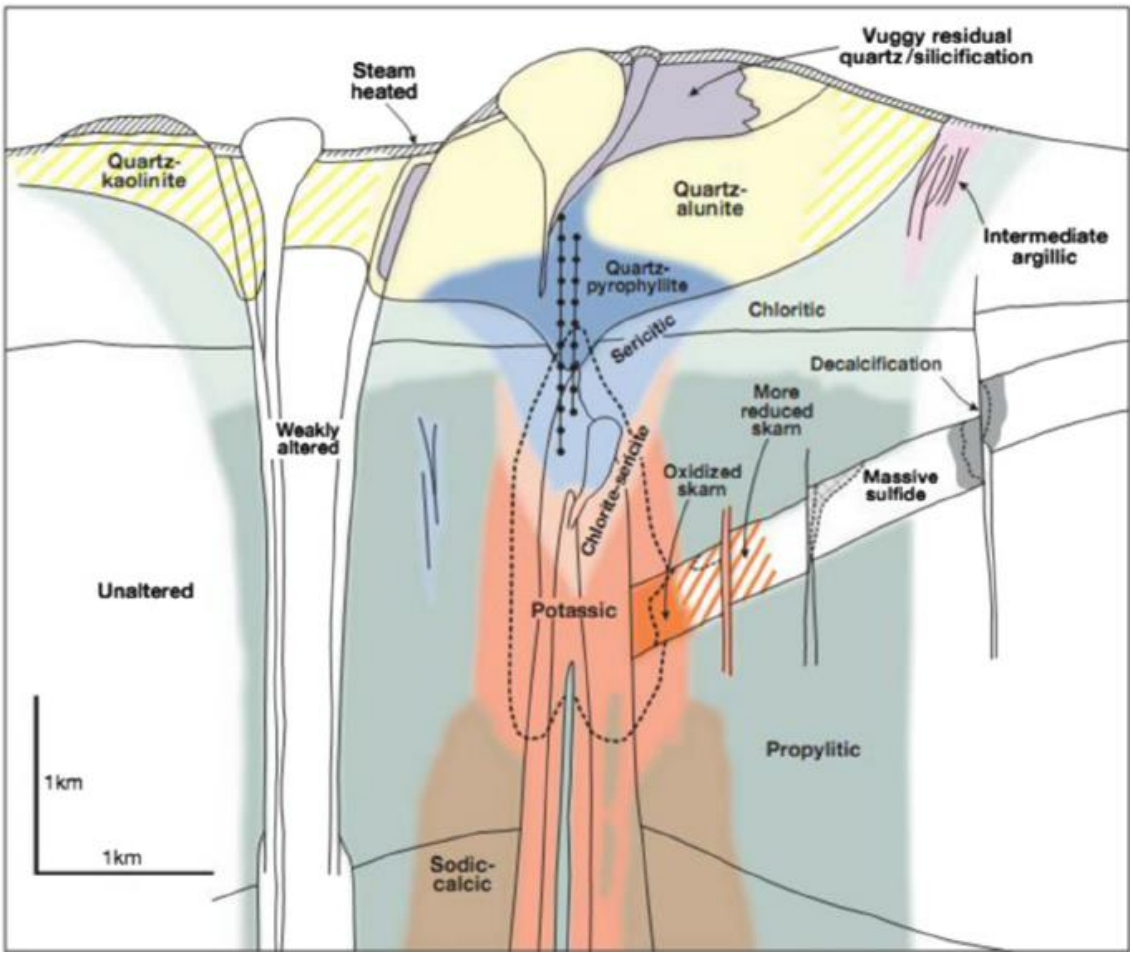

Figure 1-1 Generalised alteration-mineralisation zoning pattern for telescoped porphyry Cu deposits. Classic alteration assemblages include a potassic core with propylitic margins and a sericitic zone. From Sillitoe (2010)

1.3 Geological setting of the Galway batholith

The late Caledonian Galway Granite is a calc-alkaline batholith emplaced at circa 400 Ma. (Leggo et al. 1966; Leake 1978) with a 475-463 Ma. (Friedrich et al. 1999) metagabbro-gneiss suite to the north (Leake 1989; Leake & Tanner 1994), and Lower Ordovician greenschist facies rocks (South Connemara Group) in the south (McKie & Burke 1955; Williams et al. 1988). The Skird Rocks Fault is a major fault, predating intrusion of the batholith, which brings the South Connemara Group against the metagabbro-gneiss suite. Leake (1978) considered the Skird Rocks Fault to be a splay of the Southern Uplands Fault and to have strongly influenced the siting of the batholith. Beneath the Carboniferous rocks of the Galway Bay area a S-SE extension of several km

is indicated on gravity and aeromagnetic maps (Murphy 1952; Max et al. 1983; Madden 1987). The long axis of the batholith is therefore approximately 90km in length, trending WNW.

The NNE Shannawona Fault and the NW-trending Barna Fault are two major faults that transect the batholith (see Figure 2-1). These define the boundaries between the three principle blocks that comprise the Galway Granite batholith; the western (west of the Shannawona Fault), central (between the Shannawona Fault and Barna Fault), and eastern (east of the Barna Fault) blocks. Gravity studies by Madden (1987) show that the central block is 3-4km thinner than the western block. Leake (1978) asserted that the Granite to the east of the Shannawona Fault was upthrown and then eroded, and now exposes a correspondingly deeper level.

Many previous workers (Wager 1932; Wright 1961; Aucott 1970; Leake 1974; Claxton 1971; Lawrence 1975; Max et al 1978) showed that the western block comprises lithologies that range from granodiorite (Carna Granite) through adamellite (Errisbeg Townland Granite) to alkali granite (Murvey Granite). The two latter types are also found in the eastern block (Coats & Wilson 1971). In marked contrast, the central block exposes a significantly wider spectrum of lithologies ranging from diorite through granodiorite to alkali granite. The relatively less-evolved nature of many central block rock-types has been highlighted by previous workers (Plant 1968; Coats & Wilson 1971; Leake 1978; Max et al. 1978; Feely & Madden 1987; Feely et al. 1991; El-Desouky et al. 1996).

1.4 Physical setting

The area studied is situated approximately 55km from Galway city and approximately 3km from the village of Carna, between longitudes 9° 87’ W and 9° 89’ W and latitudes 53° 32’ N and 53° 34’ N. The area includes the townlands of Mace and Ard on the Mace Head peninsula.

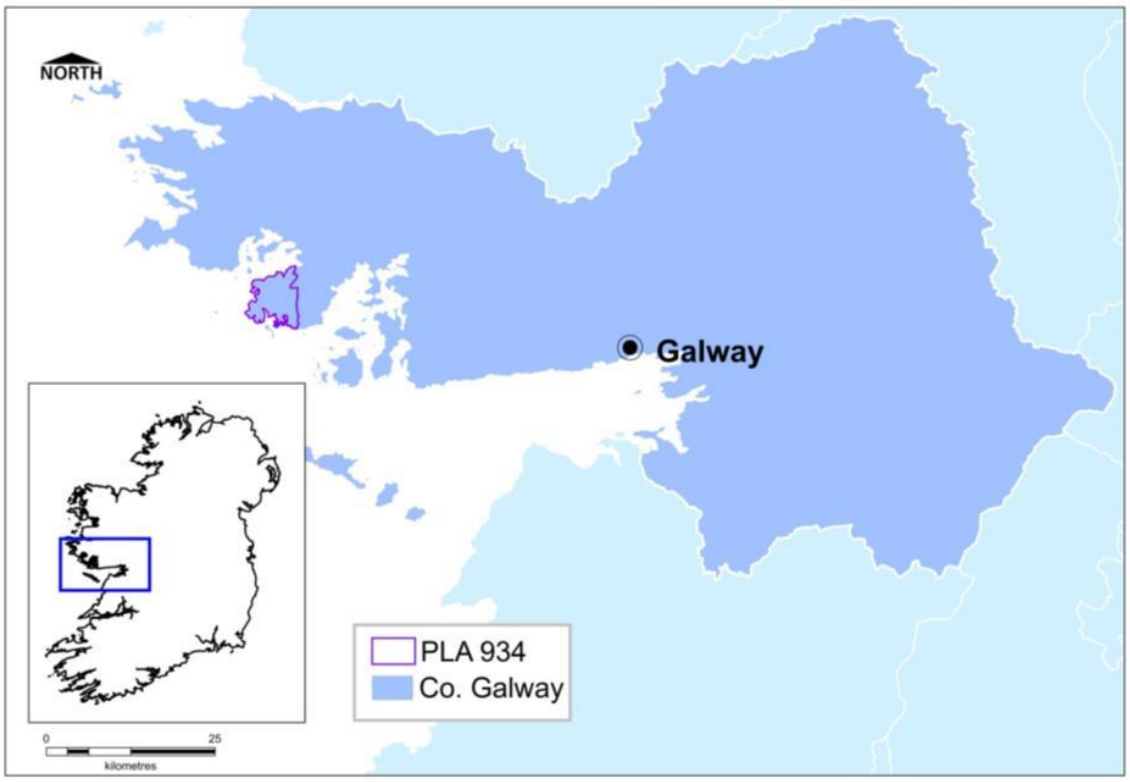

Figure 1-2 Location map of Mace Head in County Galway. From SLR Consulting Exploration Report (2016)

1.5 Granite-related molybdenite mineralisation

Disseminated and quartz vein-hosted molybdenite mineralisation occurs throughout the late-Caledonian Galway Granite and its satellite plutons (O'Raghallaigh et al. 1997). Notable occurrences are at the western end of the Galway Granite at Mace Head and Murvey (Derham 1986; Derham & Feely 1988; Max & Talbot 1986; Gallagher et al. 1992). Molybdenite-bearing quartz veins (~5–30 cm thick) at Mace Head trend NE–SW, their orientation controlled by early jointing in the host granite (Derham 1986; Max & Talbot 1986). Vein minerals also include chalcopyrite, pyrite, magnetite and muscovite. The Roundstone Murvey Granite contains both fine-grained (~5 mm) disseminated and quartz vein hosted molybdenite. There is an estimated 240,000t at 0.13% Mo in this low-grade deposit (Max & Talbot 1986).

The Omey Granite contains disseminated molybdenite (2– 4 mm) and rosettes (~5mm across) hosted in thin, discontinuous quartz veins (<5 cm across) (Feely et al. 2007) that typically contain muscovite-bearing alteration selvages similar to that encountered in

Carna Granite (at Mace Head) and Roundstone Murvey Granite molybdenite deposits (Gallagher et al. 1992). Geochemical, fluid inclusion and stable isotope (O, H, S and C) studies by Gallagher et al. (1992) indicate that the molybdenite mineralisation in the Carna Granite and Roundstone Murvey Granite was magmatic in origin. O'Reilly et al. (1997) concluded that a H2O–CO2–NaCl-bearing fluid of moderate salinity (4–10 eq. wt% NaCl) deposited late magmatic molybdenite-mineralized quartz veins. This fluid composition is similar to molybdenite-bearing vein quartz in the Omey Granite (Feely et al. 2007). Thermal Ionization Mass Spectrometry (TIMS)-based U–Pb zircon geochronology of the Galway Granite indicates that emplacement occurred over a period of at least 20 Ma from c. 400 to 380 Ma (Feely et al. 2003). Molybdenite Re–Os ages for granite related molybdenite mineralisation (Omey Granite, Roundstone Murvey Granite and Carna Granite from Mace Head) at the western end of the batholith extended the period of magmatic activity to 423-380 Ma (Selby, Creaser & Feely 2004; Feely et al. 2007), indicating that granite emplacement in the Galway batholith spanned a period of c. 40 Ma, with a similar time span for molybdenite mineralisation in the south Connemara area (Feely 2010).

1.6 Mo-Cu mineralisation at Mace Head

Mineralisation at Mace Head has generally been considered by exploration geologists (e.g. Bergey 2008, SLR 2016) to form part of the uppermost portion of a porphyry type molybdenite-copper system, with similarities to the Highmont deposit in the Highland Valley of British Columbia(Bergey 2008), but with molybdenum more important relative to copper, and a more obvious association with regional faulting. The Highmont Deposit is hosted in late Triassic to Jurassic calc-alkaline rocks with deep seated faults thought to be responsible for early emplacement and creating lines of weakness that are followed locally by younger successor faults (Bergey 2008). The molybdenite at Mace Head is predominantly emplaced in quartz veins and as fracture fill within the Carna granodiorite intrusion, which forms part of the composite Galway batholith.

The molybdenum prospect has been explored at Mace Head since the late 1960s. Talbot and Ryan (1988) identified the highest Mo concentrations in overburden in Ireland or Britain occurring in the poorly drained acidic peaty soil directly overlying the deposit

area. The paper attributed high mobility of Mo to its combined chalcophilic, lithophilic, and siderophilic characteristics. The Mo-Cu mineralisation at Mace Head extends from SW to NE along the eastern shore of Lough Bunacliffa. Strong NE-trending structural control influences mineralisation (Derham & Feely 1988). NE-trending faults contain disseminated chalcopyrite and pyrite, with molybdenite concentrations in a quartz vein stockwork and disseminated in the host granodiorite.

1.7 Historic exploration at Mace Head

Some exploration work had been carried out by the Geological Survey of Ireland prior to Anglo United Trust acquiring the prospecting licences at Mace Head and Murvey in 1960. The system was observed to be coincident with a NE trending fault swarm with moderate to intense propylitic and potassic alteration.

Geochemical exploration in the area in 1967 outlined a porphyry molybdenum-copper system related to the Galway Granite. The system was partially explored by drilling programs between 1968 and 1970 by Anglo United Trust (see Figure 1-3), which included 26 diamond and 20 percussion drill-holes totalling almost 2100m, and outlined a zone of mineralisation. The drill-holes were located in the central portion of the zone, within an area that measures 1400 m in length and up to 300 m in width. The drill-holes were shallow (mainly <50 m in depth) and mostly widely spaced (between approximately 50 m and 150 m), apart from some drill-holes spaced at approximately 50 m in length. Reporting at the time estimated that 20% to 45% of molybdenite was lost during the coring process. Drilling was also suggested to have been directed in the same direction as the veins and molybdenite-coated fractures, which was later confirmed by detailed examination of the drill logs (Bergey 2008).

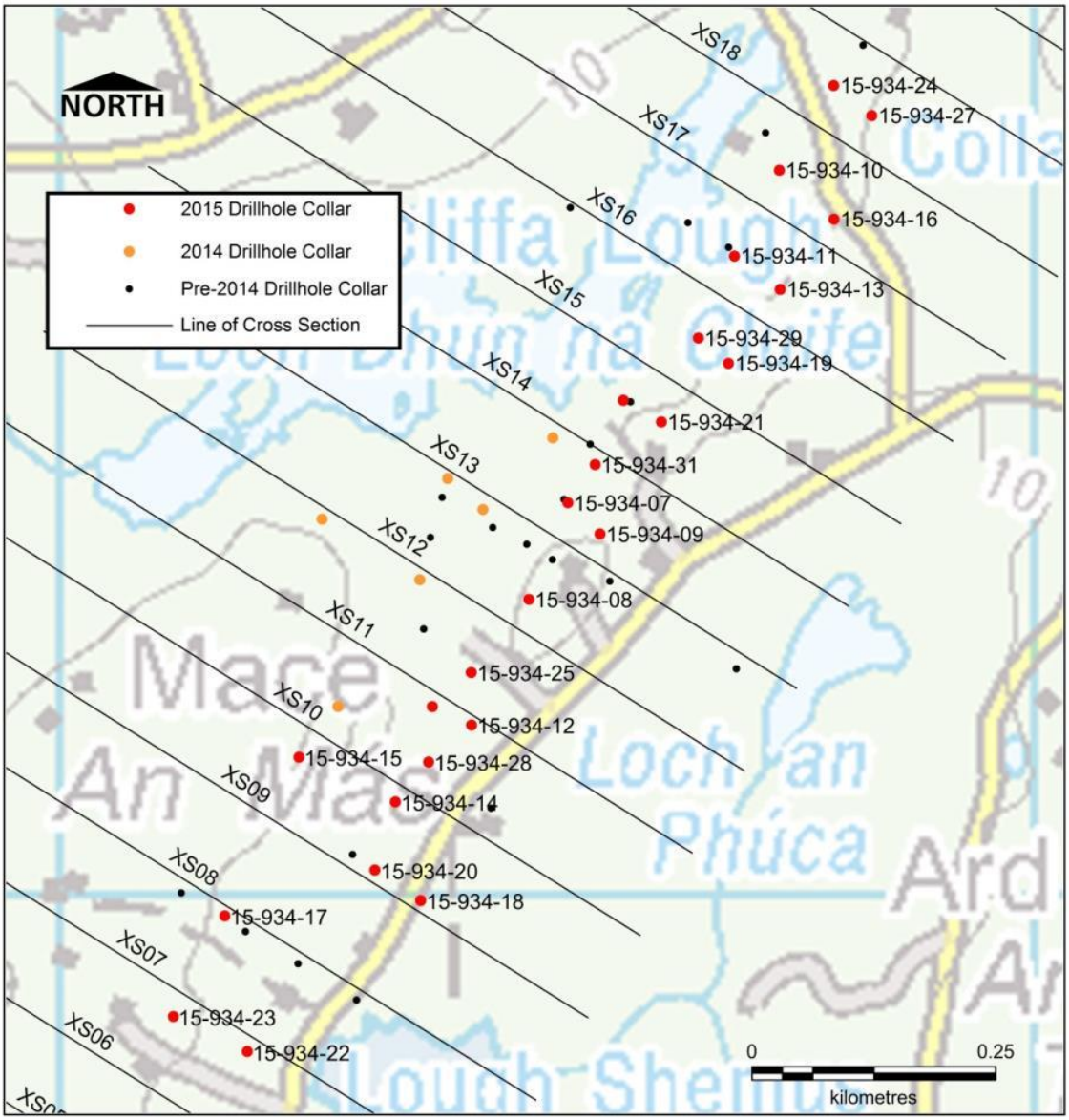

Figure 1-3 Drill Plan for Mace Head showing the locations of historic and recent drill holes (SLR 2016)

Exploration had initially focused on the Murvey prospect, approximately 10km northwest of Mace. From November 1966 to April 1967 a regional stream sediment survey was carried out over 380km^2, including several prospecting licences. The Mace molybdenum anomaly was discovered to be stronger and more widespread than suggested by the mineralisation noted in outcropping quartz veins, probably due to loss of molybdenite along fractures during glaciation. Using the results of the regional stream sediment survey, reconnaissance geochemical soil sampling for Mo and Cu was undertaken at Mace, with positive results followed up by a more detailed soil sampling

campaign that outlined two NE-trending Mo anomalies – a large anomaly of around 2km in length east of Lough Bunacliffa and a smaller anomaly 600m in length adjacent to Lough Aphuca to the southeast. Anglo United's initial drilling of 505m in 1968 was followed by additional soil sampling in the core of the soil Mo anomaly in February 1969. An induced polarisation (IP) survey at Mace was completed in March 1969, which also measured apparent resistivity of the underlying rock.

944m of diamond drilling consisting of 15 holes was carried out from January to June 1970. Burns (1970) in his summary geological report suggested that significant loss of molybdenum in the quartz veins had occurred. In late 1970 614m of percussion drilling in 20 holes was carried out, mainly along the margins of the previous drilling area. No mineral resource or reserve estimates were recorded as a result of this work, and there is no record of mineral production in the prospecting licence.

1.8 Recent exploration

Drilling at the Mace Deposit by SLR Consulting for MOAG Copper Gold Resources from 2014 to 2016 has defined a mineralised body measuring at least 1.2 kilometres (SSW-NNE axis) by 250m (ESE-WNW axis) and extending to almost 200m below sea level (Figure 1-4).

Most drill holes intersected significant (>100m) intervals averaging 0.04% Mo or better, with intervals of significantly higher grades (>0.07% Mo) common throughout.

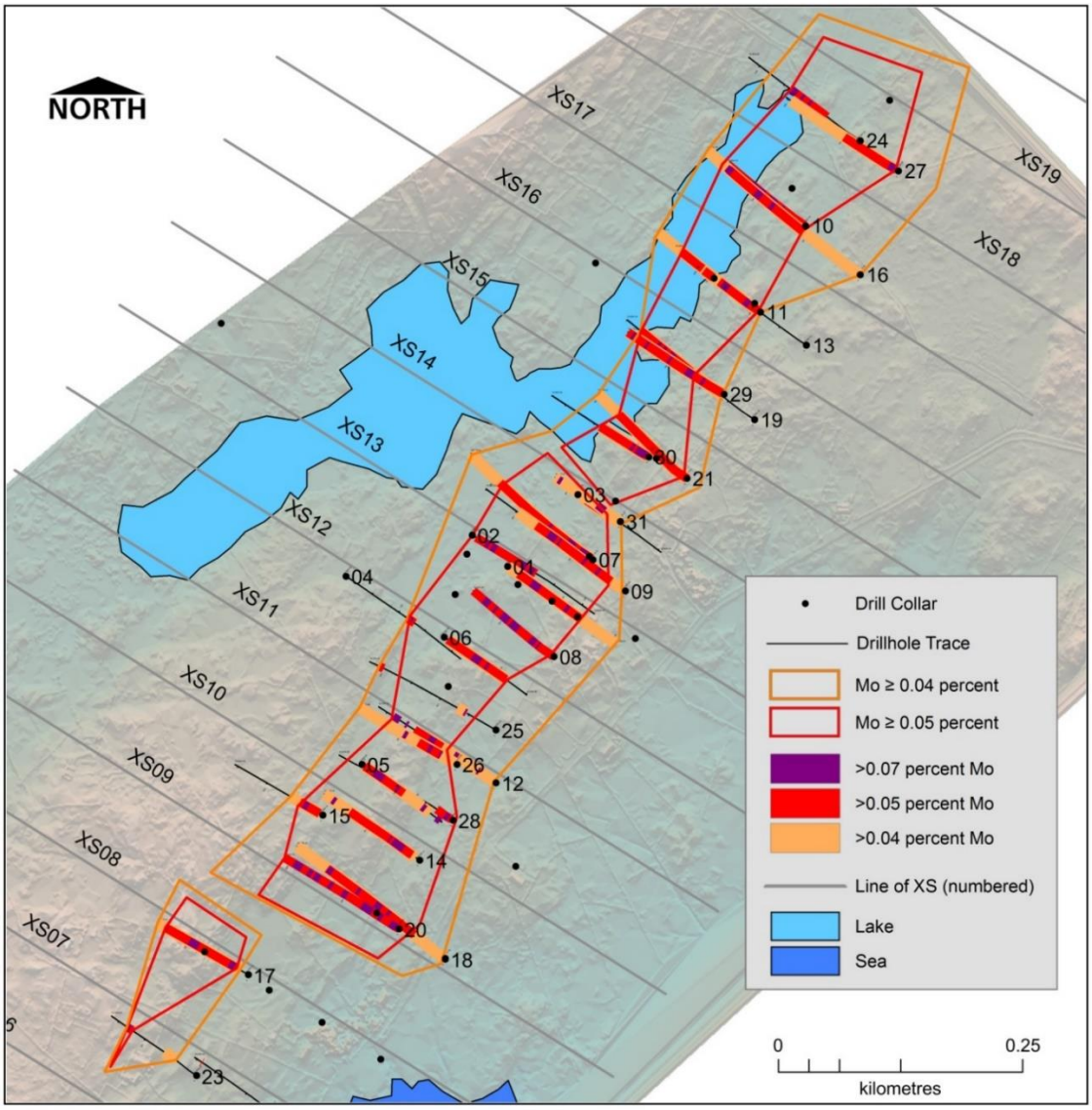

Figure 1-4 Plan view of drilling with composited assays shown downhole. Grades are averaged over a minimum downhole interval of 3.0m (SLR 2016)

The deposit is a porphyry-style deposit, hosted in granites and dacite porphyritic intrusions. Alteration is typical of a porphyry deposit, and is patchy yet seen in every drill hole. Alteration is primarily seen forming a halo around mineralised veins and it is believed that these veins originate from a deeper zone of more pervasive alteration and higher grade, consistent mineralisation (SLR 2016). Tellus (2016) magnetic survey data show an approximately circular magnetic low encompassing the deposit area and extending offshore to the SSE. SLR's (2016) Cu:Mo ratio voxel similarly shows an increase in the Cu:Mo ratio in a SSE direction, suggesting this is vectoring towards the origin of mineralising fluids at depth. It is believed that the erosion level at the deposit

is approximately at the upper-middle part of the system, indicating that significant mineralisation may exist below the levels drilled to date. Hyperspectral imaging and magnetic susceptibility have been useful tools in mapping alteration, defining areas of higher magnetic susceptibility in area of potassic alteration and fresher, less altered granite, and relatively lower susceptibility where propylitic and phyllic alteration is observed (McCarthy and Cloutier 2016, see Table 1).

Structural controls on the deposit are evident, with ENE-trending faults clearly acting as a conduit for mineralisation. Later, post-mineralisation, WNW faults have dextrally offset parts of the deposit from adjacent zones, which is consistent with observed trends at outcrop. Structural mapping by Hutton (2015) and others has indicated that there may be some as-yet untested targets in the area. Mineralisation has been well-defined to date, with very consistent zones defined at cut-off grades of 0.04% Mo and 0.05% Mo. Most drill holes intersected significant thicknesses of mineralisation averaging above those cut-off grades. Within those zones, significant intervals of >3.0m averaging above 0.07% Mo are common. One drill hole in the southern part of the deposit is mineralised throughout, and returned the highest Mo values of the recent drilling campaign. 3D modelling demonstrates that this drill hole, and surrounding drill holes, sits in an area of high Mo:Cu ratio, indicating that it is on or near an important conduit for mineralising fluids during the formation of the deposit. The zone is persistent at depth. The deposit is open in all directions, making it likely that further drilling will extend it to the NNE, SE and possibly to the east. In addition to those obvious extensions to existing drilling, there are other, untested targets in the area.

1.9 Research aims and goals

The Mace molybdenum-copper porphyry deposit is unusual in Ireland in that porphyry-style deposits are not a common occurrence in Irish granite bodies. It is important to relate the alteration and mineralisation patterns at Mace to those observed at other known porphyry systems in order to target exploration and identify vectors towards mineralisation. To do this, a clear understanding of the paragenetic sequence of alteration and mineralisation at Mace is required.

While molybdenite occurrences have been known in the Galway Granite Batholith for some years, detailed work did not begin until the 1960s. Despite the exploration work completed over the last 50 to 60 years, the true origin and nature of the deposit has been poorly understood, and attempts to model the deposit at Mace Head have not been made until the most recent exploration programme carried out by SLR Consulting for MOAG Copper Gold Resources.

Exploration work by SLR Consulting has defined the orebody within an economic grade envelope and established a Cu:Mo ratio suggesting an origin for mineralising fluid to the south-east of the deposit area, just offshore Mace Head, due to the postulated position of the Mace deposit in the context of a classic porphyry Cu-Mo deposit. SLR has postulated that the Mace Deposit is located in the upper-middle part of a larger, deeper porphyry-type deposit (see Figure 2-8). Mineralisation assemblages and alteration styles in the Mace deposit are similar to classic porphyry-type deposits.

This thesis describes textural and geochemical analysis carried out on drill core from Mace Head and the resulting commercial laboratory assays on drill core samples. A detailed petrographic analysis of representative mineralisation and alteration styles has been undertaken to help differentiate the various mineralisation phases, alteration assemblages, and mineralisation assemblages. A clear understanding of the paragenetic veining sequence is believed to be crucial in understanding the genetic nature of the deposit, and will inform the future exploration model. It is believed that the deposit may contain further concentrations of economic mineralisation, particularly at a depth not yet tested by exploration drilling.

Statistical analyses on the commercial whole rock geochemical assays obtained during exploration were used to help correlate economic mineralisation grades with mineral and alteration assemblages in the deposit.

Laboratory analytical techniques were applied to drill core samples in order to investigate trace element geochemistry of mineralisation and alteration within the deposit and establish a paragenetic sequence for vein types recorded during exploration drilling.

Such work has never been undertaken at the Mace Deposit and increases the geological understanding of a unique example of an Irish porphyry system. Most importantly, a greater understanding of the geology and mineralising system will aid exploration and drill targeting on the deposit, and contributes to the geological knowledge of this part of the composite Galway Granite Batholith.

1.10 References

Aucott, J. W., (1965): Layering in the Galway Granite: Nature, 207, 929-930

Ballard, J. R., Palin, J. M., Williams, I. S., Campbell, I. H., Faunes, A., (2001) Two ages of porphyry intrusion resolved for the super-giant Chuqui- camata copper deposit of northern Chile by ELA-ICP-MS and SHRIMP: Geology 29:383

Bergey, W. R. (2008). Geological Report On The Mace Molybdenum-Copper Prospect Connemara, County Galway, Ireland

Burns, D.J., (1970), Drilling on Licence 934, Mace, Co. Galway: West Galway Joint Project: Anglo United Trust Private Report

Carten, R.B., Geraghty, E.P., Walker, B.M., and Shannon, J.R., (1988), Cyclic development of igneous features and their relationship to high-temperature hydrothermal features in the Henderson porphyry molybdenum deposit, Colorado: Economic Geology, v. 83, p. 266–296

Claxton, C.W., (1971), The petrology, chemistry and structure of the Galway Granite in the Rosmuc area, Co. Galway: Proceedings of the Royal Irish Academy 71B, 155

Coats, J. S., & Wilson, J. R., (1971), The eastern end of the Galway Granite: Mineralogical Magazine, vol. 38, pp. I38-51

Cooke, D.R., Hollings, P., Wilkinson, J.J., and Tosdal, R.M., (2014), Geochemistry of porphyry deposits, *in* Holland, H.D., and Turekian, K.K., eds., Treatise on geochemistry, 2nd edition, v. 13: Oxford, Elsevier, p. 357–381

Crowley, Q. & Feely, M., (1997), New perspectives on the order and style of granite emplacement in the Galway Batholith, western Ireland. Geological Magazine 134, 539–48

D'Angelo et al. (2017), Petrogenesis and Magmatic Evolution of the Guichon Creek Batholith: Highland Valley Porphyry Cu ± (Mo) District, South-Central British Columbia: Economic Geology, v. 112, pp. 1857–1888

Deckart, K., Clark, A.H., Cuadra, P., and Fanning, M., (2013), Refinement of the time-space evolution of the giant Mio-Pliocene Río Blanco-Los Bronces porphyry Cu-Mo cluster, central Chile: New U-Pb (SHRIMP II) and Re-Os geochronology and 40Ar/39Ar thermochronology data: Mineralium Deposita, v. 48, p. 57–79

Deckart, K., Silva, W., Spröhnle, C., and Vela, I., (2014), Timing and duration of hydrothermal activity at the Los Bronces porphyry cluster: An update: Mineralium Deposita, v. 49, p. 535–546

Derham, J. (1986). Structural controls of sulphide mineralisation at Mace, Co. Galway: Geology and Genesis of Mineral Deposits in Ireland. Irish association for Economic Geology

Derham, J.M., and Feely, M., (1988), A K-feldspar breccia from the Mo-Cu stock work deposit in the Galway Granite, west of Ireland: Journal of the Geological Society, v. 145, p. 661-667

El Desouky, M., Feely, M., and Mohr, P., (1996), Diorite-granite magma mixing along the axis of the Galway Granite batholith, Ireland. Journal of the Geological Society, London 153, 361-7

Feely, M., McCabe, E., and Kunzendorf, H., (1991), The Evolution of Ree Profiles in the Galway Granite Western Ireland: Irish Journal of Earth Sciences, Vol. 11, No. 1 (1991), pp. 71-89

Feely, M., Coleman, D., Baxter, S., and Miller, B., (2003), U-Pb zircon geochronology of the Galway Granite, Connemara, Ireland: implications for the timing of late Caledonian tectonic and magmatic events and for correlations with Acadian plutonism in New England: Atlantic Geology 39. 175-84

Feely, M., Selby, D., Conliffe, J. and Judge, M., (2007), Re-Os geochronology and fluid inclusion microthermometry of molybdenite mineralisation in late-Caledonian Omey Granite, western Ireland: Applied Earth Science 116, 143-9

Feely, M., Selby, D., Hunt, J. and Conliffe, J. (2010) Long-lived granite-related molybdenite mineralisation at Connemara, western Irish Caledonides. Geological Magazine 147, 886-894

Feely, M., and Madden, J. S., (1987), The Spatial Distribution of K, U, Th and Surface Heat Production in the Galway Granite, Connemara, Western Ireland: Irish Journal of Earth Sciences, Vol. 8, No. 2, pp. 155-164

Gallagher, V., Feely, M., Hoegelsberger, H., Jenkin, G. R. T., & Fallick, A. E., (1992), Geological, fluid inclusion and stable isotope studies of Mo mineralisation, Galway Granite, Ireland: Mineralium Deposita 27, 314–25

Grumbley, N. L., (2015), The Geological Evolution of the Haib Cu-Mo Porphyry, Namibia, Unpublished MSc thesis, Trinity College Dublin, Ireland

Hutton, D. H. W., (2015), Report on the Mace Granite Prospect - June 2015: Internal Report to MOAG Copper Gold Resources

Keith, J. D., Whitney, J. A., Hattori, K., Nallantyne, G. H., Christiansen, E. H., Barr, D. L., Cannan, T. M. & Hook, C. J., (1997), The role of magmatic sulphides and mafic alkaline magmas in the Bingham and Tintic mining districts, Utah, Journal of Petrology, vol. 38, pp. 1979-1990

Lawrence, G., (1975), The use of Rb/Sr ratios as a guide to mineralisation in the Galway granite, Ireland. *in* Elliot, I.L. and Fletcher, W.K. (eds) Geochemical Exploration, Elsevier, Holland, 353

Leake, B., (1974), The crystallization history and mechanism of emplacement of the western part of the Galway Granite, Connemara, Western Ireland: Mineralogical Magazine, v. 39, p. 498-513

Leake, B. E., (1978), Granite Emplacement the granites of Ireland and their origin *in* Bowes, D R and Lake, B E (eds), Crustal evolution in northwestern Britain and adjacent regions: Geological Journal Special Issues 10, 221-248

Leake, B., (1989), The metagabbros, orthogneisses and paragneisses of the Connemara complex, western Ireland: Journal of the Geological Society, v. 146, p. 575-596

Leake, B.E., and Tanner, P. W. G., (1994), The geology of the Dalradian and associated rocks of Connemara, western Ireland: Dublin. Royal Irish Academy

Leggo, P. J., Compston, W., and Leake, B. E., (1966), The geochronology of the Connemara granites and its bearing on the antiquity of the Dalradian series: Quarterly Journal of the Geological Society of London 122, 91-188

Li, C. Y., Wang, F. Y., Hao, X. L., Ding, X., Zhang, H., Ling, M. X., Zhou, J. B., Li, Y. L., Fan, W. M., & Sun, W. D., (2012), Formation of the world's largest molybdenum metallogenic belt: a plate-tectonic perspective on the Qinling molybdenum deposits: International Geology Review, 54:9, 1093-1112

Norman, D. K., Parry, W. T., Bowman, J. R., (1991), Petrology and geochemistry of propylitic alteration at Southwest Tintic, Utah: Economic Geology, 86 (1): 13–28

Madden, J. S., (1987), Gamma-ray spectrometric studies of the main Galway Granite, Connemara, west of Ireland: Unpublished PhD thesis, National University of Ireland

Max, M.D., Long, C.B. and Geohagen, M.A., (1978), The Galway Granite: Geological Survey of Ireland, Bulletin 2

Max, M. D., Ryan, P. D., and Inamdar, D. D., (1983), Magnetic deep structural geology interpretation of Ireland: Tectonics 2, 431-4

Max, M.D. and Talbot, V., (1986), Molybdenum concentrations in the western end of the Galway Granite and their structural settings: Irish Assoc. for Economic Geology, Geology & Genesis of Mineral Deposits of Ireland

McKie, D., & Burke, K. C., (1955), The geology of the Islands of South Connemara: Geol Mag. 92, 487

Murphy, T., (1952), Measurements of gravity in Ireland, gravity survey of central Ireland: Dublin Institute for Advanced Studies, Geophysics Memoir, 2, Part 3, 31 pp

O'Raghallaigh, C., Feely, M., McArdle, P., MacDermott, C., Geoghegan, M. & Keary, R., (1997), Mineral localities in the Galway Bay Area: Geological Survey of Ireland, Report Series, RS97/1 (Mineral Resources), 70 pp

Plant, A., (1968), Geology of the Leam-Shannawona District, Connemara, Ireland: Unpublished PhD thesis, University of Bristol

Selby, D., Creaser, R.A. and Feely, M., (2004), Accurate and precise Re-Os molybdenite dates from the Galway Granite, Ireland. Critical comment on "Disturbances of the Re-Os chronometer of molybdenites of the Late Caledonian Galway Granite, Ireland, by hydrothermal fluid circulation" by Suzuki et al, Geochemical Journal, 35, 29-35, 2001. Geochemical Journal 38, 291-94 Selby, Creaser & Feely, 2004

Sillitoe, R. H., (2010), Porphyry copper systems: Economic Geology, v. 105, p. 3–41

Sillitoe, R.H., and Mortensen, J.K., (2010), Longevity of porphyry copper formation at Quellaveco, Peru: Economic Geology, v. 105, p. 1157−1162

Sinclair, W.D., (2007), Porphyry deposits, *in* Goodfellow, W.D., ed., Mineral Deposits of Canada: A Synthesis of Major Deposit-Types, District Metallogeny, the Evolution of Geological Provinces, and Exploration Methods: Geological Association of Canada, Mineral Deposits Division, Special Publication No. 5, p. 223-243

SLR Environmental Consulting (Ireland) Ltd, Internal Exploration Reports to MOAG Copper Gold Resources, 2015-2016

Tellus Programme of the Geological Survey of Ireland, accessed 15th March 2017, www.tellus.ie

Wager, L.R., (1932), The geology of the Roundstone district, County Galway: Proceedings of the Royal Irish Academy 41B, 46-72

Wilkinson, J. J., Chang, Z., Cooke, D. R., Baker, M. J., Wilkinson, C. C., Inglis, S., Chen, H., Gemmell, J. B., (2015), The chlorite proximitor: A new tool for detecting porphyry ore deposits: Journal of Geochemical Exploration 152 (2015) 10–26

Williams, D.M., and Harper, D.A.T., (1988), A basin model for the Silurian of the Midland Valley of Scotland and Ireland: Journal of the Geological Society, London 145, 741-8

Williams, T. J., Candela, P. A. & Piccoli, P. M., (1995), The partitioning of copper between silicate melts and two-phase aqueous fluids: an experimental investigation at 1kbar, 800°C and 0.5kbar, 850°C, Contributions to Mineralogy and Petrology, vol. 121, pp. 388-399

Wright, P. C., (1961), The petrology and geochemistry of the Galway granite, of the Carna district, Connemara, Eire: Ph.D. Thesis of the University of Bristol

2.0 CHAPTER 2 MACE HEAD GEOLOGY

2.1 Introduction

The Mace molybdenum-copper deposit is hosted in the Carna Pluton of the Galway Granite. It is a Devonian age (Feely et al. 2003), composite, east-west trending pluton of granodiorite to leucogranite composition that outcrops along the northern margin of Galway Bay and extends inland for 20 km (SLR 2016 The Carna Pluton covers an area of approximately 600 km^2. The northern edge of the pluton is bordered by metamorphic rocks of the Connemara Massif. The Galway Granite was emplaced into the 490Ma metagabbro-gneiss suite to the north (Leake 1989; Leake & Tanner 1994) and into Lower Ordovician greenschist facies rocks (South Connemara Group) to the south (McKie & Burke 1955; Williams et al. 1988) during the late stages of major regional shearing, near the southern margin of the Dalradian miogeosyncline on the north-eastern margin of the Lower Palaeozoic Iapetus Ocean. A major fault, the Skird Rocks Fault, predates intrusion of the batholith and brings the South Connemara Group against the metagabbro-gneiss suite. It is considered by Leake (1978) to be a splay of the Southern Uplands Fault and to have strongly influenced the siting of the batholith. Available geochronological data indicate that emplacement occurred between c.423Ma and c.380Ma (Feely et al. 2010), with initial emplacement in the NW of Connemara and later granites (c. 410 to 380 Ma) sited to the south and east, along the extension of the Southern Uplands Fault (the Skird Rocks Fault), including the Carna Pluton. Molybdenite in the deposit area has been dated to 407±1.5Ma (Feely et al. 2010).

2.2 Prospect geology

The Connemara Geological Bedrock Map Sheet 10 published by the Geological Survey of Ireland (Morris et al. 1995) shows that the rocks in the Carna Dome, which forms the core of the western portion of the Galway batholith, are composed mainly of grey granodiorite (Carna-type) and pink monzogranite (Cuilleen-type).

Hunt et al. (2006) demonstrates that the sequential emplacement of the main phases of the Galway Batholith was controlled by the WNW-ESE to E-W trending Skird Rocks

Fault, that provided a general progression of granite emplacement to the south and east, south of the Connemara E-W metamorphic belt (Feely et al. 2010).

Reverse block movement on the NNE-trending Shannawona Fault and NNW-trending Barna Fault downfaulted the Carna Granite suite after it was intruded into the roof zone of the main batholith (Hunt et al. 2006).

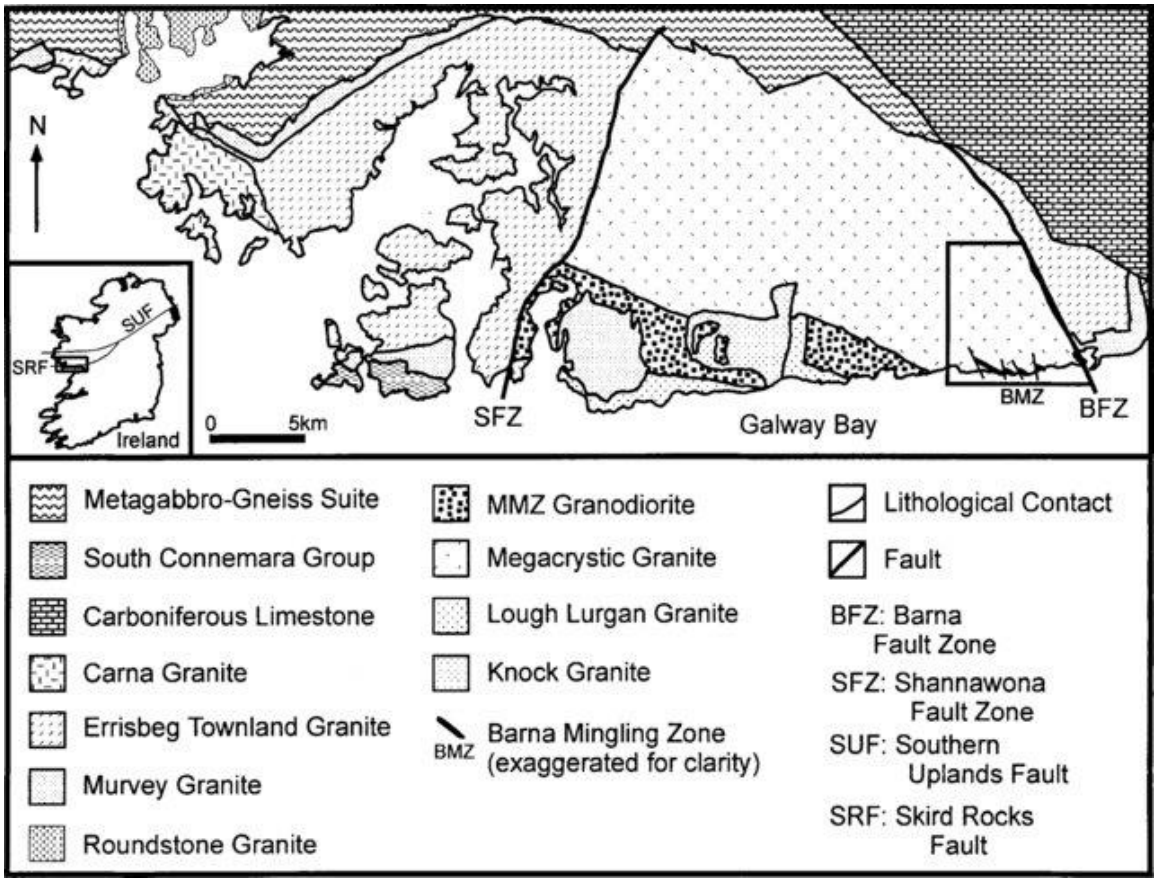

Figure 2-1 Geological map showing progressive phases of the Galway Granite Batholith (from Baxter & Feely 2002)

The WNW-ESE Skird Rocks Fault, NNE-trending Shannawona and NNW-trending Barna Faults played a key role in the progressive emplacement and distribution of the Galway intrusive complex (Hunt *et al*. 2006).

Leake (2011) provided further detailed interpretation of the Galway Granite and its emplacement mechanisms through progressive outward stoping, by mapping of distinctive phases of the Western Ring Complex of the batholith.

Leake indicated that the newly named Mace-Ards Granite, of which the southwestern edge of Mace Head is composed (*shown in Figure 2-2 below*) intruded the Carna and Cuilleen phases (mapped by Derham (1993), see Figure 2-3) of the granite within the ring complex, with this subsequently intruded by the later Murvey Granite phases. Crowley and Feely (1997) indicate that in the roof zone of the batholith marginal mixing of the partly crystallised Carna Granite magma and Errisbeg Townland Granite magmas occurred during emplacement. All of the granites are comprised of plagioclase, quartz and K-feldspar, ranging from granodiorite through granite to alkali-feldspar granite. (Leake 2011). Leake's detailed mapping indicates that the Mace-Ards Granite lacks hornblende and titanite but contains minor oligoclase and biotite, with k-feldspar rich phases on the western side of Mace Head.

Derham (1993) revised the chronology of the younger intrusive rocks of the Carna Dome during detailed geological mapping in the area of the Mace prospect (see Figure 2-2). The Carna phase is the oldest unit in the area and is intruded by the Cuilleen phase, which had previously been considered an orthoclase-rich division of the Carna phase, due to potassic metasomatism. After initial emplacement of the batholith at c. 420 Ma to the north and northwest of the Skird Rocks Fault (see Figure 2-1) generally south and eastward progression of granite emplacement and molybdenite mineralization along the Skird Rocks Fault followed at c. 410 Ma (Roundstone Murvey and Carna granites), at c. 400 Ma (Errisbeg Townland, Megacrystic, MMZ Granodiorite, Lough Lurgan and Kilkieran Murvey granites) and at c. 380 Ma (Costelloe Murvey, Shannapheasteen and Knock granites) (Feely et al. 2010).

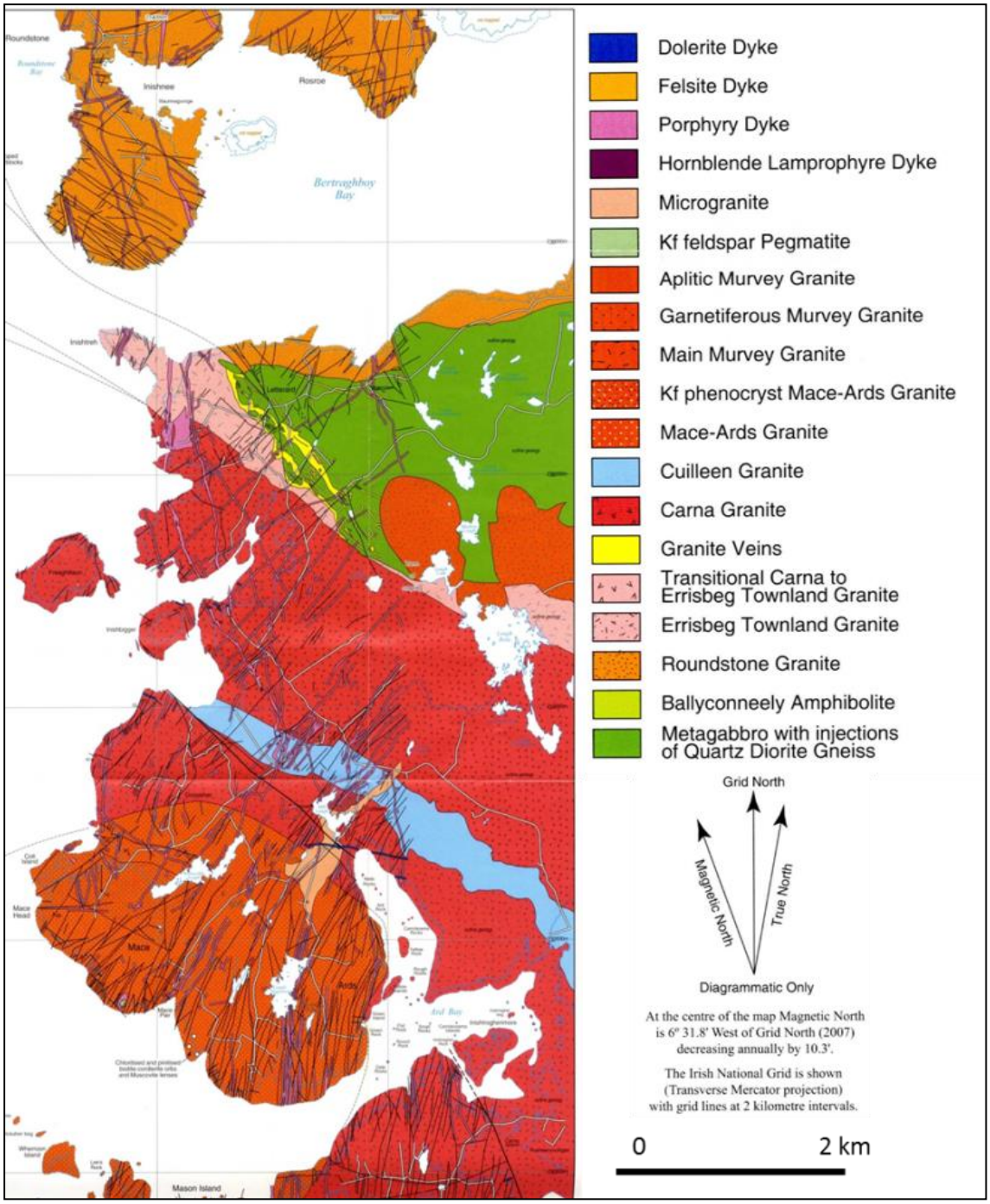

Figure 2-2 Geology of Mace Head, Co. Galway (Leake 2011)

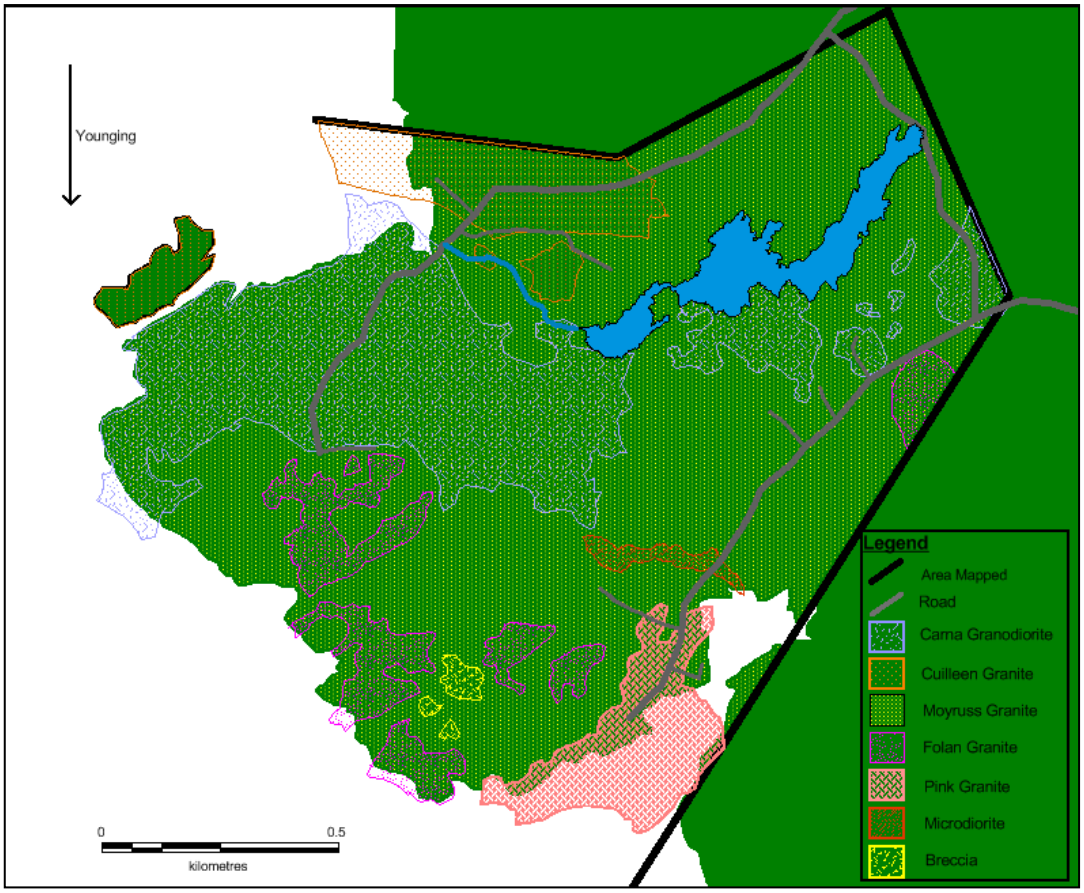

Figure 2-3 Principal Granite Lithologies of the Mace Head area (after Derham 1993)

There is a distinctive WNW trend in the margins of the principal granite lithotypes, but a NNE orientation of mapped outcrops, Mace Pier inlet and Lough Bunnacliffa lake margins.

2.2.1 Structure

Leake (2011) suggests that the west end of the Galway Batholith is a major, near-roof, ring complex, emplaced by outward stoping and progressive inward intrusion, combined with central uplift. Mapping carried out by Hutton for SLR (2016), on behalf of MOAG Copper Gold Resources, suggests that the Mace-Ards granite may in fact be a lacolith, with mapped features (presence of aplitic granites, drusy or vuggy cavities in granite, and tourmaline) indicative of a high level emplacement in the roof zone of the system (thus concurring with Leake). Disseminated patches of molybdenite and chalcopyrite observed during mapping appear to be controlled by very fine cross cutting quartz stringers, rather than being part of the melt, with the Mo-Cu ratio decreasing

away from these mineralised veins.; copper is more evenly distributed through the deposit than molybdenum. This observation is further supported by petrographic examination by SLR of samples taken during mapping.

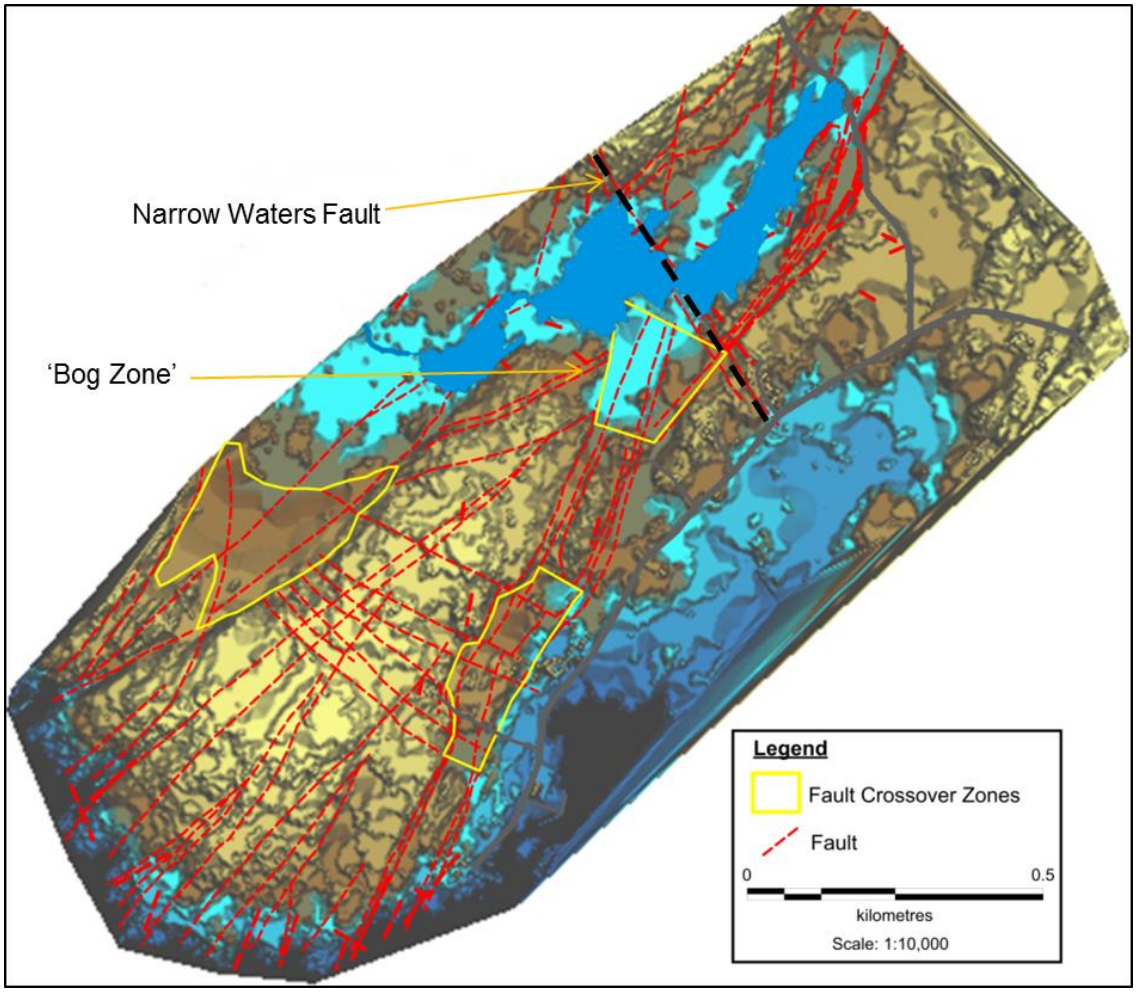

Figure 2-4 Results of structural mapping by Hutton (2015) during recent exploration

The NNE trend of Mo-Cu mineralised zone and dyke trends, which are observed perpendicular to the WNW long axis of the Galway Granite and the Skird Rocks fault, may be reflective of stress relaxation fractures that appear to control emplacement of dacite dykes during cooling and consolidation of the batholith (Hunt & Mohr 2007). The Narrow Waters Fault (Figure 2-4) is thought have offset mineralisation dextrally (SLR 2016), resulting in the 'Bog Zone' area of increased mineralisation.

2.3 Alteration and mineralisation

Exploration drilling on the Mace Deposit has shown that alteration and mineralisation are inherently associated (SLR 2016). Higher grade mineralisation (> 1.0% Mo and/or Cu) most often occurs in the presence of moderate to strong alteration.

Mineralisation and veining are closely related at Mace, with quartz veins hosting the majority of the molybdenum and copper mineralisation. Numerous vein types were observed during the early drilling programme and seven distinctive categories of veins (V1-V7) were defined by SLR geologists (2016). For simplicity during the exploration programme, dacite dykes and aplite/pegmatite horizons in the granite body were assigned as “V5” (dykes) and “V6” (aplite/pegmatite) for the purposes of classification. These two categories are related to the development of the batholith, while four vein types were interpreted to be related to mineralisation, and one interpreted as a late stage alteration phase. The vein types were categorised by SLR as follows:

- **V1**: These veins are typically 1cm wide, extensional quartz veins and are common throughout the drill core. They often host molybdenite patches at vein contacts. Extension cracks within the veins are observed perpendicular to the veins’ short axes. The extension cracks are interpreted to indicate multiple phases of extension and subsequent quartz precipitation.
- **V2**: This type describes the widest quartz veins encountered during drilling. V2 veins vary in width from 0.2m to 1.5m wide, are typically milky white and host the highest molybdenum and copper grades. Mineralisation is concentrated at vein contacts, but molybdenite, chalcopyrite and pyrite patches may occur throughout the vein. They typically occur in zones with several V2 type veins and an overall increase in quartz veining. These zones are characterised by strong epidote-chlorite-silica alteration, which can be several meters wide. Epidote, chlorite and silica are the main alteration phases defining the halo, bleaching the granite to apple to dark green.
- **V3:** A molybdenite vein, coating on fracture/ joint surfaces defines this vein type. This is best observed when the fracture has opened and molybdenite can be seen on both planes of the fracture, but can be inconspicuous when the fracture

remains closed in core. The molybdenite coating is usually <1mm wide, but has been observed up to 1cm wide, in localised, high grade zones. Slickensides are commonly observed on the surface of the molybdenite coating, due to the soft nature of the mineral, indicating shearing during or just after emplacement. These features were also observed at outcrop during field mapping.

- **V4:** This vein type encompasses quartz stringers (<1mm wide veinlets) and disseminations that occur throughout the granite. The stringers contain patches of molybdenite, chalcopyrite and pyrite.
- **V5:** K-feldspar dominated pegmatites that are commonly observed in drill core define the V5 vein set. The contacts are diffuse, and the pegmatites are dominated by potassic alteration. They are commonly vuggy, with black pyrolusite (MnO_2) infill and are often related to an increase in mineralisation. Both pyrite and molybdenite patches have been observed in some of the vugs, significantly increasing Mo grade, compared to the surrounding granite.
- **V6:** Fine-grained porphyritic dacite dykes, seen in drill core and mapped on surface. The dykes have been classified as either mineralised or unmineralised. The mineralised dykes are usually medium to light grey in colour, with some green epidote alteration; they are often silicified. They contain pink feldspar porphyroblasts (<1cm wide) in a very fine-grained matrix. These dykes are commonly cut by mineralised quartz veins (V2 and V4, rarely V3), often with a fine grained potassic alteration halo, and report very similar molybdenum and copper grades to the surrounding host granite. These dacitic dykes are inferred to have been intruded during (and possibly at a late stage of) mineralisation of the granite. The unmineralised dykes are typically dark grey and gritty in texture and have been observed to cut mineralised quartz veins. They are interpreted to have been intruded post-mineralisation at a late stage of emplacement.
- **V7:** These are cream coloured calcite and light purple fluorite stringers that occur at a high angle (c.45 degrees from vertical), usually parallel or sub-parallel to the long core axis. They are not related to mineralisation and appear wavy, with several growth stages. They have been interpreted as a form of late stage veining as the system cools.

2.3.1 Alteration

Typical of a porphyry style deposit, three main types of alteration were observed in core from the Mace drilling programme (see Figure 2-5).

- Potassic alteration, medium to coarsely crystalline and pink or pinkish-brown in colour;
- Phyllic alteration, which takes the form of sericite replacement of the primary minerals;
- Propylitic (epidote-chlorite) alteration, which is typically expressed as green to dark green altered granite, often on the margins of larger brecciated and mineralised veins.

The phyllic alteration is fine grained and subtly observed, and has mainly been confirmed by means of hyperspectral analysis (McCarthy and Cloutier 2015). McCarthy and Cloutier do not draw a distinction between phyllic and propylitic alteration, regarding all fractured, green-colour altered granite as having undergone phyllic alteration.

Potassic, phyllic and propylitic alteration phases are all associated with Mo-Cu mineralisation, with slightly higher grades generally occurring in the potassic zones. These alteration styles are typical of porphyry style mineralisation, with confirmation of the occurrence of these types of alteration suggesting that there may be potential for further mineralisation at depth with pervasive higher temperature alteration. Magnetic susceptibility was found by McCarthy and Cloutier (2015) to be low in epidote altered areas and areas of phyllic alteration but relatively high in potassically-altered areas.

Dacitic dykes (like the one in the bottom of the image in Figure 2-5(b) below) were emplaced at Mace throughout the emplacement and mineralisation history of the host granite. Many dykes show magma mixing with the granite, meaning they were emplaced early in the history of their emplacement history, while other dykes both cross-cut the granite and show signs of Mo-Cu sulphide mineralisation, suggesting that some of the dykes are coeval with mineralisation. Other dykes are emplaced along faults and many are either cut by quartz veins or cut the quartz veins, indicating that

they were most likely emplaced between development of the fault zone through emplacement of the first quartz veins and into the dextral faulting from NW to SE. Hutton's (2015) work identified the dykes as a feature of the area emplaced in an approximate NE-SW trending swarm. Most of the dykes contain minor amounts of mineralisation, with bulk rock assays (SLR 2016) showing molybdenum and copper values roughly the same as those found in the surrounding granite host.

Propylitic alteration is generally associated with larger quartz veins and with brecciation and faulting in the deposit. Potassic alteration is also associated with mineralisation, often as an alteration halo surrounding mineralised veins, and occasionally in relation to areas of brecciation.

Late stage "V7" veining, which usually contains calcite, chlorite and fluorite as a late lower temperature phase, is usually not observed to contain Mo-Cu mineralisation.

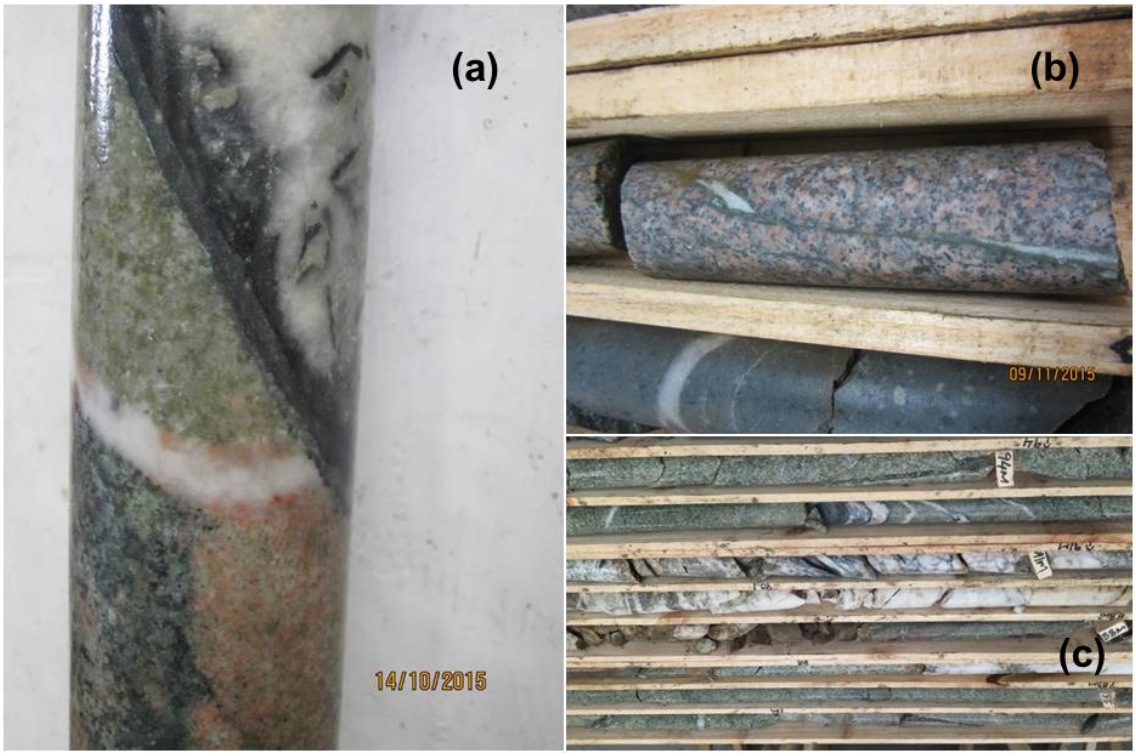

Figure 2-5 Typical alteration phases observed in SLR drilling; (a) potassic (pink) and propylitic (green) alteration styles shown, separated by "V1" extensional quartz vein in core from 15-934-18; (b) Top: potassic alteration associated with narrow quartz-Mo-Cu veins and speckled Mo in groundmass. Bottom: dacitic porphyry dyke; (c) Epidote (propylitic) alteration above and below large breccia and mineralised quartz vein. Core shown is NQ size (4.8cm across)

2.3.2 Magnetic susceptibility

SLR used a magnetic susceptibility meter during the 2015 drilling campaign to record magnetic susceptibility readings at 1m intervals during core logging. Broad correlations could be made using this simple technique, showing where magnetic highs occurred in biotite-rich, competent, fresher granite. The measuring technique used is useful for relative comparisons between different lithologies and alterations, but did not provide reliable, absolute values, so its use was confined to a pilot study of seven drill holes.

Potassic alteration results in relatively high readings, while strong propylitic alteration has a noticeably low magnetic susceptibility. McCarthy and Cloutier (2016) found that

magnetic susceptibility is also relatively low in sericitic (phyllic) alteration. Magnetic susceptibility readings are summarised in **Table 1** below.

Table 1 Summary of magnetic susceptibility readings from drill core at Mace (from McCarthy and Cloutier 2016)

Lithology or alteration type	Magnetic Susceptibility Average
Granite with weak epidote alteration and/or potassic alteration	3.71
Granite with potassium feldspar (unaltered)	2.61
Granite with epidote & potassic alteration	2.50
Felsite/dacite dykes	1.39
Granite with strong epidote alteration	0.56
Aplite	0.29
Fault gouge/No recovery	0.09
Breccias and Veins	0.06

The two primary alteration styles associated with Mo-Cu mineralisation, phyllic/propylitic and potassic, show distinctly different magnetic susceptibility responses in drill core. Phyllic alteration exhibits low magnetic susceptibility and high fracture intensity. This suggests that phyllic alteration is magnetically destructive and the fluids responsible for the alteration used the fracture zones as pathways during the mineralisation and alteration events. Potassic alteration is associated with a higher magnetic susceptibility and a decrease in fracture intensity, relative to zones exhibiting phyllic alteration (McCarthy and Cloutier 2016).

The de-magnetising nature of the fluids associated with phyllic alteration links well with the findings of the Geological Survey of Ireland's Tellus Survey (see Figure 2-6), which shows a well-defined low magnetic anomaly, centred on the Mace Deposit and to the south-east, and which corresponds with the observed increase in Cu-Mo ratio to the south-east seen in SLR's voxel model using drilling assay results.

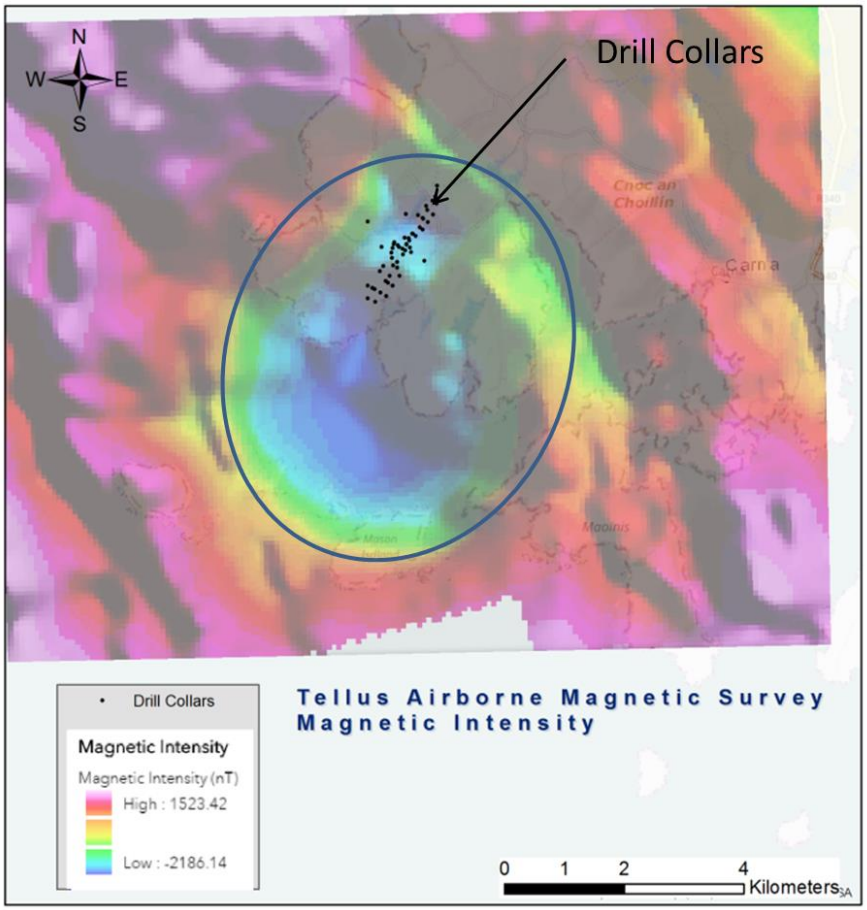

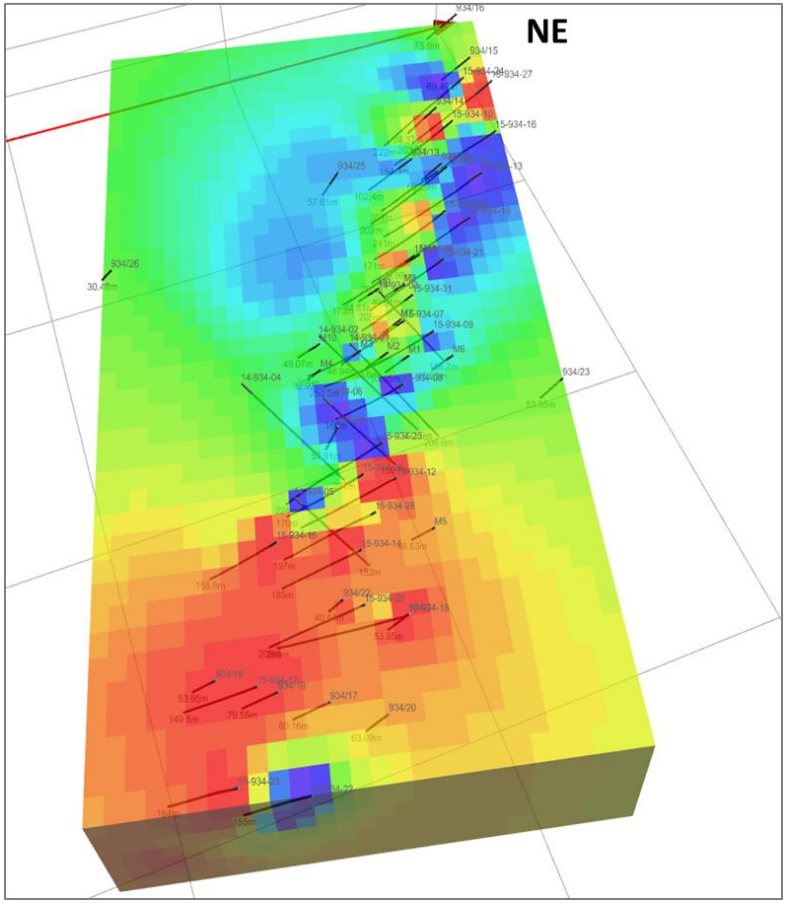

Figure 2-6 Left: Tellus airborne magnetics data, released 2016, showing a distinct low magnetic anomaly centred on Mace Head; Right: SLR's 2016 Cu-Mo drilling results voxel showing increasing Cu-Mo ratio to the south of the deposit area (red = high, blue = low)

2.3.3 Mineralisation

The molybdenum of interest at the Mace Deposit occurs as molybdenite (MoS_2), with copper primarily present as chalcopyrite ($CuFeS_2$) or rarely as bornite (Cu_5FeS_4). Pyrite is common to abundant throughout most of the deposit area. A north-northeast (NNE)-trending zone lying parallel to mapped veins near Mace Pier contains molybdenite, chalcopyrite, pyrite and occasional galena, extending from the seashore for at least 2km to the northeast within the Mace-Ards Granite (see Figure 2-1). Mineralisation is hosted in the Mace-Ards granite (Figure 2-2), dominated by plagioclase, quartz and K-feldspar, with common felsite intrusives and rare greisen-style, K-feldspar pegmatites. Significant epidote-K-feldspar alteration of the host granite was observed as hydrothermal alteration linked to the mineralising system. Molybdenite occurs variably as patches, disseminations in quartz veins, striated and unstriated smears on slickensides, rosettes on partly recrystallized surfaces, and on open joint planes. Chalcopyrite occurs primarily as patches and disseminations within quartz veins and as disseminations within the granite. The ratio of molybdenum to copper has been observed to decrease away from mineralised veins, with copper disseminated more evenly through the deposit than molybdenum (SLR 2016). The results of SLR's block modelling and Tellus magnetic survey data released in 2016 highlight this observation (see Figure 2-6 (b))).

Mo mineralisation is hosted in narrow to wide (0.1cm - 1m), steeply dipping quartz veins and stringers (see Figure 2-5 and Figure 2-7). These veins are generally sub-vertical to 85° dip and strike north-north-easterly (020°). Along the vein selvages, molybdenite also occurs as disseminations in the altered host granite. Many of the observed quartz veins and stringers appear to be late and crosscut the granite host. Mineralisation has been well-defined by drilling to date, with very consistent zones defined at cut-off grades of 0.04% Mo and 0.05% Mo. Most drill holes intersected significant thicknesses of mineralisation averaging above those cut-off grades. Within those zones, significant intervals of >3.0m averaging above 0.07% Mo are common.

Drilling intersected significant visible chalcopyrite, pyrite and molybdenite at Mace, hosted in quartz veins, veinlets and stringers, as well as in localised brecciated zones. An example of typical mineralised textures is presented below (*Figure 2-7*).

Figure 2-7 Quartz vein-breccia with molybdenite, chalcopyrite and pyrite. Observe also the green epidote and pink-K-feldspar alteration in the vein selvage. Field of view approximately 25cm.

Late porphyritic dacite dykes cross-cut the granite, but many also show signs of Mo-Cu sulphide mineralisation, suggesting that at least some of the dykes are coeval with a late phase of mineralisation. Faulting can be observed locally with significant fault intersections in at least two drill holes. Fault zones observed in drill core have been interpreted to correspond well to some of the faults mapped on the surface. South of the Narrow Waters Fault (see Figure 2-4) on the southern shore of Lough Bunacliffa, two 20m wide fault zones were intersected, at 86–109m and 130–150m (downhole depths), each consisting of highly broken and weathered granite, felsite and quartz veins, with weathered sulphides throughout. Significant fault zones were also observed in other drill holes.

2.4 Conclusions

The Mace Deposit has many of the classic characteristics of a porphyry style deposit. It is hosted in felsic intrusive rocks, with the three major styles of alteration (propylitic, phyllic and potassic) observed and mineralogy typical of a Mo-Cu porphyry, with

molybdenite, chalcopyrite and bornite as the main economic minerals and common-to-abundant pyrite throughout.

Due to the nature of mineralisation and alteration seen in drilling and during mapping of the deposit area, it is thought that the erosion level at the Mace deposit is in the upper part of a typical porphyry deposit (see Figure 2-8). A classic porphyry style stockwork has not been intersected at Mace, although it is believed that there is potential to intersect such a system below the latest drilling depth of just over 200 vertical metres.

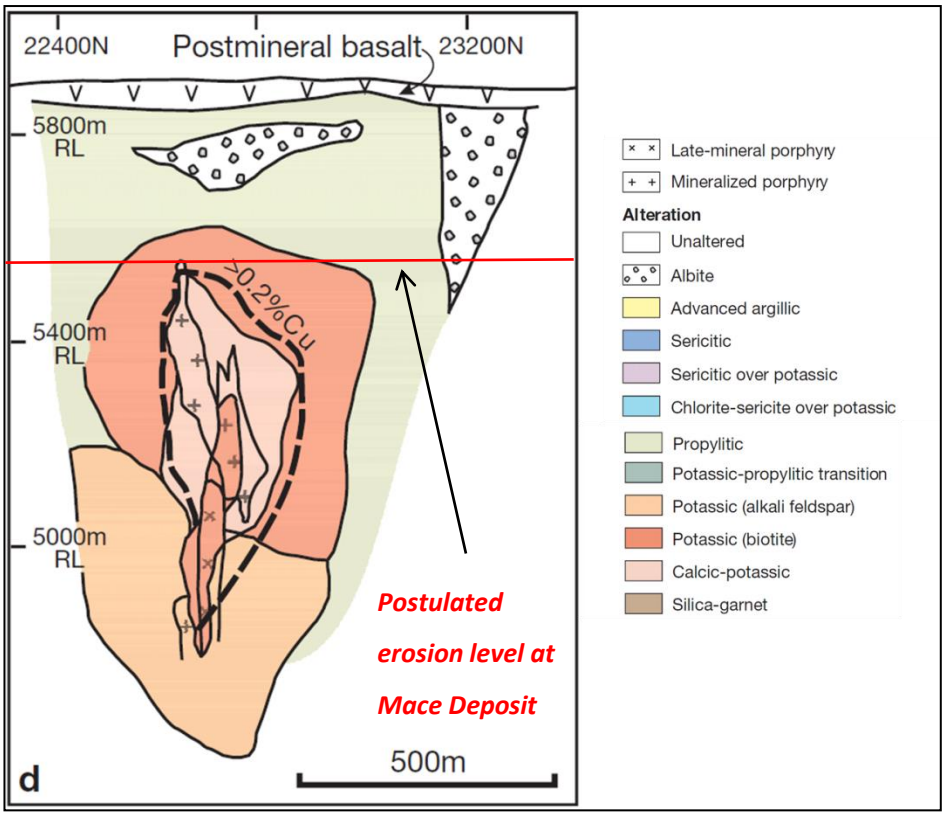

Figure 2-8 Schematic representation of a porphyry system (from Sillitoe 2010)

Structural controls on the deposit are well defined, with ENE-trending faults acting as a conduit for mineralisation and WNW faults offsetting the deposit dextrally, most notably at the Narrow Waters Fault that can be seen to dextrally offset the topography of Lough Bunacliffa directly to the NW of the deposit area.

Mineralisation has been well defined by drilling in the area, and most drill holes encountered significant grades of Mo. Drilling confirmed that mineralisation is more

consistently observed in drill holes towards the south of the deposit, with this zone persisting at depth, which correlates with the Tellus magnetic anomaly and the Cu-Mo modelling carried out by SLR. This evidence indicates that these vectors point towards an important conduit for mineralising fluids during deposit formation at depth and to the south.

The intimate association between mineralisation and alteration suggests that mineralising fluid transport and alteration of the host granites was coeval and multi-stage. Mineralised quartz veins are associated with higher temperature potassic alteration, while some of the largest quartz veins both in terms of thickness and Mo grade are associated with strong propylitic (epidote-chlorite) alteration. Unaltered granite in the deposit area has been observed to contain “barren” quartz veins – those where the only sulphide present is pyrite – suggesting that the first phases of economic mineralising fluid entering the system were the same fluids responsible for alteration textures seen at Mace. Using Sillitoe’s (2010) classifications, this may be indicative of a sequence from an initial high temperature fluid evidenced by potassic alteration, through progressively lower temperature propylitic-phyllic phases, and with a final “cool” unmineralised calcite-fluorite-chlorite assemblage overprinting the deposit at a late stage in its history.

2.5 References

Baxter, S. & Feely, M., (2002), Magma mixing and mingling textures in granitoids: Examples from the Galway Granite, Connemara, Ireland. Mineralogy and Petrology 76, 63-74

Bergey, W. R. (2008), Geological Report On The Mace Molybdenum-Copper Prospect Connemara, County Galway, Ireland

Crowley, Q. & Feely, M., (1997), New perspectives on the order and style of granite emplacement in the Galway Batholith, western Ireland. Geological Magazine 134, 539–48

Hutton, D. H. W., 2015, Report on the Mace Granite Prospect - June 2015: Internal Report to MOAG Copper Gold Resources

Hunt, J. Feely, M. Yates, M. Selby, D. Creaser, R. Leake, B. (2006). *Deconstructing the late-Caledonian Galway Batholith: P-T-t perspectives of granite magmatism in Connemara, western Ireland*. Paper presented at Harrisburg symposium, New Brunswick (2006)

Hunt, J. & Mohr, P. *A Composite Breccia and Magmatic Dacite Dike in the Galway Granite Batholith*. Irish Journal of Earth Sciences 25 (2007), pp 39-53

Feely, M. Selby, D. Hunt, J. & Conliffe, J. (2010*). Long-lived granite-related molybdenite mineralisation at Connemara, western Irish Caledonides*. Geol. Mag. 147 (6), pp.886-894. Cambridge University Press

Leake, B., (2011), Stoping and the mechanisms of emplacement of the granites in the Western Ring Complex of the Galway granite batholith, western Ireland. Earth and Environmental Science Transactions of the Royal Society of Edinburgh, v. 102, p. 1-16

McCarthy, W. & Cloutier, J. 2016. *Hyperspectral reflectance and magnetic alteration of the Mace Mo-Cu deposit, Co Galway*. Report to MOAG. University of St. Andrews

Morris, J.H., Long, C.B., McConnell, B. and Archer, J.B., (1995), Geology of Connemara: Geological Survey of Ireland [To accompany Bedrock Geology Map Series Sheet 10, Connemara]

Sillitoe, R. H., (2010), Porphyry copper systems: Economic Geology, v. 105, p. 3–41

Talbot, V. and Ryan, P., (1988), High molybdenum land values in Ireland: Possible implications: Science of The Total Environment, vol.76, Issues 2–3, pp. 217-228

3.0 CHAPTER 3 PETROGRAPHY

3.1 Introduction

To further investigate petrographic descriptions at Mace Head, a suite of 17 half-core samples were collected from drill holes in the Mace deposit, from depths ranging from 27 to 200m (down-hole depths).

60µm polished and uncovered thin sections were made from samples that had been selected to give a representative selection across alteration and vein types in the deposit area (see Appendix 1 for detailed descriptions). The samples were prepared in the Geology Department at Trinity College Dublin, and thin sections were made by Thin Section Labs in Toul, France. The thin sections were examined in the Centre for Microscopy and Analysis at Trinity College Dublin under reflected and transmitted light and under plain-polarised and crossed-polar light using a Nikon Eclipse LV100 light microscope with a Nikon DS-Ri2 camera attachment.

The main findings of the petrographic study will be outlined in this chapter, which will include the petrographic features of the main rock types and alteration assemblages described during exploration work on the deposit. Detailed descriptions of the primary and secondary mineral assemblages and a petrographic model for Mace Head are presented.

3.2 Laboratory analytical techniques and methods

3.2.1 Materials and methods

All equipment was available in Trinity College laboratories, while thin sections were prepared at Thin Section Labs, France.

3.2.2 Sample selection and preparation

Bulk geochemical assay results and the 3D drill section model created during SLR's exploration drilling programme were used to select drill core samples from the MOAG drill core stored at the core store in Carna. The core was available as split half-core, with permission granted from MOAG Copper Gold Resources to remove representative

sections as necessary. Samples were selected to give a representative selection across alteration and vein types in the deposit area (see Table 2 and detailed descriptions in Appendix 1). 14 areas were selected from four drill holes across the deposit area, focusing mainly on the central mineralised “Bog Zone”.

Table 2 Locations and depths of samples selected for thin-section. Depths are down-hole

Sample Number	Hole Number	From (m)	To (m)
39207	16-934-36	118.61	118.74
39208	16-934-36	110.69	110.81
39209	14-934-05	151.09	151.28
39210	14-934-05	141.63	141.78
39211	15-934-12	154.4	154.55
39212	15-934-12	165.09	165.25
39213	15-934-12	174	174.38
39214	15-934-12	182.79	182.9
39215	15-934-12	197.12	197.34
39216	16-934-36	103	103.2
39217	15-934-18	27.75	28.05
39218	15-934-18	72.18	72.4
39219	15-934-18	122.8	123.07
39220	15-934-18	123.21	123.39

The samples, principally of granite and dacite dyke lithologies with both mineralised and unmineralised veins, were prepared and polished using a Vibroplate and polishing plates

in Trinity College, after which areas of interest were selected and marked for creation of thin sections at Thin Section Labs in France.

17 thin sections were produced, to reflect the variety of alteration and vein styles found in the deposit. The thin sections were prepared for SEM backscattered electron imaging of mineral and vein relationships, X-Ray mapping, and LA-ICP-MS.

3.2.3 Light microscopy and scanning electron microscopy

In order to maximise the efficiency of the limited available time using the MIRA SEM, all thin sections were photographed using a Nikon light microscope and examined for suitable close inspection under the SEM. The images were photographed under both reflected and transmitted light in order to maximise visibility of features within each section (see Appendix 3 Light Microscope Imagery). Each image was analysed and areas of interest for SEM study were selected, paying particular attention to alteration minerals and patterns, interactions between vein types including crosscutting relationships and mobility of minerals across and within veins, and mineralisation in the host rock groundmass both related and unrelated to hydrothermal vein fluids.

Most of the SEM work used the back-scattered electron (BSE) detector on Trinity College's MIRA Scanning Electron Microscope. Back-scattered electrons enhance material contrast of the sample and result in heavier elements appearing as a lighter colour under the microscope.

The BSE detector is of the scintillation type. An annular (YAG) mono-crystal scintillator with a conductive surface is placed in the optical axis directly under the lower pole extension of the objective. The high energy back-scattered electrons impinge the scintillator without any additional acceleration and excite the scintillator atoms that emit visible radiation photons successively. The photons are carried, by means of the light guide, through the side outlet of the scintillator to the cathode of the photo-multiplier. They are then processed in the same way as the signal coming from the secondary electrons. The BSE detector is manufactured in an R-BSE (Retractable BSE) version. This modification allows retraction of the detector from under the pole piece

position if the detector is not used. This allows the specimens to be moved as close as possible to the objective when viewed by other detectors.

3.3 Rock type petrography

3.2.1 Granite

The host granite at Mace Head is a granodiorite intrusion composed mainly of medium- to coarse-grained textural varieties of granodiorite to leucogranite composition, variously exhibiting potassic, propylitic and phyllic alteration typical of porphyry-type deposits. The granite types at Mace are comprised of plagioclase, quartz and K-feldspar, and range from granodiorite through granite to alkali-feldspar granite (Leake 2011)._ Leake's detailed mapping indicates that the Mace-Ards Granite lacks hornblende and titanite but contains minor oligoclase and biotite (<5%), with k-feldspar rich phases on the western side of Mace Head.

Alteration of the granite is observed to increase towards mineralised intervals, as is typical of many porphyry mineralisation systems. Increased quartz veining and partial brecciation is accompanied by strong but patchy propylitic-potassic alteration in the host rock, which persists as a halo surrounding molybdenite-infilled, <40cm wide brecciated quartz veins. Although mineralised veins and fracture planes are observed throughout, a strong correlation between intense alteration and increased sulphide content, including chalcopyrite and pyrite, has been noted (SLR 2016).

Three main types of alteration can be seen in the host rock:

- Potassic alteration is observed as a pale pink to red gradational halo of potassium feldspar (k-feldspar), several centimetres wide, associated with mineralised quartz veins.

- Propylitic alteration is most commonly observed as an increase in green epidote with chlorite, associated with increases in quartz veining, brecciation and elevated molybdenum (Mo) and copper (Cu) values.

- Phyllic alteration, indicated by fine muscovite (sericite), is noted by Bergey (2008) in some historic drill logs, but it is not as common as the epidote-chlorite alteration minerals typical of propylitic alteration. The phyllic alteration is fine grained and subtly observed, and has mainly been confirmed by means of hyperspectral analysis (McCarthy and Cloutier 2015).

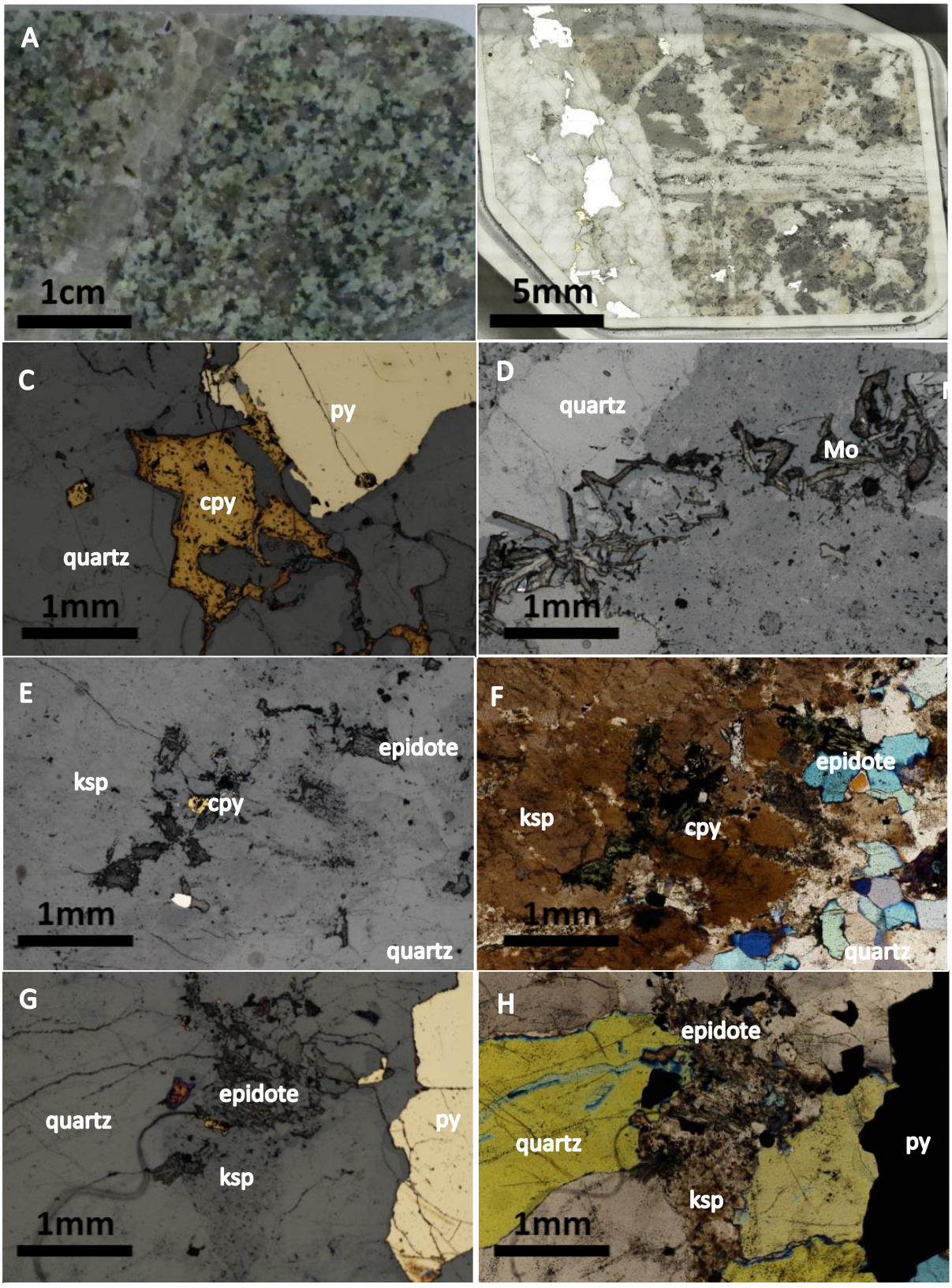

Figure 3-1 Examples from Sample No.39207 half-core and thin section of epidote-altered granite with quartz extension veins: A) Typical greenish epidote-chlorite alteration in polished half core section with visible pink-brown K-feldspar and 1cm quartz extension vein; B) Reflected light microscope image showing quartz vein with sulphides crosscutting quartz-molybdenite vein; C) PPL image showing late chalcopyrite overgrowing pyrite grain in quartz vein; D) molybdenite stringer (a) with muscovite mica (b) crosscutting quartz vein E) & F) PPL & XPL images of epidote and chalcopyrite in groundmass K-feldspar next to quartz; G) & H) PPL & XPL images of K-feldspar grain heavily included with sericite alteration with chalcopyrite and epidote in quartz and k-feldspar groundmass

3.2.2 Hydrothermal brecciation

Brecciation occurs associated with quartz veining throughout the deposit. It is most commonly associated with larger quartz veins having related propylitic and phyllic alteration of the granite host rock. Epidote-chlorite alteration is often seen in close association with some of the larger brecciated quartz veins, which commonly contain some of the highest recorded molybdenum assay values. The propylitic alteration appears to form a halo around these large veins, often extending several metres from the vein margins. Brecciation usually occurs in a quartz matrix, although common calcite-quartz matrix has been observed (Figure 3-3D)). A calcite matrix may indicate a later, lower temperature hydrothermal fluid phase, as calcite-fluorite veining is commonly seen in drill core as a clear final overprinting phase post-mineralisation.

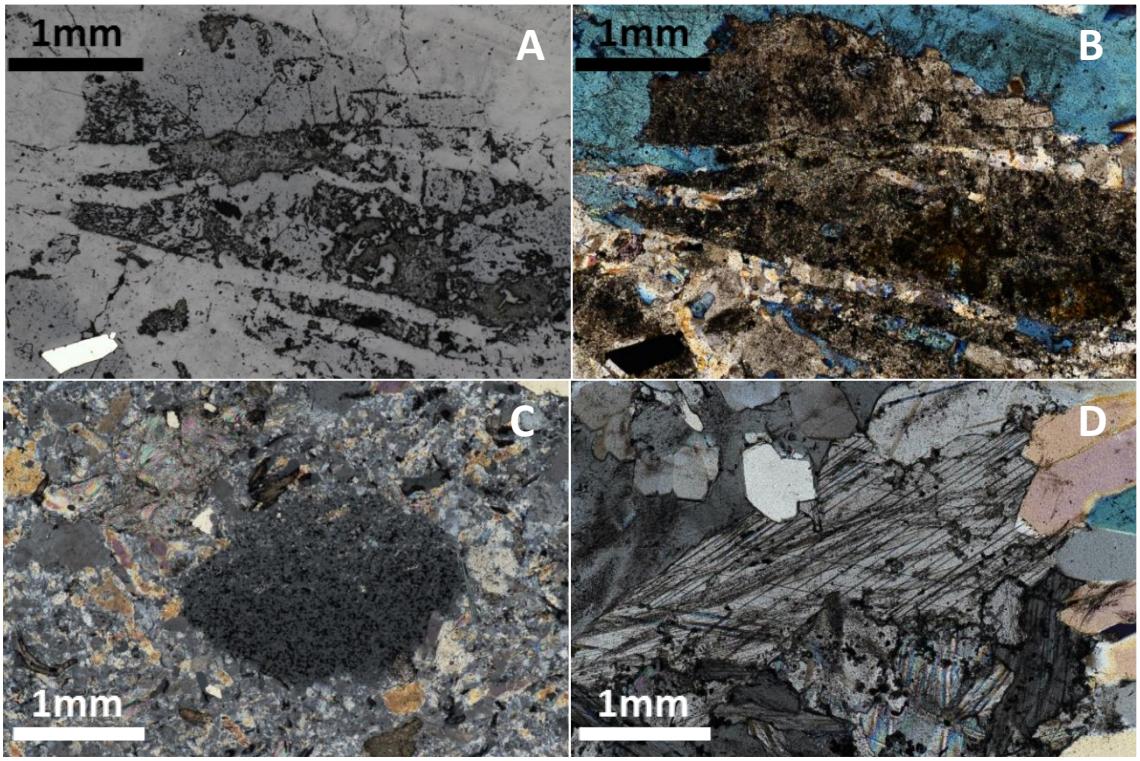

Figure 3-2 A) & B) PPL and XPL images of brecciated and epidote altered k-feldspar at quartz vein margin with chalcopyrite grain in bottom left; C) altered clast in breccia with epidote, sericite and sulphides; D) large calcite crystals with quartz in breccia

3.2.3 Quartz veins

One of the earliest vein types at Mace Head are extensional quartz vein systems; These are typically sulphide-bearing, granular quartz-dominated veins. Quartz veins typically occur as around 1cm wide and contain minor amounts of pyrite. Other than pyrite, the principal sulphides are molybdenite and chalcopyrite, which may be observed at the contacts between veins and host rock.

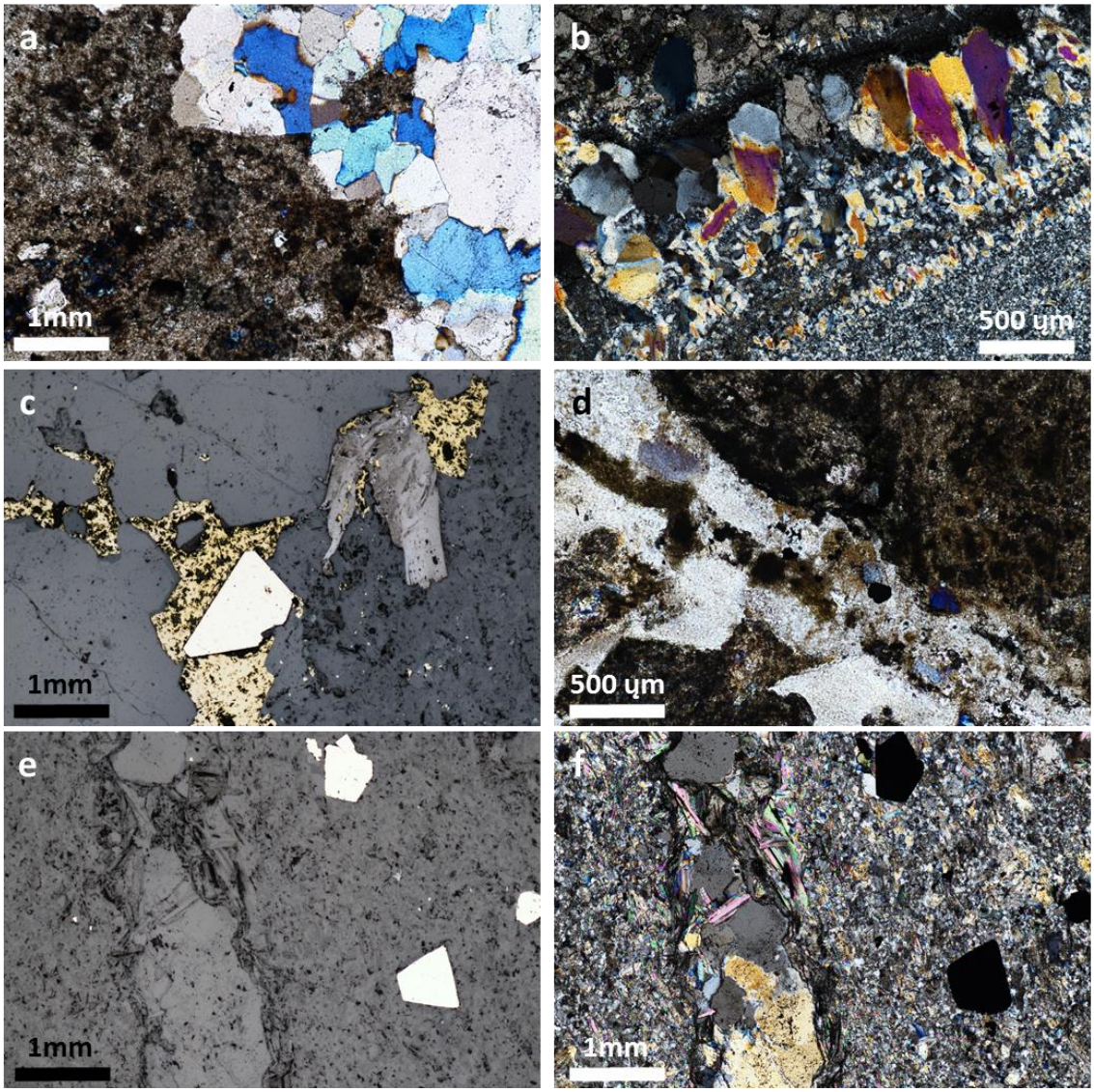

Figure 3-3 Examples of quartz veins and relationships between pyrite and other sulphides (chalcopyrite and molybdenite) within and at the margins of quartz veins a) & b) contact of quartz veins with sericite alteration of k-feldspar c) chalcopyrite overgrowth around euhedral pyrite (centre) and molybdenite (top right) d) fine grained sericite alteration e) & f) PPL and XPL images of euhedral pyrite crystals in sericite altered groundmass

3.2.4 Molybdenite veins and veinlets

A molybdenite coating on fracture/ joint surfaces defines this vein type. It is best observed when the fracture has opened and molybdenite can be seen on both planes of the fracture but can be inconspicuous when the fracture remains closed in core.

Slickensides are common on molybdenite coating fracture surfaces. Molybdenite may be seen overgrowing earlier pyrite at vein margins and in the host granite in alteration selvages.

3.2.5 Porphyritic dacite dykes

Fine-grained feldspathic dacite dykes can be seen throughout drill core and on surface exposures in the Mace Head area. These dykes have been classified as either mineralised or unmineralised during logging by SLR geologists in the field. Hutton (2015) noted that the dykes are a feature of the area that were emplaced in an approximate NE-SW trending swarm ranging from early in the granite history to coeval with mineralising events in the area. Mixing with the host granite is evident at the margins of some dykes, implying emplacement early in the history of the region. Some dykes are emplaced along faults and many may either cut quartz veins or have been cut by quartz veins. Slickenside relationships show that quartz and sulphides often crystallised synchronously with fault movement. These syn-tectonic veins are often cut by a set of NW-SE trending dextral faults.

The dacite dykes seen in the study area contain mainly remnant k-feldspar with common sericite replacement. Other common minerals in the porphyry dykes include quartz, plagioclase feldspar, amphibole, and chlorite. Dykes previously classified as “mineralised” and “unmineralised” by logging geologists show little difference in petrographic study. Chlorite-epidote alteration is common where the host granite is altered.

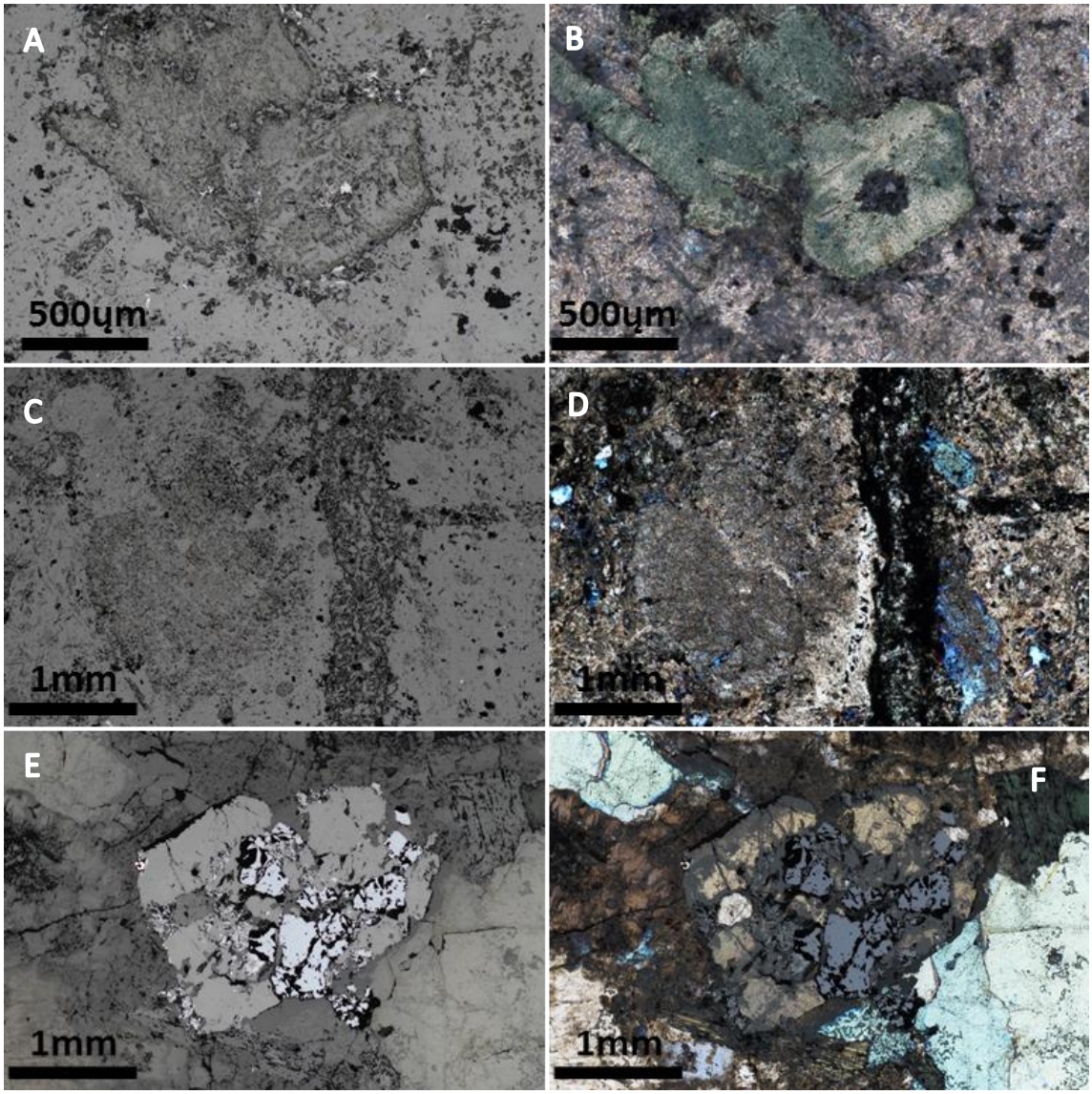

Figure 3-4 Alteration and mineralisation textures in felsic dacite dykes; A) & B) PPL and XPL images of a large epidote grain in sericitised k-feldspar dyke groundmass with molybdenite at centre of grain; C) & D) PPL and XPL images of vein through highly sericite-altered groundmass of dyke; E) & F) PPL and XPL images of a large fractured k-feldspar grain with molybdenite replacement at centre

3.2.6 Pink pegmatite/aplite

Pink pegmatite/aplite veins are generally assumed to be a product of magma mixing in the granite host and are therefore dated prior to mineralisation. Small patches and disseminations of sulphides can sometimes be observed in aplitic or pegmatitic sections of core, but these occurrences generally correspond to amounts observed in

surrounding rock types. Aplitic sections are occasionally cut by mineralised quartz veins and several fluid phases. Figure 3-8 C) shows molybdenite and chalcopyrite intergrowth with chlorite around pyrite in sericitised k-feldspar from an aplite vein through granite.

3.2.7 Calcite-chlorite-fluorite veins

Cream coloured calcite and light purple fluorite stringers usually occur parallel or sub-parallel to Mace drill core (around 45 degrees from vertical). They are not related to mineralisation and have uneven margins, with several growth stages. They have been interpreted by exploration geologists (Bergey 2008, SLR 2016) as a form of late-stage veining as the system cools and can form an overprinting texture along vein lineaments.

3.4 Alteration

Alteration in the Mace deposit is observed to increase towards mineralised intervals, as is typical of many porphyry mineralisation systems. Areas in drill core with a higher prevalence of quartz veining and partial brecciation are accompanied by strong but patchy propylitic-potassic alteration, which persists as a halo surrounding molybdenite-infilled, <40cm wide brecciated quartz veins. Although mineralised veins and fracture planes are observed throughout, a strong correlation between intense alteration and increased sulphide content, including molybdenite, chalcopyrite and pyrite, can be seen both in core and in thin section.

Three main types of alteration are encountered both in core and in thin section:

• Potassic alteration, characterised by K-feldspar that is medium to coarsely crystalline and pink or brown in colour. Potassic alteration is commonly observed in the groundmass near quartz veins with chalcopyrite and chalcopyrite-molybdenite mineralisation. Potassic alteration is generally observed in more structurally competent rock, and is often associated with narrow mineralised quartz-molybdenite veins. Potassic alteration is characteristic of high temperature alteration in porphyry systems (Sillitoe 2010). At Mace Head, potassic alteration is also associated with higher magnetic susceptibility (McCarthy and Cloutier 2015, SLR 2016) and a decrease in fracture intensity relative to zones exhibiting phyllic alteration. Disseminated molybdenite and

narrow molybdenite-rich veins are observed to cross cut the potassic assemblage (Figure 3-6 C)), with an overall molybdenum grade generally higher than in other mineralised vein styles in the deposit. This overprinting suggests that these vein types may post-date alteration.

• Phyllic alteration, which takes the form of sericite replacement of the primary minerals. Sericite replacement of k-feldspar is pervasive in many of the samples described here, often proximal to zones of epidote-chlorite alteration of primary k-feldspar and amphibole in groundmass (Figure 3-5 & Figure 3-6 D, E, F).

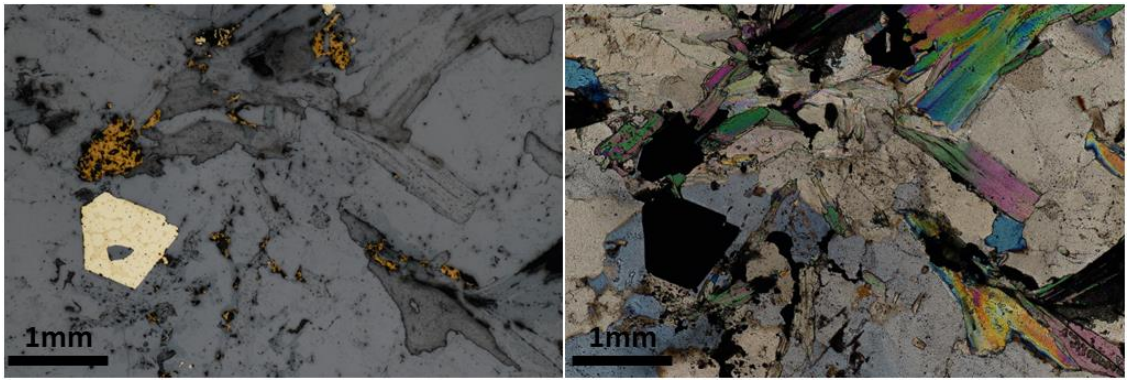

Figure 3-5 PPL and XPL images of euhedral pyrite and anhedral chalcopyrite in mica and quartz vein

• Propylitic (epidote-chlorite) alteration, which is typically expressed as green to dark green altered granite, often on the margins of larger brecciated and mineralised veins. Dacite dykes studied petrographically show propylitic alteration together with sericite alteration of remnant k-feldspar crystals. Propylitic alteration appears to exist concurrently or as alternating sequences with potassic alteration phases in the granite at Mace Head. Propylitic alteration was the most commonly reported alteration type in Bergey's (2008) report on historic drill logs, although propylitic alteration was not mentioned by Talbot and Max (1984). Epidote-chlorite alteration is often seen in close association with some of the larger brecciated 'V2' type quartz veins, which commonly contain some of the highest recorded molybdenum assay values. Increased quartz veining and partial brecciation in drill core is accompanied by strong but patchy

propylitic alteration which appears to form a halo around these large veins, often extending several metres from the vein margins.

The main propylitic and potassic alteration styles may be interpreted as hydrothermal alteration linked to the mineralising system (Figure 3-8 G) & H)). Much of the alteration is spatially associated with mineralised veins and it is deduced that mineralisation and alteration are closely related. There is a strong correlation between more intense alteration, particularly propylitic and potassic alteration, and increased sulphide presence. Potassic alteration, as a pale pink gradational halo, is associated with mineralised quartz veins, while propylitic alteration associated with chlorite, epidote and sericite, is commonly observed associated with increases in quartz veining, brecciation and the highest Mo and Cu values

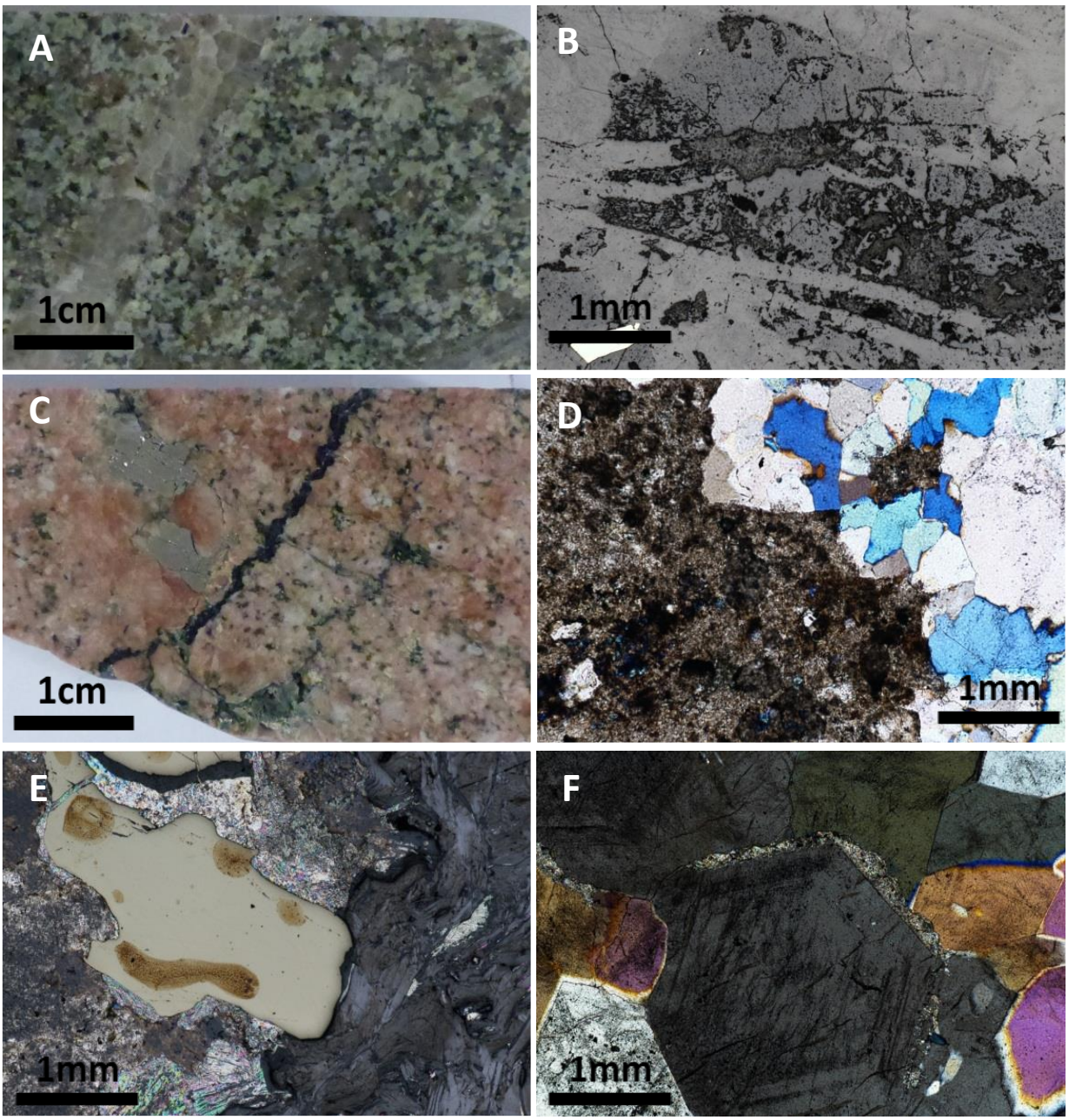

Figure 3-6 Alteration textures seen in samples from Mace Head A) typical greenish epidote-chlorite alteration in polished half core section with visible brecciated pink-brown K-feldspar and 1cm quartz extension vein; B) epidote alteration of k-feldspar grain with brecciation and quartz veining; C) classic potassic alteration of granite. Large pyrite crystals and molybdenite stringers are visible in this polished half core sample; D) sericite and chlorite replacement of K-feldspar crystal next to quartz grains; E) chalcopyrite crystal growing in k-feldspar grain showing strong sericite replacement next to molybdenite vein; F) sericite rim forming around hexagonal quartz crystal

3.5 Mineralisation

Mineralisation at Mace Head is hosted within fault-related quartz veins, with a SE-NW orientation. Three main mineral assemblages and textures are evident from petrographic analyses of samples taken from the deposit.

A *pyrite* assemblage is the most widespread in the deposit. This consists mainly of large pyrite crystals and disseminations of pyrite hosted in the earlier and larger quartz veins found in the deposit. Chalcopyrite, and more rarely molybdenite, is sometimes common as an overgrowth texture or exhibiting growth synchronous with pyrite

A *chalcopyrite* assemblage can be seen throughout veins and groundmass as individual grains or clusters of grains without a clear vein-host relationship. These chalcopyrite grains occur predominantly in areas of potassic alteration, implying a higher temperature fluid phase, and can sometimes occur associated with minor amounts of molybdenite.

A *molybdenite and chalcopyrite-molybdenite* assemblage is generally quartz vein hosted and is often seen as a second phase of mineralising fluid reactivating older quartz vein conduits. Chalcopyrite and molybdenite can be observed as secondary growth around pyrite and quartz in veins and around k-feldspar and quartz in groundmass in close proximity to quartz veins. Molybdenite-rich veins and stringers can also crosscut older quartz veins and often contain chalcopyrite.

Chalcopyrite can be commonly observed replacing pyrite, where the margins of pyrite grains have been partially replaced in quartz veins due to a later phase of mineralising fluid along reactivated conduits. Fracturing and minor brecciation of pyrite grains with subsequent chalcopyrite infill implies reactivation of vein pathways by higher temperature potassic fluids.

Examples of the growth patterns of sulphide grains can be seen in Figure 3-7 and Figure 3-8. Pyrite overgrowing and replacing chalcopyrite has not been observed in the studied samples.

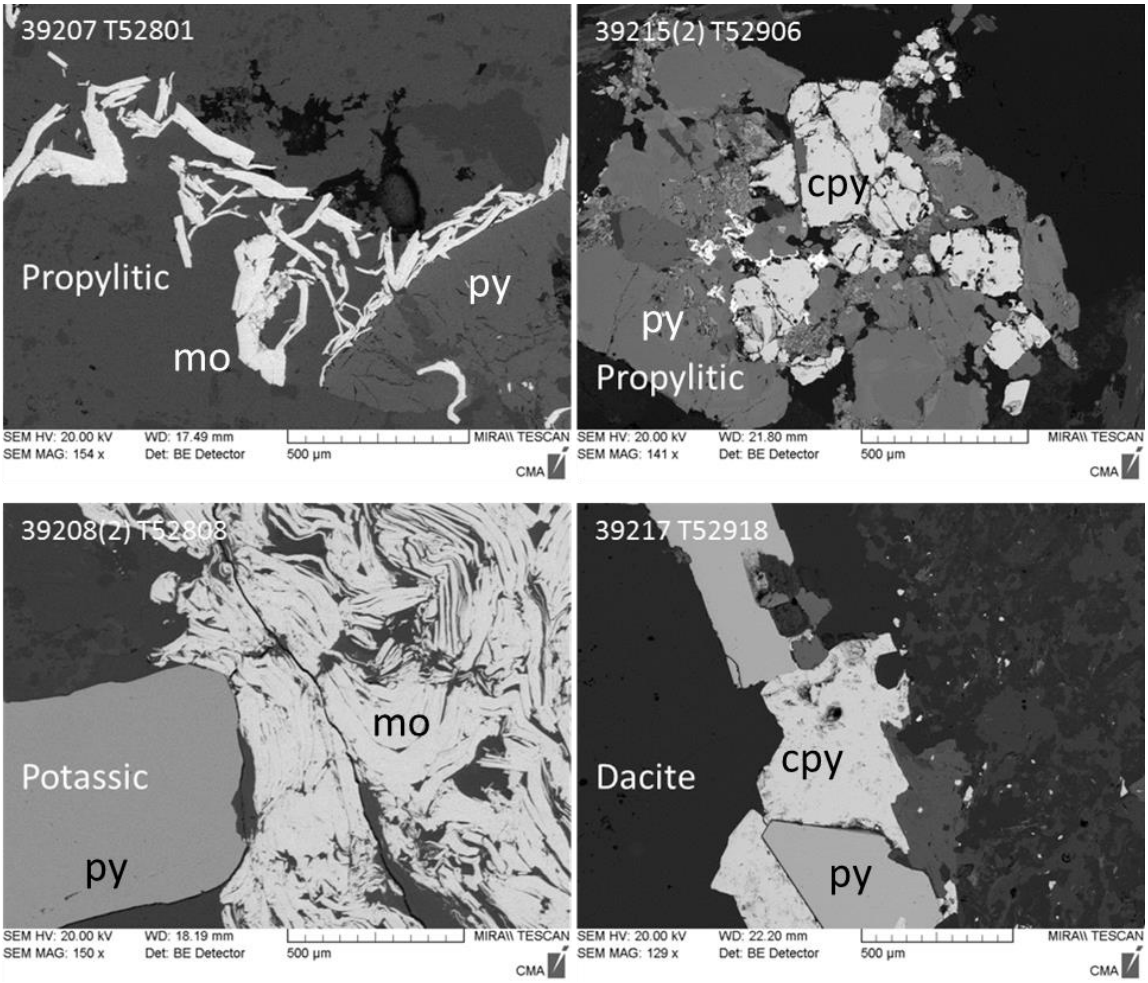

Figure 3-7 Examples of Cu and Mo sulphides in relation to earlier pyrite grains as seen under SEM. Chalcopyrite and molybdenite overgrowth of pyrite is clearly visible, particularly where potassic or propylitic alteration is strongly apparent

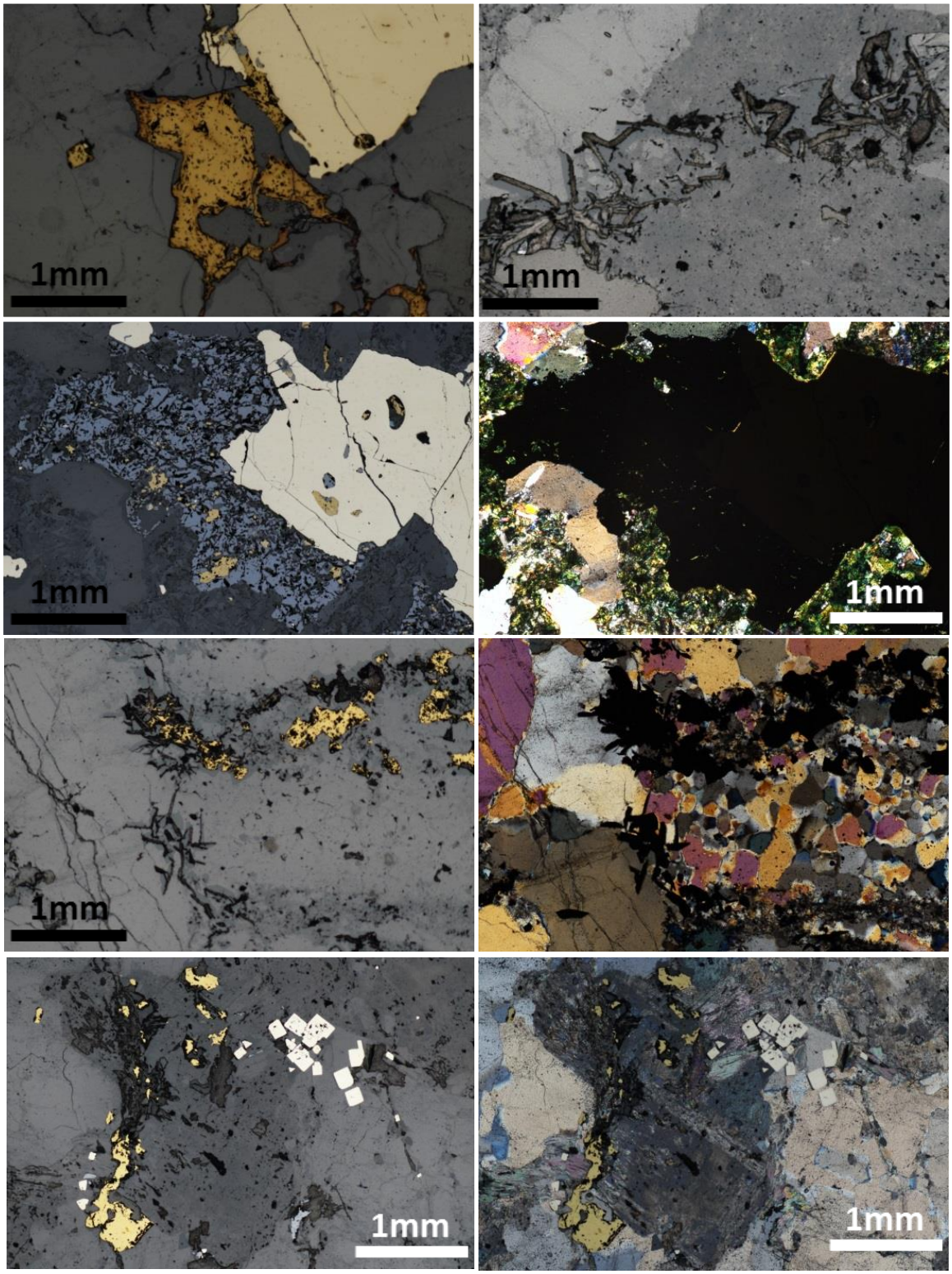

Figure 3-8 Mineralisation styles in thin section A) chalcopyrite replacing and overgowing pyrite in quartz vein; B) molybdenite stringer crosscutting quartz vein; C) & D) molybdenite and chalcopyrite intergrowth with chlorite around pyrite in sericitised k-fsp; E) & F) molybdenite and chalcopyrite intergrowth in the centre and margins of quartz vein crosscut by larger quartz vein; G) & H) euhedral pyrite grains and anhedral chalcopyrite in chlorite-epidote alteration of feldspar

3.6 References

Bergey, W. R. (2008), Geological Report On The Mace Molybdenum-Copper Prospect Connemara, County Galway, Ireland.

SLR Environmental Consulting (Ireland) Ltd, Internal Exploration Reports to MOAG Copper Gold Resources, 2015-2016

Derham, J.M., and Feely, M., (1988), A K-feldspar breccia from the Mo-Cu stock work deposit in the Galway Granite, west of Ireland: Journal of the Geological Society, v. 145, p. 661-667.

McCarthy, W. & Cloutier, J., (2016), Hyperspectral reflectance and magnetic alteration of the Mace Mo-Cu deposit, Co Galway. Report to MOAG. University of St. Andrews.

Sillitoe, R. H., (2010), Porphyry copper systems: Economic Geology, v. 105, p. 3–41.

Talbot, V. and Max, M.D., (1984), Application of various geophysical exploration techniques to Cu and Mo mineralisation in Galway Granite, Ireland: Trans. Instn. Min. Metall. (Section B).

Talbot, V. and Ryan, P., (1988), High molybdenum land values in Ireland: Possible implications: Science of The Total Environment, vol.76, Issues 2–3, pp. 217-228

Tellus Programme of the Geological Survey of Ireland, accessed 15th March 2017, www.tellus.ie

4.0 CHAPTER 4 GEOCHEMISTRY AND GEOSTATISTICS

4.1 Introduction

This chapter describes statistical analyses carried out on the whole rock geochemistry assays collected as part of SLR's (2016) drilling campaign on the Mace deposit, and Laser Ablation ICP-MS for trace element mapping of representative areas of interest from the polished thin-sections described in Chapter 3.

Most previous geochemical work on the Galway Granite Batholith has mainly focused on other geographic areas (e.g. El-Desouky, Feely & Mohr 1996; Crowley & Feely 1997; Baxter et al. 2005; Feely et al. 2006; and Leake 2006) or on molybdenum age ranges (Feely et al 2010). Prior to the SLR campaign at Mace Head, geochemical studies have not been carried out on the deposit area. The geochemical data produced by SLR (2016) has not been investigated in any detail, so this work represents the first systematic geochemical study of the deposit. Therefore, this geochemical characterisation of the mineralisation at Mace provides novel information for future exploration on the deposit.

Principal Component Analysis was applied to the assay results to identify clusters of trace elements related to mineralising fluids as part of the Mo-Cu porphyry system. Element mapping of the cluster using laser ablation inductively-coupled-plasma mass spectroscopy (LA-ICP-MS) was carried out in order to characterise the mineralising fluids in relation to their trace element composition.

4.2 Geostatistics

7122 whole rock samples were assayed using a commercial assay suite from ALS Global Laboratories in Loughrea, Co. Galway. These data were produced from assays results of drill core obtained during recent drilling campaigns, and are proprietary to MOAG Copper Gold Resources and used with permission. Full details of analytical methods used by ALS Laboratories are provided on their website www.alsglobal.com. These sample assays were statistically analysed in R Studio (RStudio Team 2015) to investigate relationships between elements within the assay group. Principal Component Analysis

(PCA) is a technique to study the linear relationship of variables by converting a set of observations into a smaller set of (linearly uncorrelated) variables (Wagstaff et al. 2001). PCA calculates the principle components of the data as sets of eigenvalues and eigenvectors of the covariance matrix of the data (an eigenvector is a non-zero vector which, when multiplied by a square matrix, yields a constant times the vector). Figure 4-1 shows the initial PCA point cloud in two dimensions, signifying the relationships between major components within each sample.

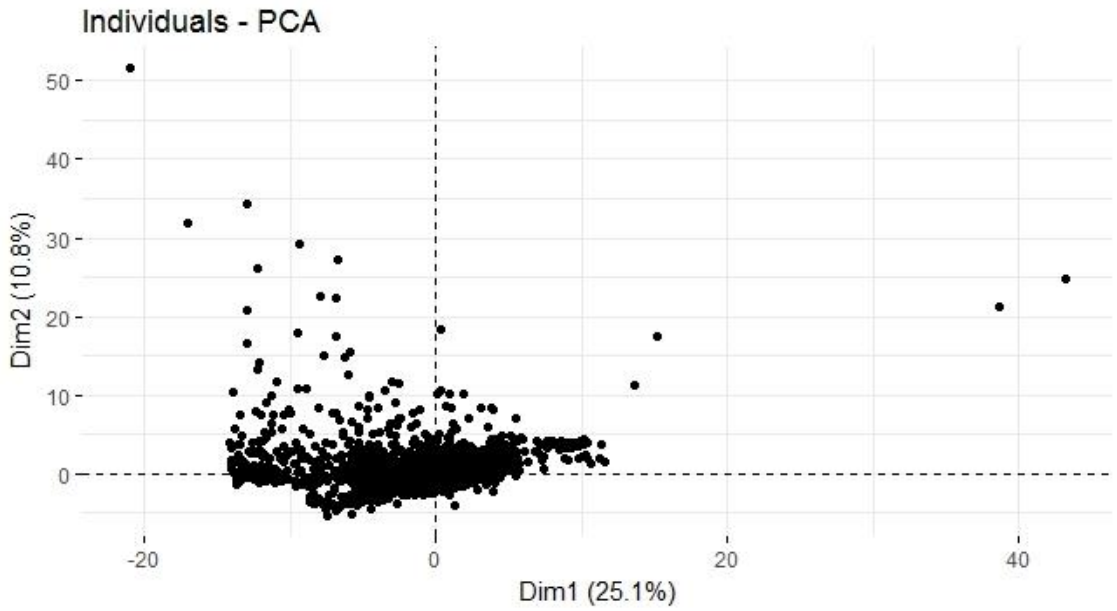

Figure 4-1 Principal Component Analysis for whole rock geochemistry assays of Mace drill core showing general clustering of individual components.

PCA of the whole rock geochemistry assays identified three distinct groups of elements in the assay data (see Table 3). K-means clustering was applied to the PCA results in order to group the samples.

K-means clustering is a method commonly used to automatically partition a data set into k groups. It proceeds by selecting k initial cluster centres and then iteratively refining them. The algorithm converges when there is no further change in assignment of instances to clusters (Wagstaff et. al 2001). The goal of k-means clustering is to obtain a qualitative and quantitative understanding of large amounts of N-dimensional data by providing reasonably good similarity groups (MacQueen 1967).

Initial k-means clustering (Figure 1-2) shows one distinct group, interpreted as representing the mineralising component of the bulk rock assays, with a larger group of elements interpreted to represent elements unrelated to the mineralising component (i.e. predominantly related to magmatic processes which pre-date mineralisation events).

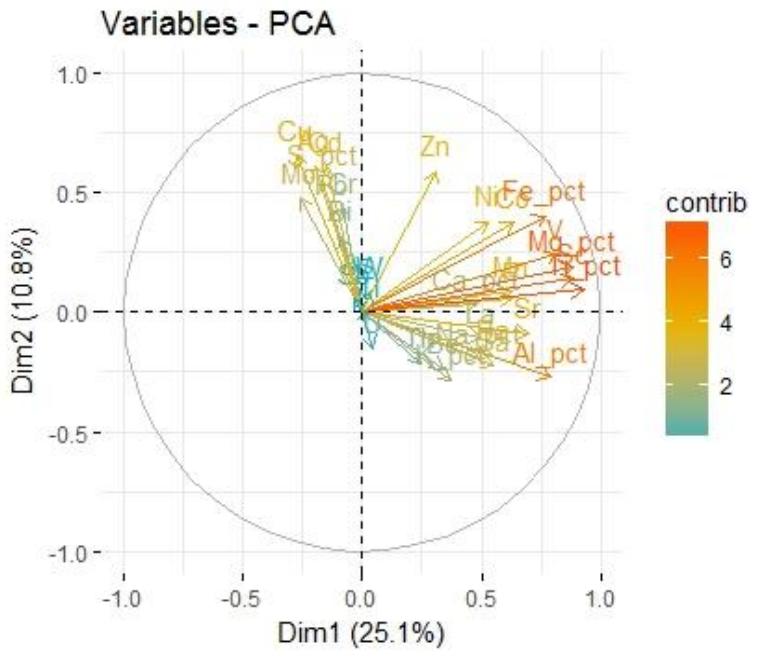

Figure 4-2 Initial Principal Component Analysis loadings plot of commercial assay results from Mace Head drilling; closer vectors indicate positive correlations of labelled elements in assays.

Further analysis of the PCA results was then able to classify the element groups into felsic, mafic, and mineralising components. Figure 4-3 shows related grouping of elements in Cluster 1 which corresponds to mineralising fluids carrying copper, molybdenum, and other trace elements into the host granite. Cluster 2 shows the felsic magmatic component minerals of the granite host rock, while cluster 3 shows evidence of a more mafic host rock component. Figure 4-3 indicates a strong negative correlation between elements related to mineralisation and felsic members of the granite suite, and a slightly more positive correlation with the mafic components of the host rock. There is, however, a relatively strong negative correlation between the elements that comprise the granite host rock and the elements that are related to Mo-Cu

mineralisation at the Mace deposit (see Table 3). The felsic and mafic components of the analysed sample assays show much closer correlation than the mineralising component.

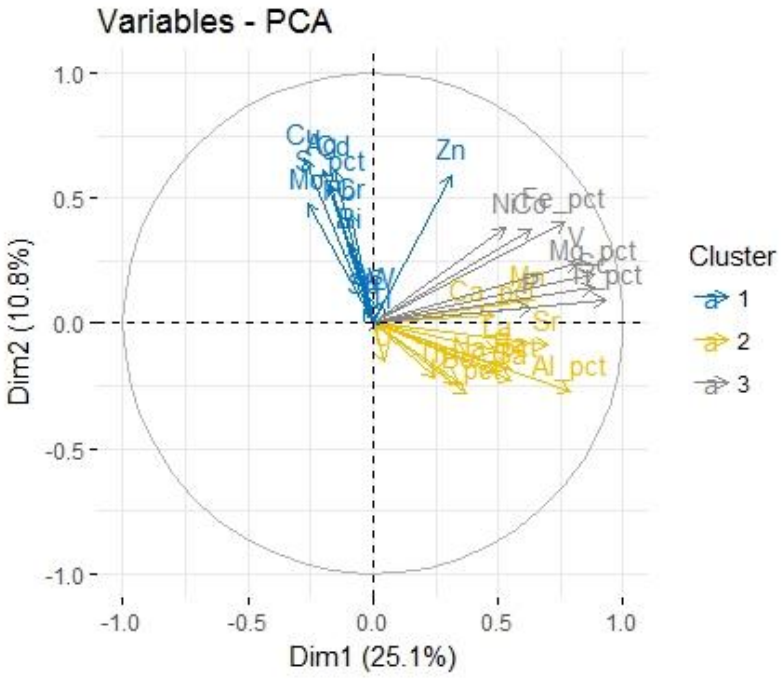

Figure 4-3 K-means clustering results showing 3 major groups of elements through Principal Component Analysis

Table 3 Element groupings through K-means clustering of whole rock assay results from drill core

Cluster 1 Mineralising Component	Cluster 2 Felsic Component	Cluster 3 Mafic Component
Silver, Ag	Iron, Fe	Aluminium, Al
Arsenic, As	Nickel, Ni	Calcium, Ca
Bismuth, Bi	Cobalt, Co	Manganese, Mn
Cadmium, Cd	Magnesium, Mg	Lanthanum, La
Copper, Cu	Phosphorous, P	Strontium, Sr
Molybdenum, Mo	Vanadium, V	Sodium, Na
Lead, Pb	Titanium, Ti	Thorium, Th
Sulphur, S	Scandium, Sc	Beryllium, Be
Antimony, Sb		Barium, Ba
Thallium, Tl		Potassium, K
Tungsten, W		Uranium, U
Zinc, Zn		Gallium, Ga
Chromium, Cr		

4.2.1 Laser ablation ICP-MS

LA-ICP-MS experiments were carried out in April and September 2018 at the Geochemistry Laboratories of Trinity College, Dublin. A Photon Machines Excite 193 nm excimer Ar-F laser system with a Helex 2-volume ablation cell and He-Ar carrier gas (ca. 0.8 l/min He and ca. 0.7 l/min Ar) was used. The mass spectrometer used was a Thermo SCIENTIFIC iCAP Q (model s) Quadrupole inductively-coupled-plasma mass spectrometer. A variable volume device was used for signal smoothing between the laser and the mass spectrometer without significantly compromising spatial resolution (Ubide *et. al* 2015). Three separate standard reference materials were used for calibration before and after analyses (see Table 4).

Table 4 Standard Reference Materials used during laser ablation ICP-MS at Trinity College, Dublin

Standard	Description	Origin	Source
MUL-ZnS-1	Sphalerite Pellet	Synthetic	University of Leoben, Austria (Onuk et al. 2016)
MASS-1	Synthetic Polymetal Sulphide Pellet	Synthetic	U. S. Geological Survey (Wilson et al 2002)
BCR-G2	Basalt Glass	Columbia River Basin, North Western Oregon, USA	U.S. Geological Survey (Wilson 1997)

The samples were analysed for a suite of trace elements in sulphide grains. Chalcopyrite grains appear to have grown in equilibrium with the surrounding fluid and showed little variation in trace element composition across the grain, whereas pyrite grains appear influenced in their growth by multiple stages of fluid influx. Molybdenite did not ablate well under the laser, possibly because of the softness of the mineral. This resulted in poor results for molybdenite element maps.

The MASS-1 standard was used as the primary standard for the sulphide grains ablated. Three lines of each standard were ablated prior to ablation of the target mapping area. The amounts of nebuliser gas, laser power, and ablation intensity were tuned to give optimal results for the selected standards.

Table 5 summarises the instrument set-up conditions.

Table 5 Running conditions for laser ablation ICP-MS at Trinity College, Dublin

Parameter	Description
ICP Instrument Model	Thermo-Scientific iCAP-Qs (quadrupole)
Plasma RF Power (W)	1475
Plasma gas flow (L/min)	2.0
Monitored Masses	^{34}S, ^{39}K, ^{57}Fe, ^{59}Co, ^{60}Ni, ^{65}Cu, ^{75}As, ^{77}Se, ^{95}Mo, ^{107}Ag, ^{111}Cd, ^{121}Sb, ^{182}W, ^{197}Au, ^{203}Tl, ^{208}Pb, ^{209}Bi
LA Instrument Model	Photon Machines Analyte 193
Laser	ATLEX-SI 193nm ArF excimer
Fluence (J/cm²)	0.5
Reception rate (Hz)	40
Delay between analyses (s)	15
Slit length (ųm)	20
Slit width (ųm)	20
Scan speed (ųm/s)	40

4.2.2 Data processing

The raw data generated from laser ablation ICP-MS were processed using Igor Pro software and the Iolite plug-in (Paton et al. 2011). Data processing included several steps; 1) baseline corrections; 2) defining integrations for sulphide laser maps; 3) defining integrations by type; 4) defining integrations by beam intensity; 5) specifying and modifying the relevant Data Reduction Scheme in order to process the data.

The Trace Elements Image data reduction scheme (Woodhead et al. 2007) was used in Igor Pro to minimise discordance in each sample and standard. It was used to produce qualitative element maps and CellSpace Images of trace element concentrations in the mapped area of each individual sample.

Processed element maps were inspected for patterns in relation to variations in elemental concentration, or variation in element ratios in sulphide grains. This produced a clear visual pattern for the occurrence of certain elements in the analysed grains. Subsequently, profile lines were selected at three uniform intervals across grains of interest and the resultant data were exported to Microsoft Excel, and variations along these lines of section were plotted. This produced quantitative plots for each sample grain and allowed for ratio maps of certain elements to be visualised.

LA-ICP-MS analysis was performed in sulphide grains from thin-sections of core taken from areas that had strong concentrations of the two main alteration types seen in the Mace deposit, propylitic and potassic alteration. The monitored masses for this work were chosen as a result of statistical analysis detailed in Section 4.2 above, where elements related to porphyry mineralisation were identified. These elements were selected to attempt to compare and contrast known alteration textures with mineralising elements.

4.2.3 Element ratios

Element maps of thin sections 39208(2) and 39211 were selected for closer analysis of element ratios. 39208(2) shows potassic alteration whereas 39211 consists of a strongly propylitically altered granite breccia.

Figure 4-5 to Figure 4-22 below illustrate the results of the graphing of profile lines across the top, middle, and bottom of laser-mapped pyrite grains. For clarity, the mapped image shows Fe abundance in the grain, which gives the clearest view of the entire grain and its context in the groundmass. The lower graphs are ratio plots of cobalt-nickel or copper-molybdenum, while the upper graphs show individual comparisons between cobalt and nickel or copper and molybdenum. Cobalt-nickel ratios were chosen as a clear zonation pattern was evident in the initial element maps created from laser mapping data. Copper-molybdenum ratios were chosen to test the evidence from SLR's (2016) voxel model (Figure 4-4) showing an increase in the Cu-Mo ratio towards the south east and the postulated source of mineralisation.

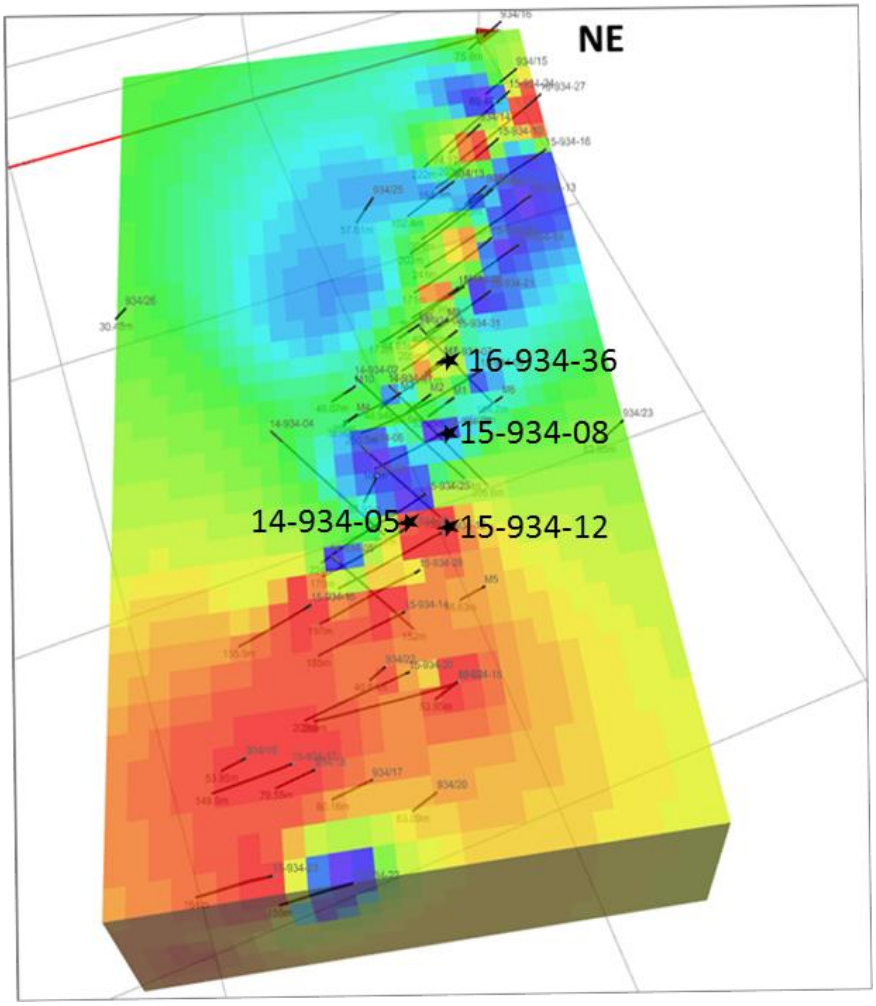

Figure 4-4 Thin-sections were created from core selected from four drill holes, shown here in relation to SLR's (2016) Cu:Mo voxel model.

SLR's work has shown that the ratio of molybdenum to copper in whole rock assays is observed to decrease away from mineralised veins, with copper disseminated more evenly through the deposit than molybdenum. The element maps shown for reference in the below figures use iron as the element that provides greatest definition between the sulphide grain and groundmass. Clear spikes are common in both single-element and ratio graphs corresponding to grain boundaries.

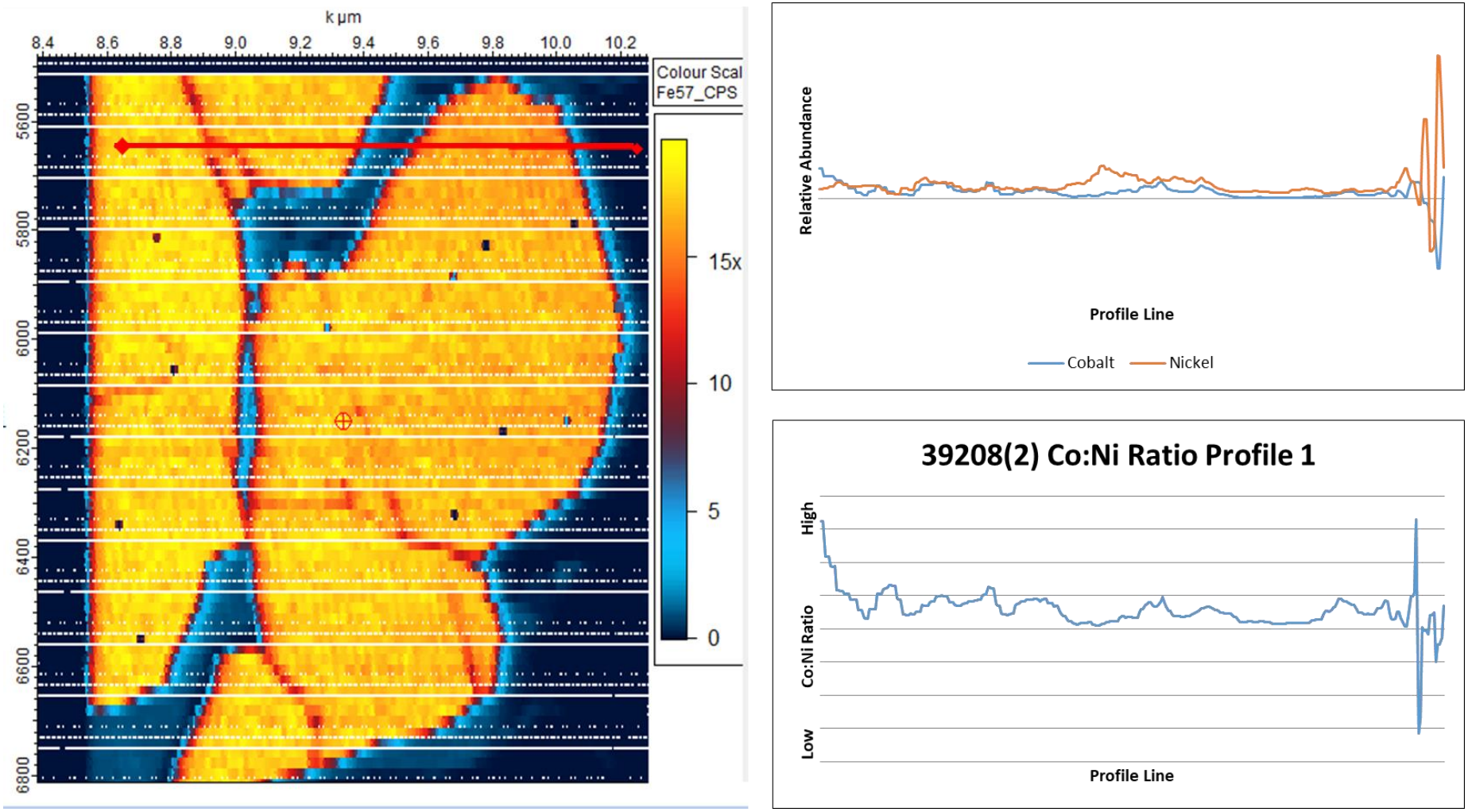

Figure 4-5 Element graphs for cobalt and nickel in sample 39208(2) Profile 1. The red line on the element map (left) indicates the profile line from which the values were exported. The upper graph shows single-element values for cobalt and nickel. The lower graph shows the Co:Ni ratio across the profile line.

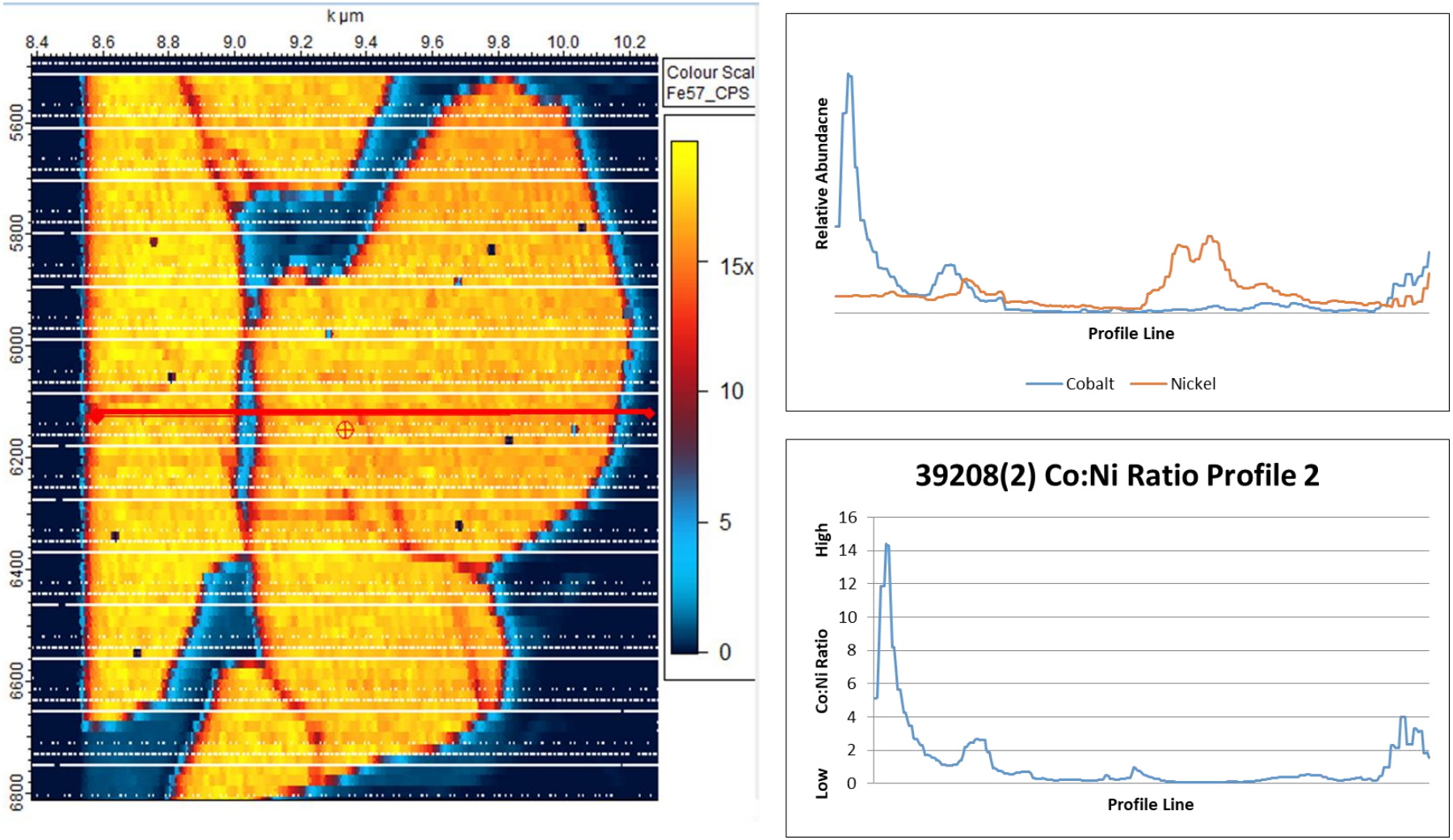

Figure 4-6 Element graphs for cobalt and nickel in sample 39208(2) Profile 2. The red line on the element map (left) indicates the profile line from which the values were exported. The upper graph shows single-element values for cobalt and nickel. The lower graph shows the Co:Ni ratio across the profile line.

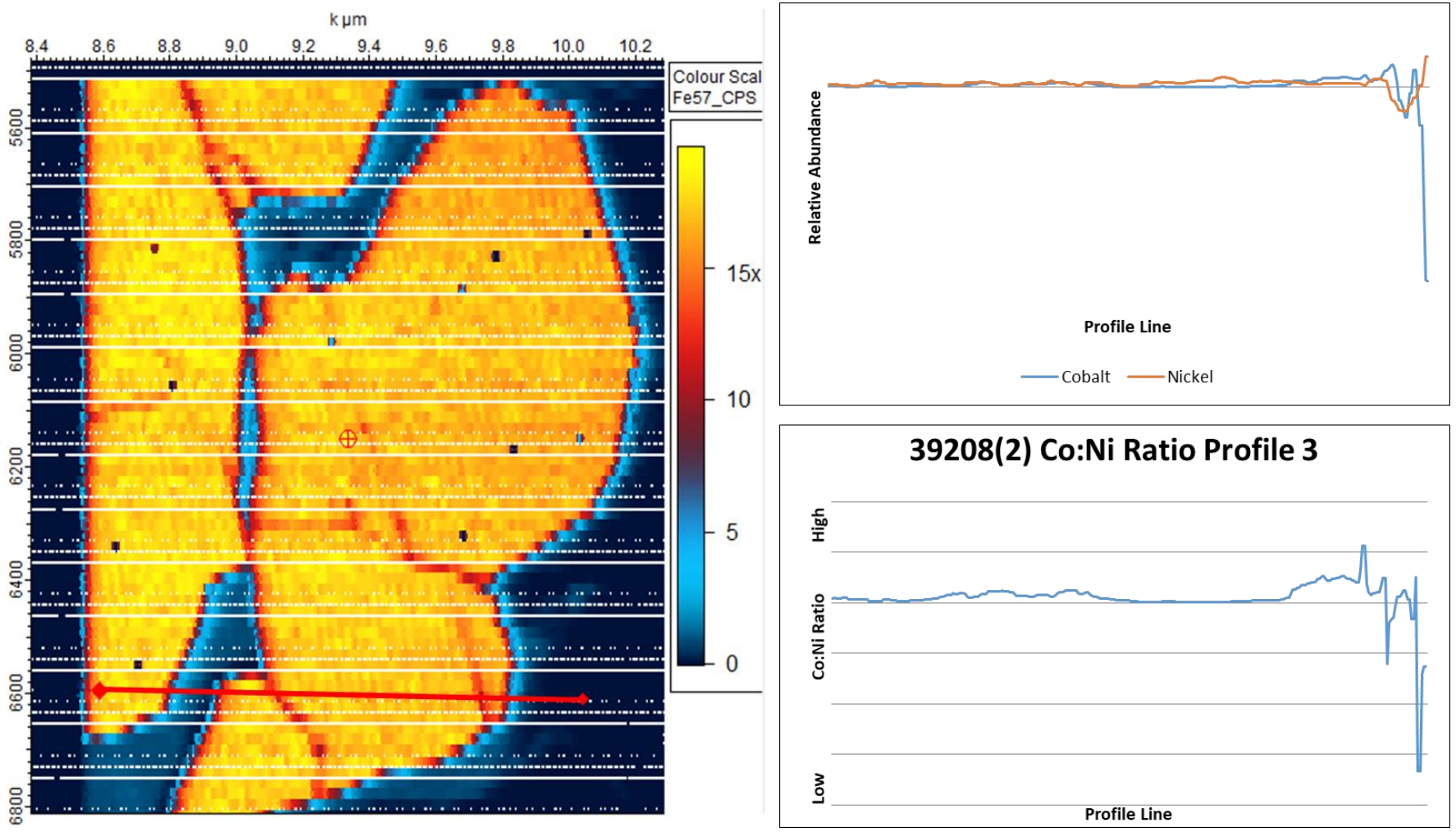

Figure 4-7 Element graphs for cobalt and nickel in sample 39208(2) Profile 3. The red line on the element map (left) indicates the profile line from which the values were exported. The upper graph shows single-element values for cobalt and nickel. The lower graph shows the Co:Ni ratio across the profile line.

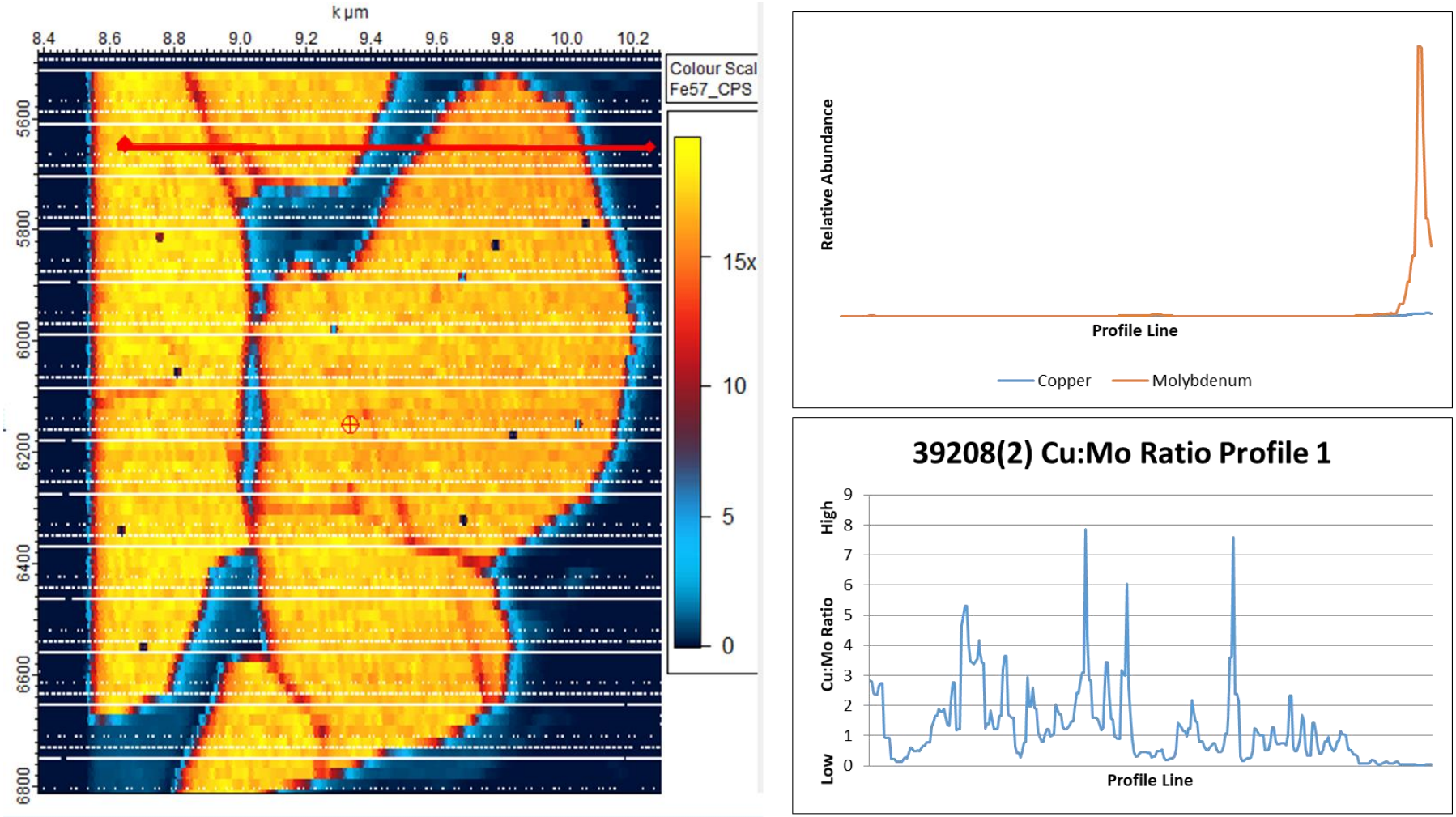

Figure 4-8 Element graphs for copper and molybdenum in sample 39208(2) Profile 1. The red line on the element map (left) indicates the profile line from which the values were exported. The upper graph shows single-element values for copper and molybdenum. The lower graph shows the Cu:Mo ratio across the profile line.

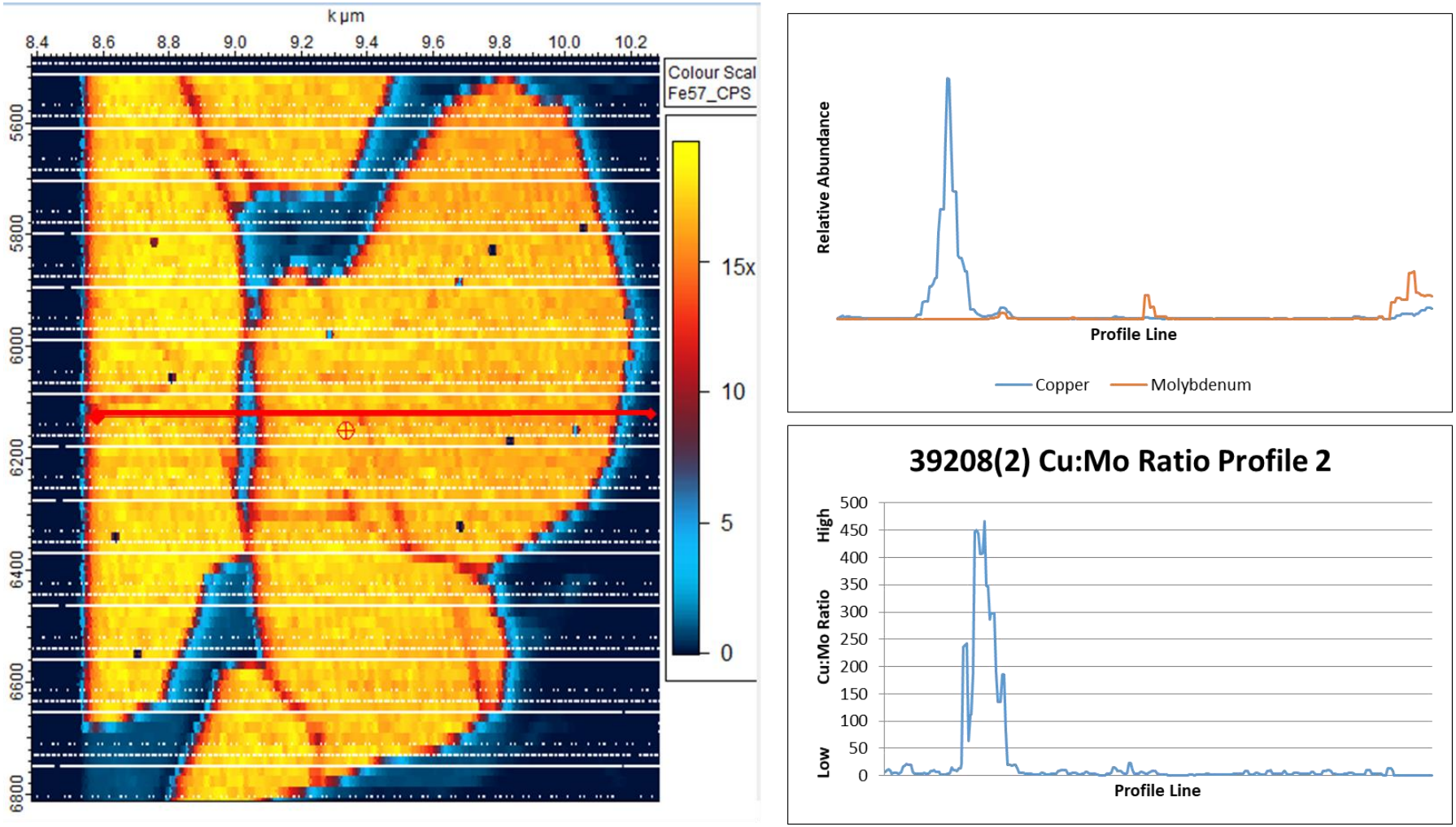

Figure 4-9 Element graphs for copper and molybdenum in sample 39208(2) Profile 2. The red line on the element map (left) indicates the profile line from which the values were exported. The upper graph shows single-element values for copper and molybdenum. The lower graph shows the Cu:Mo ratio across the profile line.

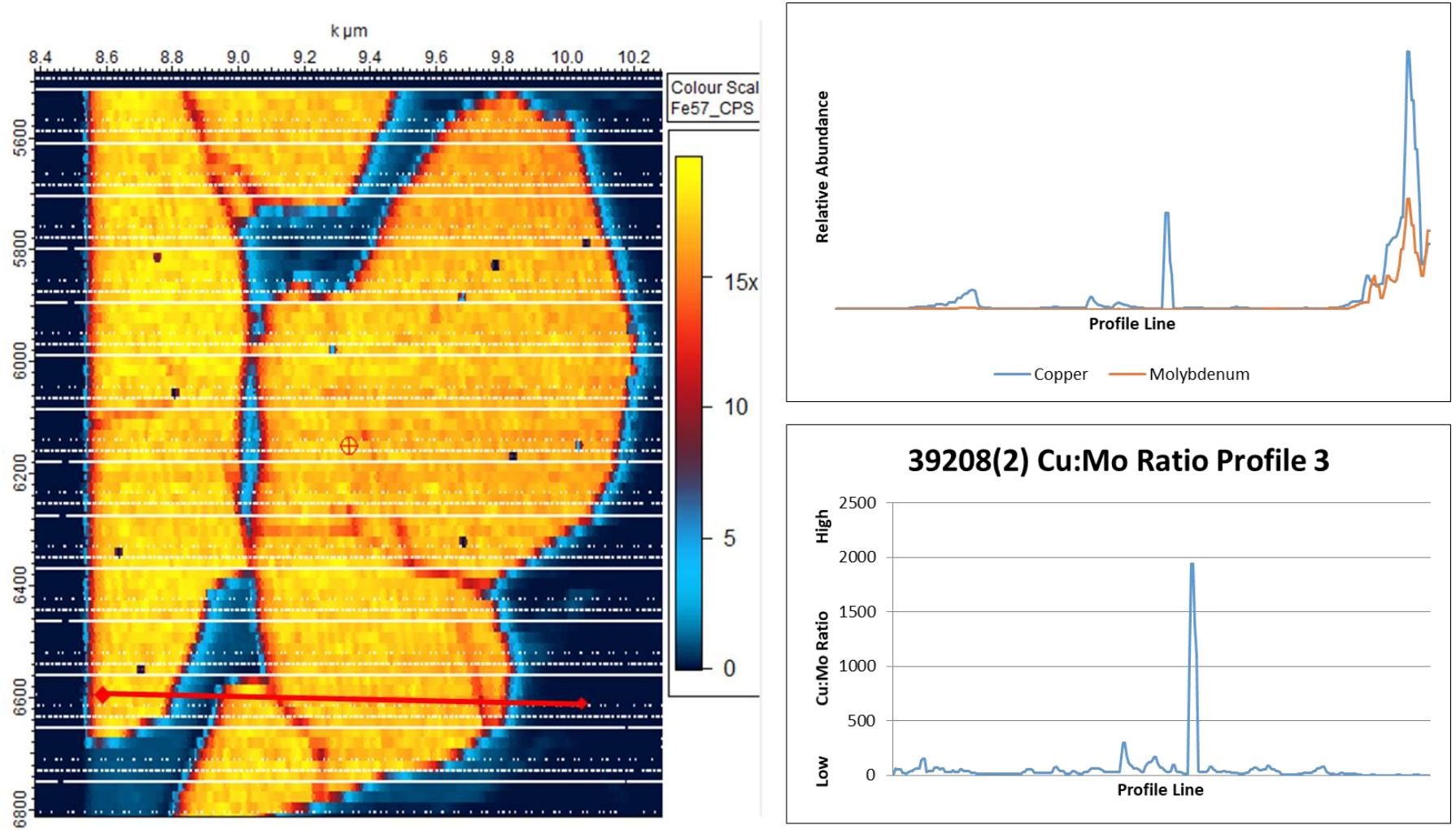

Figure 4-10 Element graphs for copper and molybdenum in sample 39208(2) Profile 3. The red line on the element map (left) indicates the profile line from which the values were exported. The upper graph shows single-element values for copper and molybdenum. The lower graph shows the Cu:Mo ratio across the profile line.

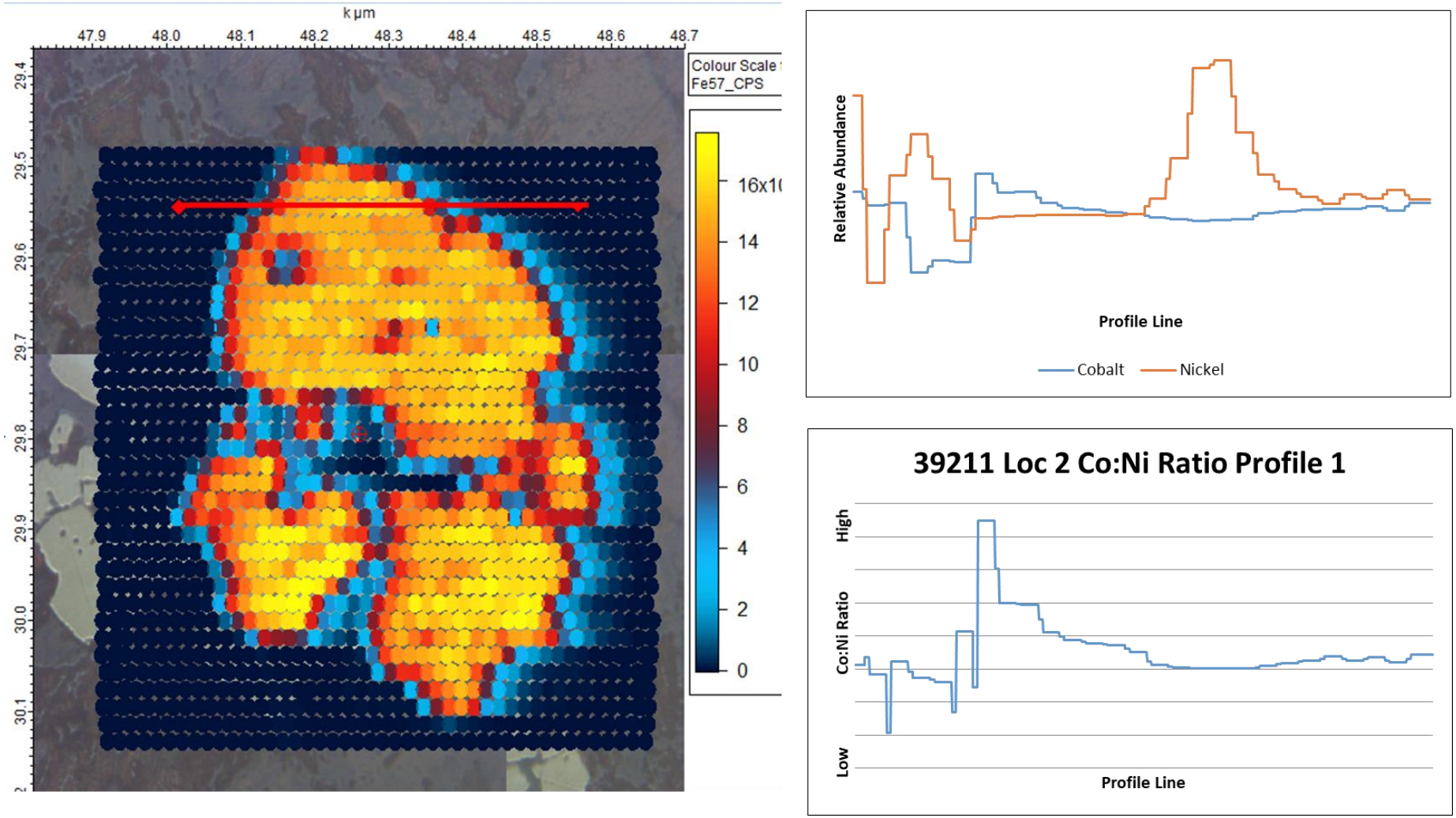

Figure 4-11 Element graphs for cobalt and nickel in sample 39211 Location 2 Profile 1. The red line on the element map (left) indicates the profile line from which the values were exported. The upper graph shows single-element values for cobalt and nickel. The lower graph shows the Co:Ni ratio across the profile line.

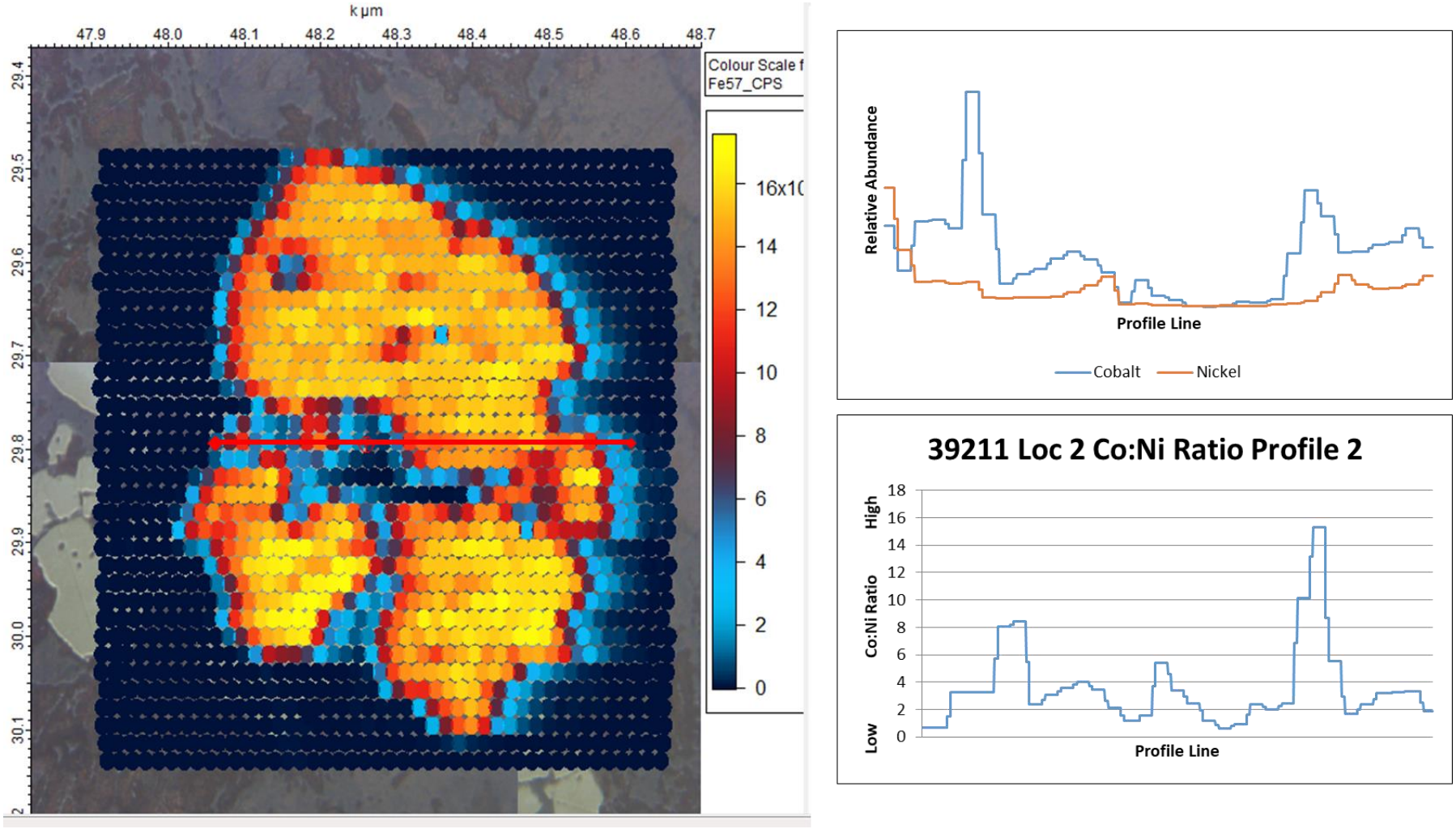

Figure 4-12 Element graphs for cobalt and nickel in sample 39211 Profile 2. The red line on the element map (left) indicates the profile line from which the values were exported. The upper graph shows single-element values for cobalt and nickel. The lower graph shows the Co:Ni ratio across the profile line.

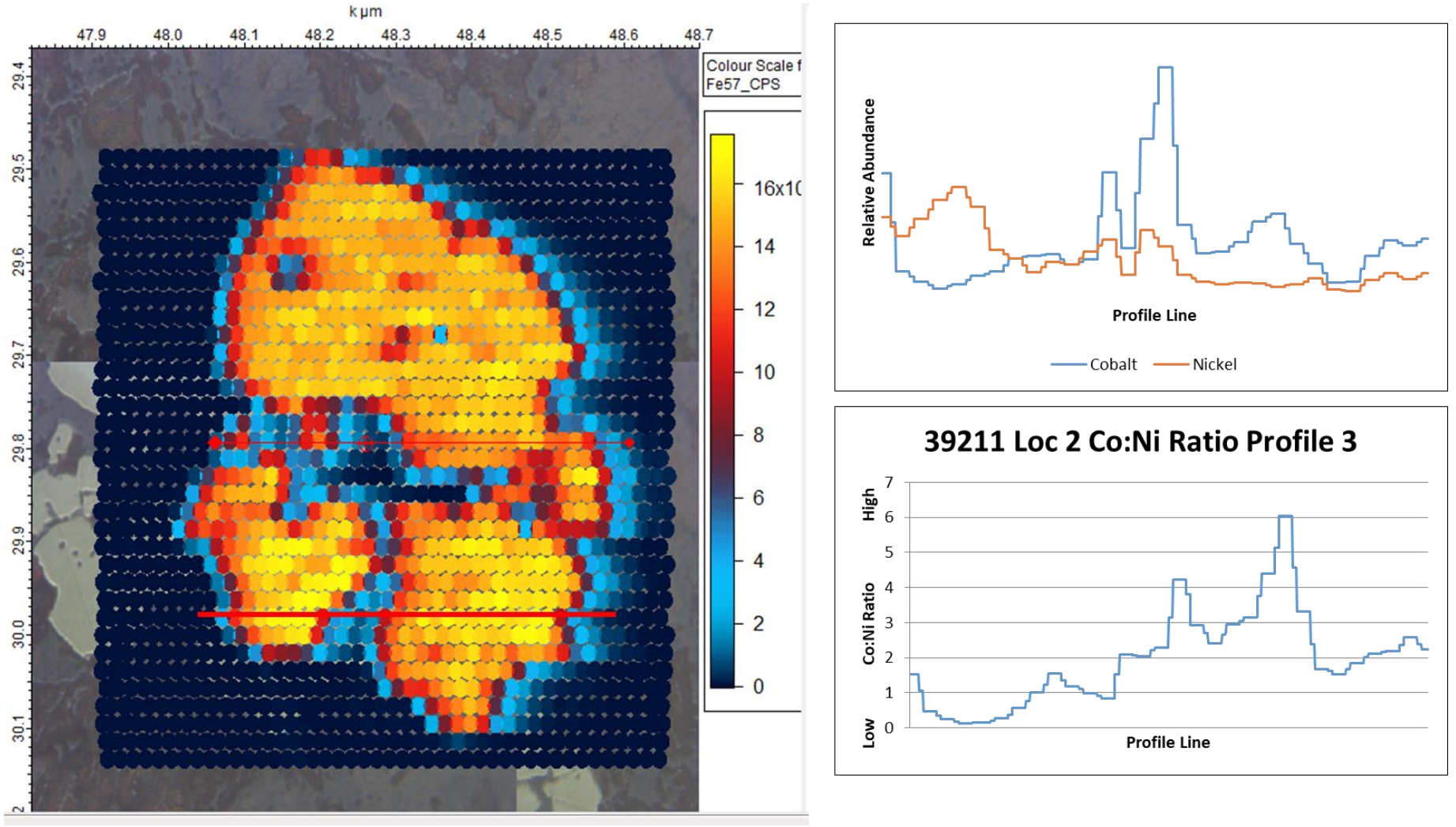

Figure 4-13 Element graphs for cobalt and nickel in sample 39211 Profile 3. The red line on the element map (left) indicates the profile line from which the values were exported. The upper graph shows single-element values for cobalt and nickel. The lower graph shows the Co:Ni ratio across the profile line.

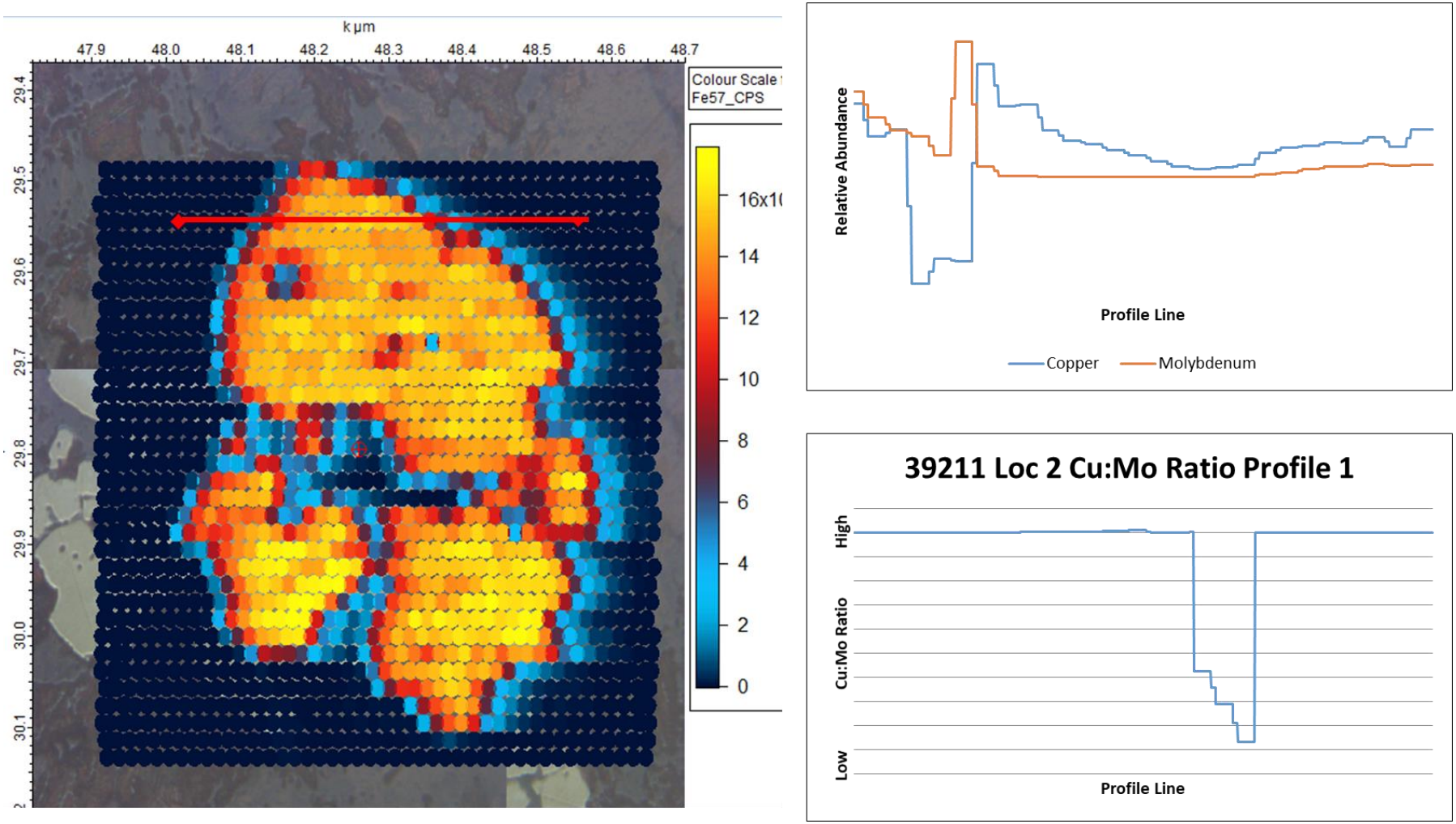

Figure 4-14 Element graphs for copper and molybdenum in sample 39211 Location 2 Profile 1. The red line on the element map (left) indicates the profile line from which the values were exported. The upper graph shows single-element values for copper and molybdenum. The lower graph shows the Cu:Mo ratio across the profile line.

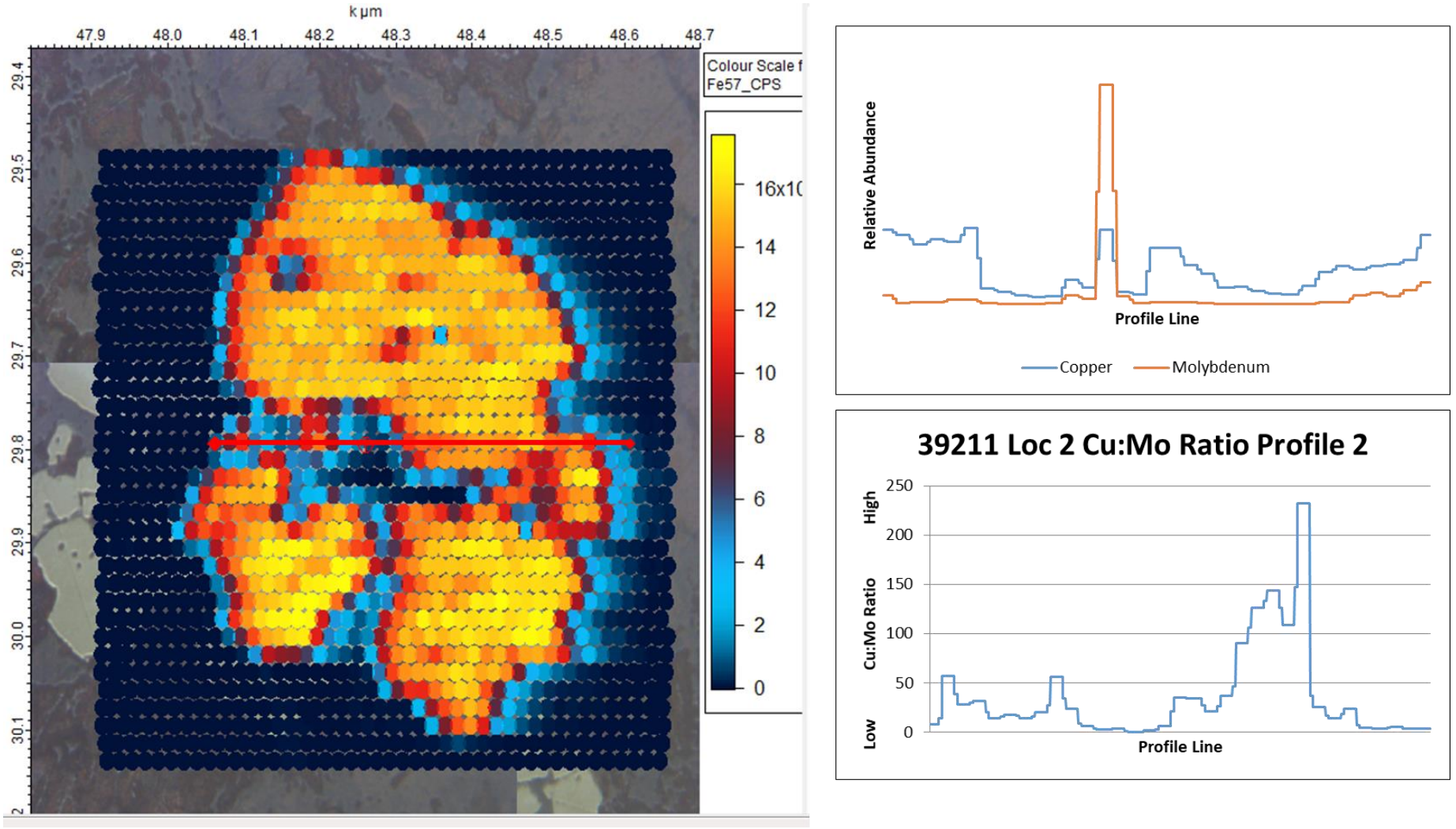

Figure 4-15 Element graphs for copper and molybdenum in sample 39211 Location 2 Profile 2. The red line on the element map (left) indicates the profile line from which the values were exported. The upper graph shows single-element values for copper and molybdenum. The lower graph shows the Cu:Mo ratio across the profile line.

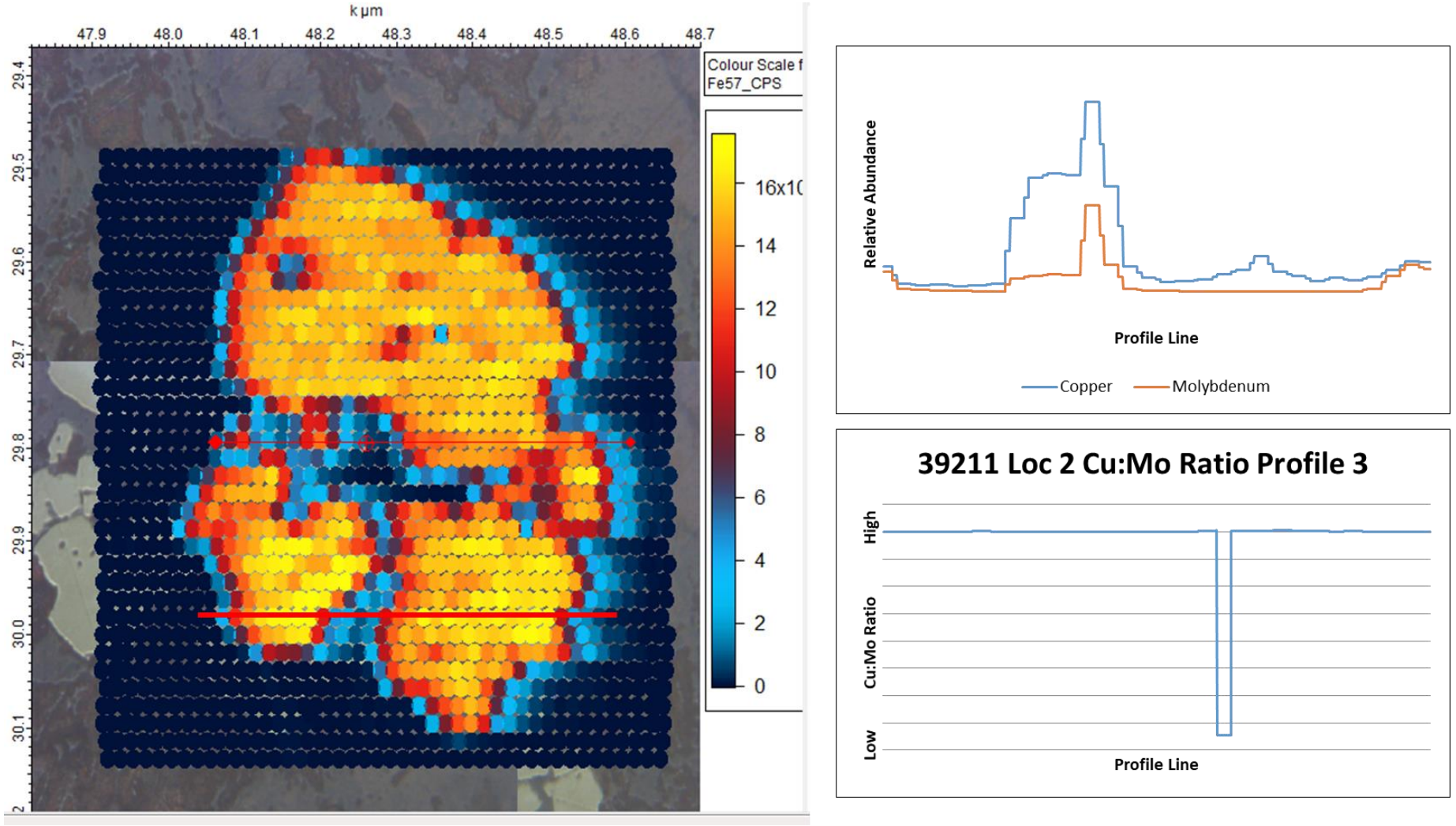

Figure 4-16 Element graphs for copper and molybdenum in sample 39211 Location 2 Profile 3. The red line on the element map (left) indicates the profile line from which the values were exported. The upper graph shows single-element values for copper and molybdenum. The lower graph shows the Cu:Mo ratio across the profile line.

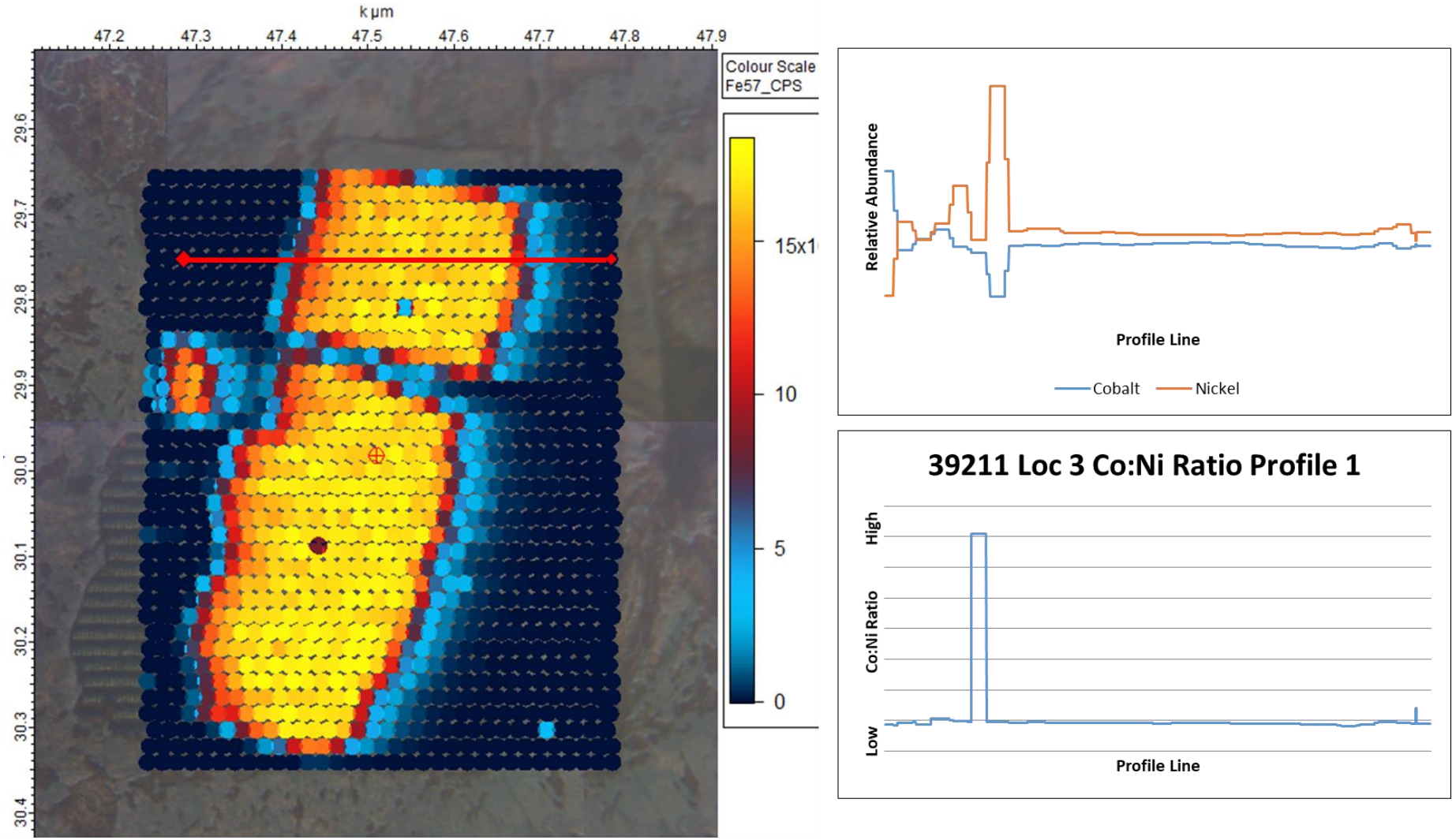

Figure 4-17 Element graphs for cobalt and nickel in sample 39211 Location 3 Profile 1. The red line on the element map (left) indicates the profile line from which the values were exported. The upper graph shows single-element values for cobalt and nickel. The lower graph shows the Co:Ni ratio across the profile line.

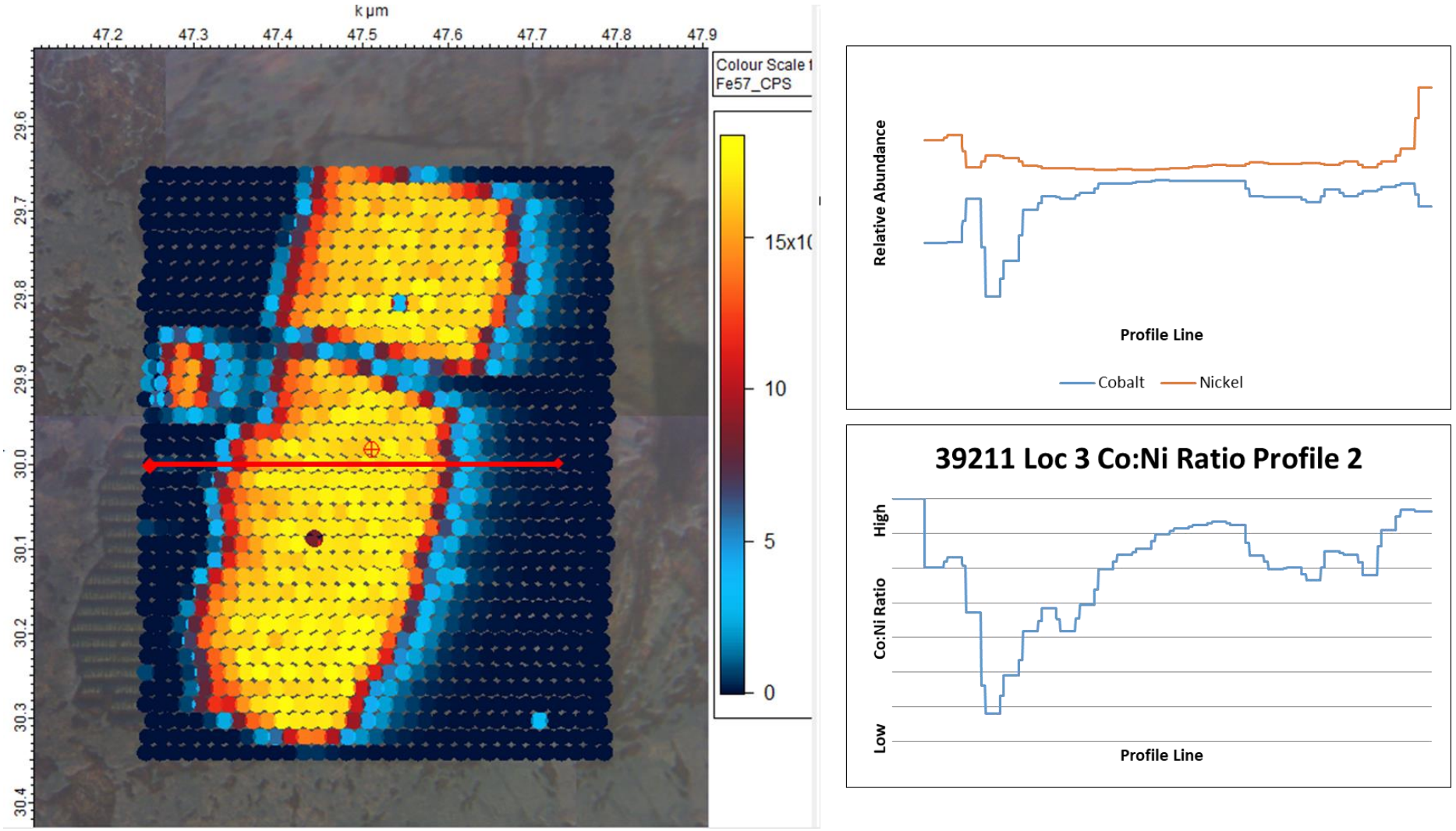

Figure 4-18 Element graphs for cobalt and nickel in sample 39211 Location 3 Profile 2. The red line on the element map (left) indicates the profile line from which the values were exported. The upper graph shows single-element values for cobalt and nickel. The lower graph shows the Co:Ni ratio across the profile line.

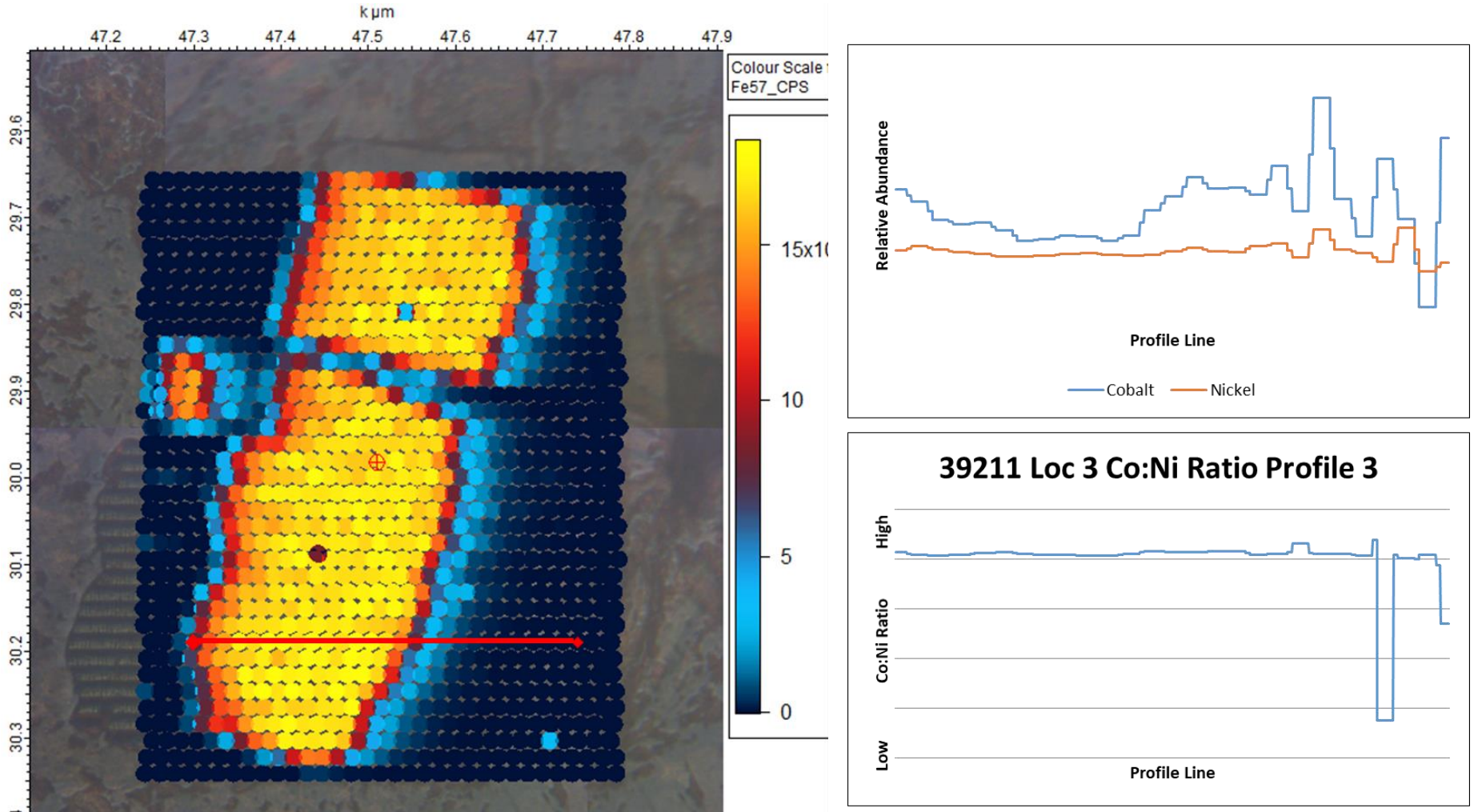

Figure 4-19 Element graphs for cobalt and nickel in sample 39211 Location 3 Profile 3. The red line on the element map (left) indicates the profile line from which the values were exported. The upper graph shows single-element values for cobalt and nickel. The lower graph shows the Co:Ni ratio across the profile line.

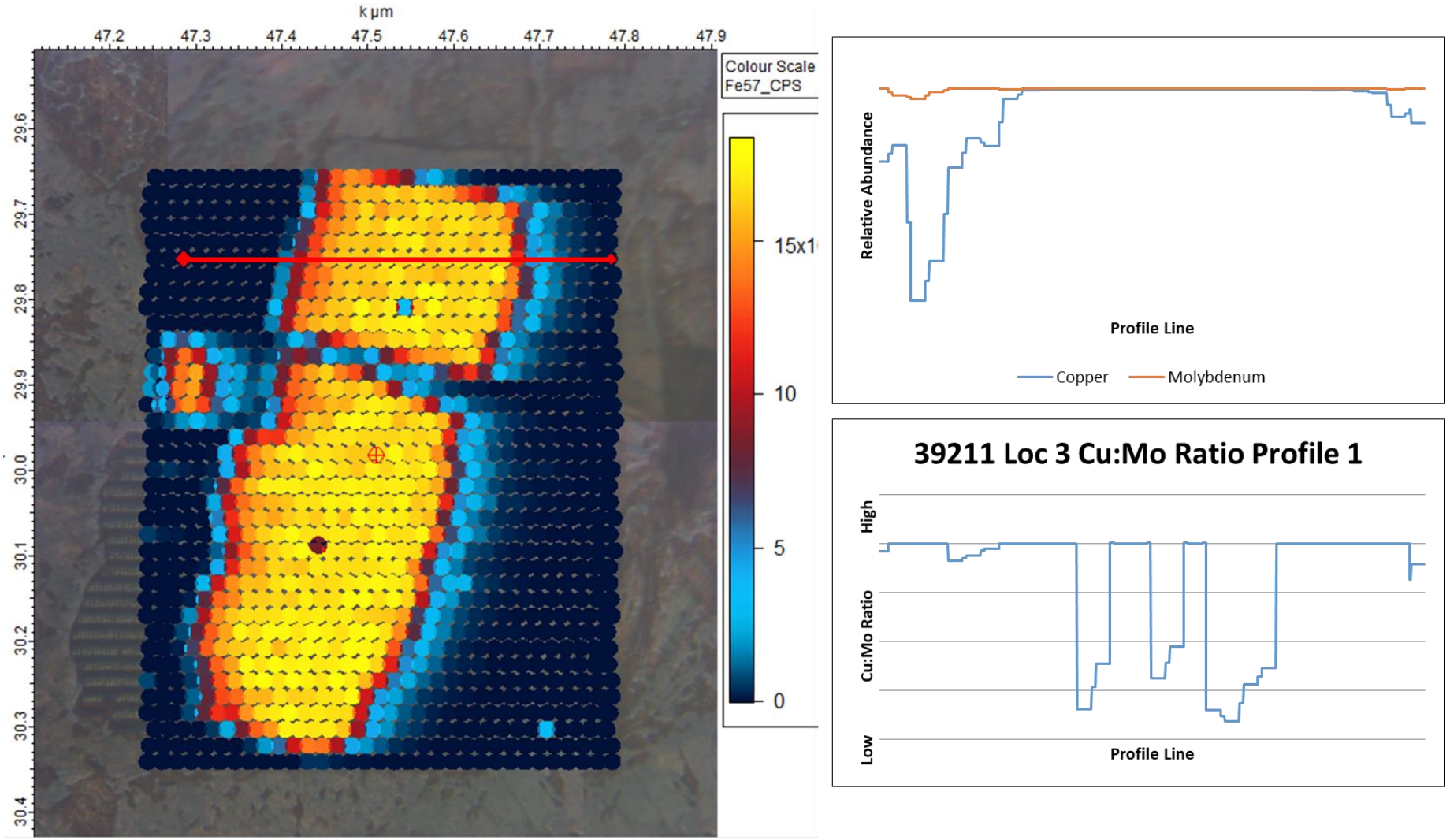

Figure 4-20 Element graphs for copper and molybdenum in sample 39211 Location 3 Profile 1. The red line on the element map (left) indicates the profile line from which the values were exported. The upper graph shows single-element values for copper and molybdenum. The lower graph shows the Cu:Mo ratio across the profile line.

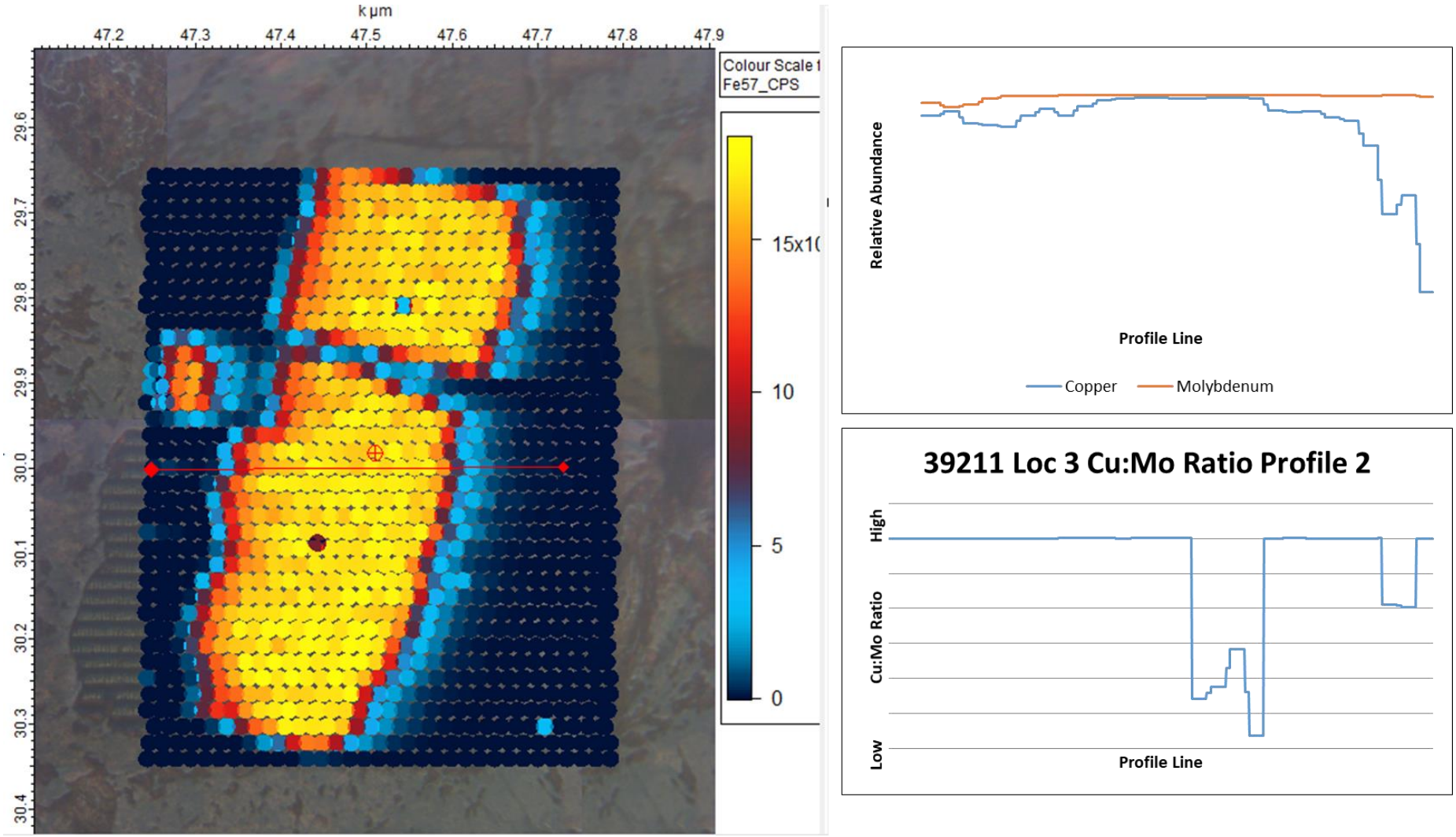

Figure 4-21 Element graphs for copper and molybdenum in sample 39211 Location 3 Profile 2. The red line on the element map (left) indicates the profile line from which the values were exported. The upper graph shows single-element values for copper and molybdenum. The lower graph shows the Cu:Mo ratio across the profile line.

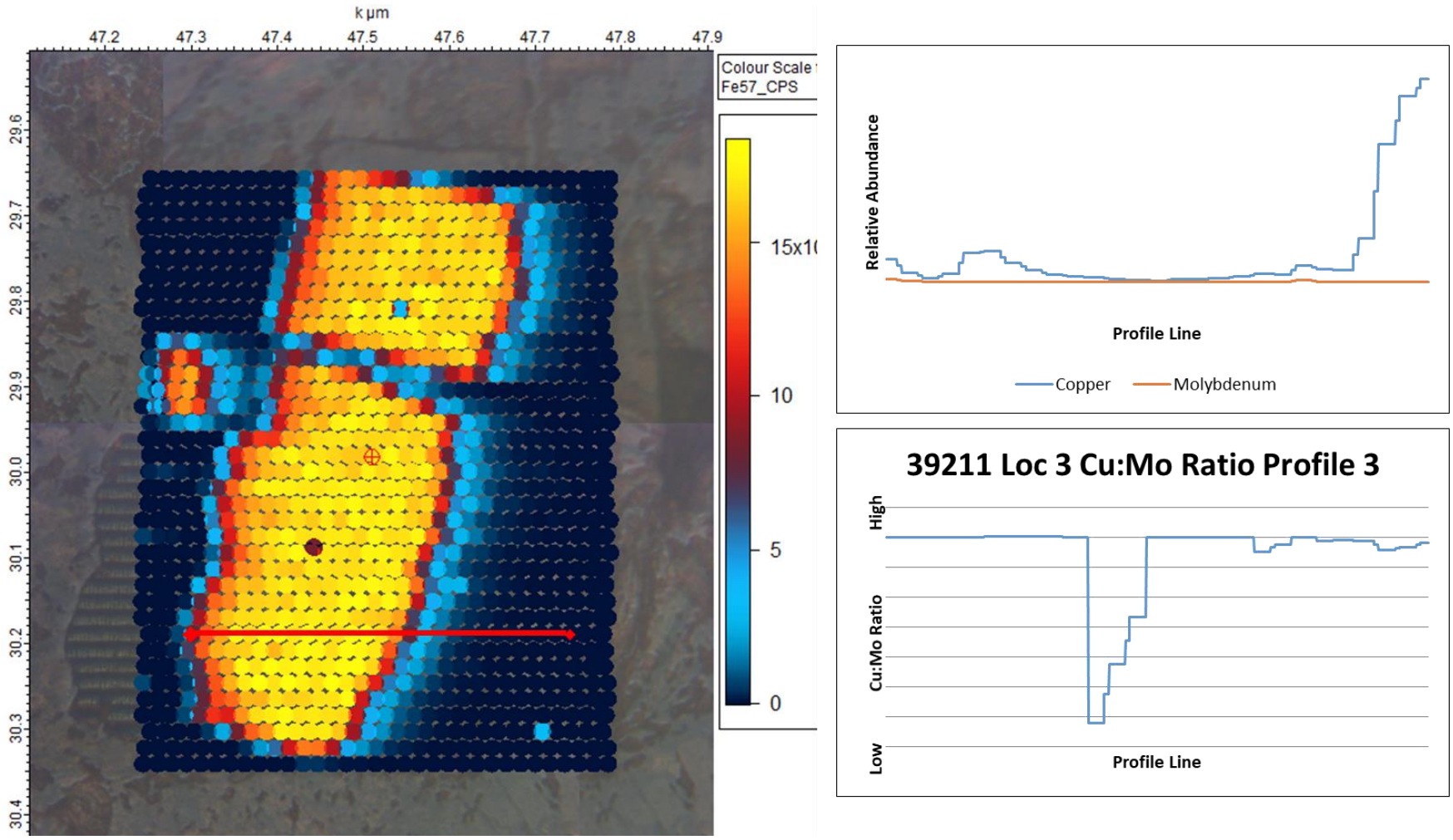

Figure 4-22 Element graphs for copper and molybdenum in sample 39211 Location 3 Profile 3. The red line on the element map (left) indicates the profile line from which the values were exported. The upper graph shows single-element values for copper and molybdenum. The lower graph shows the Cu:Mo ratio across the profile line.

4.2.4 Element zonation

Element maps were created in Iolite to investigate Cu-Mo mineralisation in relation to the alteration types present in the Mace Deposit area.

Sample 39207-Location 1 shows a very clear zoning pattern for cobalt, nickel, and selenium, with the cobalt map in particular having strongly defined growth patterns across the entire grain. The groundmass of 39207 consists of propylitically altered medium-coarse granite with some k-feldspar between epidote grains. Quartz extension veins and some molybdenite stringers are visible in thin section as well as pyrite in quartz veins. Zonation of cobalt, nickel, and selenium is evident in the pyrite grain.

39207-Location 3 shows a euhedral pyrite grain surrounded by secondary anhedral chalcopyrite overgrowth.

Sample 39208 has strong potassic alteration with common dark Mo veins/stringers and large pyrite crystals. Zoning is clearly defined in the mapped pyrite sample here.

Figure 4-23 illustrates examples from select samples of zonation of cobalt, nickel, and selenium in pyrite grains. This zoned pattern is common throughout the samples analysed, and most grains analysed show a strong correlation between cobalt, nickel, and selenium.

A negative correlation between cobalt and nickel/selenium zonation may be inferred from the element maps, with relative enrichment of nickel in pyrite grains accompanied by depletion of cobalt from the rim to the centre of the grain. Cobalt, nickel and selenium appear to have the most variation across grains. Further work may be recommended in order to investigate the causes and potential correlation with alteration and mineralisation in the porphyry system at Mace.

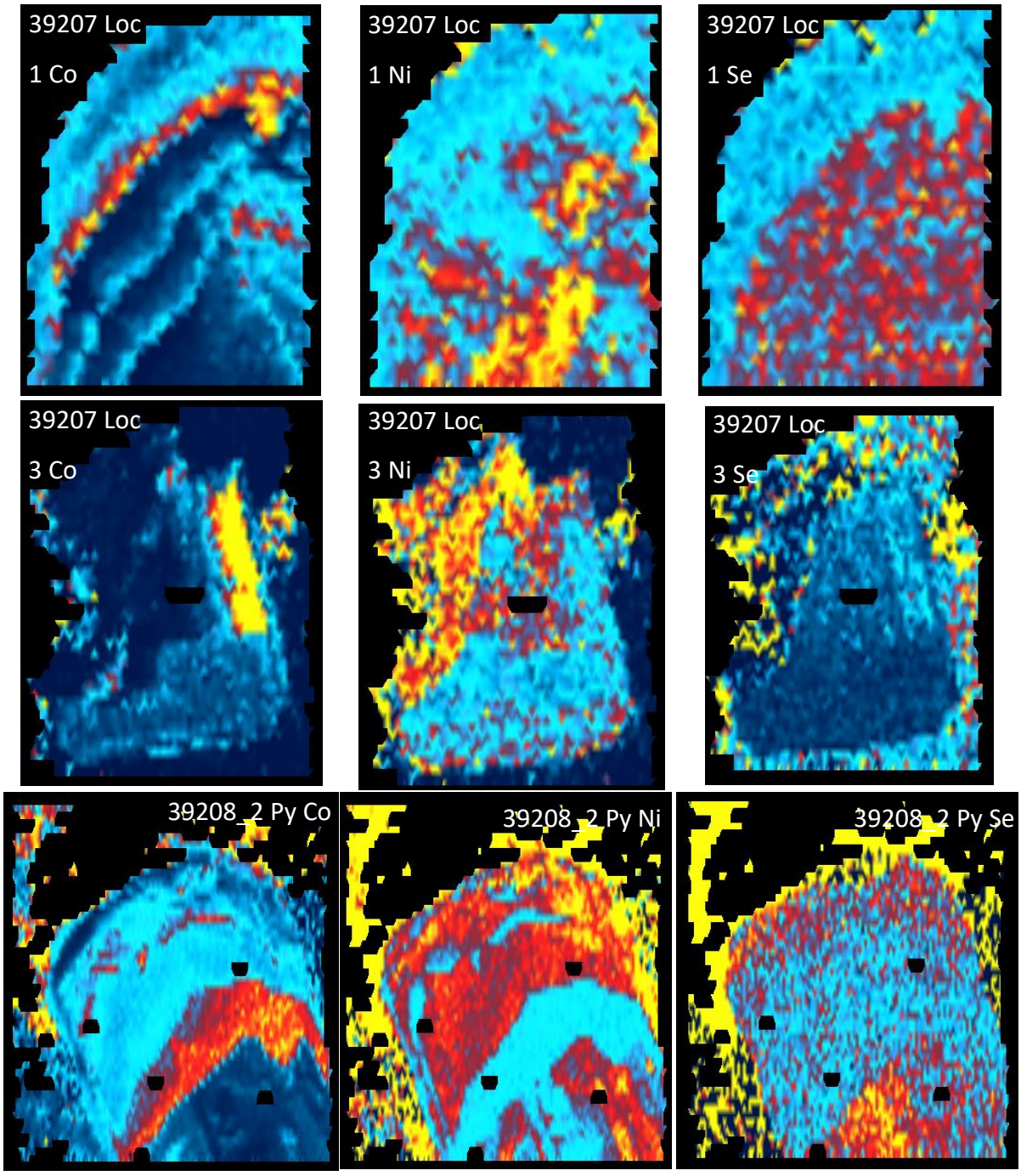

Figure 4-23 Cobalt, nickel and selenium zonation in pyrite grains from sample 39207 Location 1 (top row), 39207 Location 2 (middle row), and 39208(2) (bottom row). Colour scale: yellow and red = high, light and dark blue = low

4.2.5 Fluid phases

Pyrite textures and trace element zonation evident through LA-ICP-MS mapping suggests **a** multiphase process of fluid enrichment in the studied samples**.** Figure 4-24 and Figure 4-25 show the sequence in three stages from initial formation of the pyrite grains, through zoned cobalt-nickel-selenium, and finally a crosscutting overgrowth consisting of elements of the mineralising component identified in Chapter 3 of this thesis. This three-stage pattern is much more clearly developed in areas of increased potassic alteration; while Co-Ni-Se zonation is apparent in areas of propyllitic alteration, mineralising fluid overprinting is much less clearly defined (see Figure 4-26).

Figure 4-27 shows clear evidence of this sequence of 1) sulphide growth 2) Co-Ni-Se zonation 3) mineralising fluid intrusion. Overgrowth of chalcopyrite and molybdenite in this manner is common around pyrite grains and in fractures throughout the study area.

During statistical analysis the mineralising component of the whole rock geochemistry assay results was found to consist of the elements Ag, As, Bi, Cd, Cu, Mo, Pb, S, Sb, Tl, W, and Zn, and all of those elements which were analysed by LA-ICP-MS for this study show similar late-stage crosscutting patterns overprinting pyrite grains.

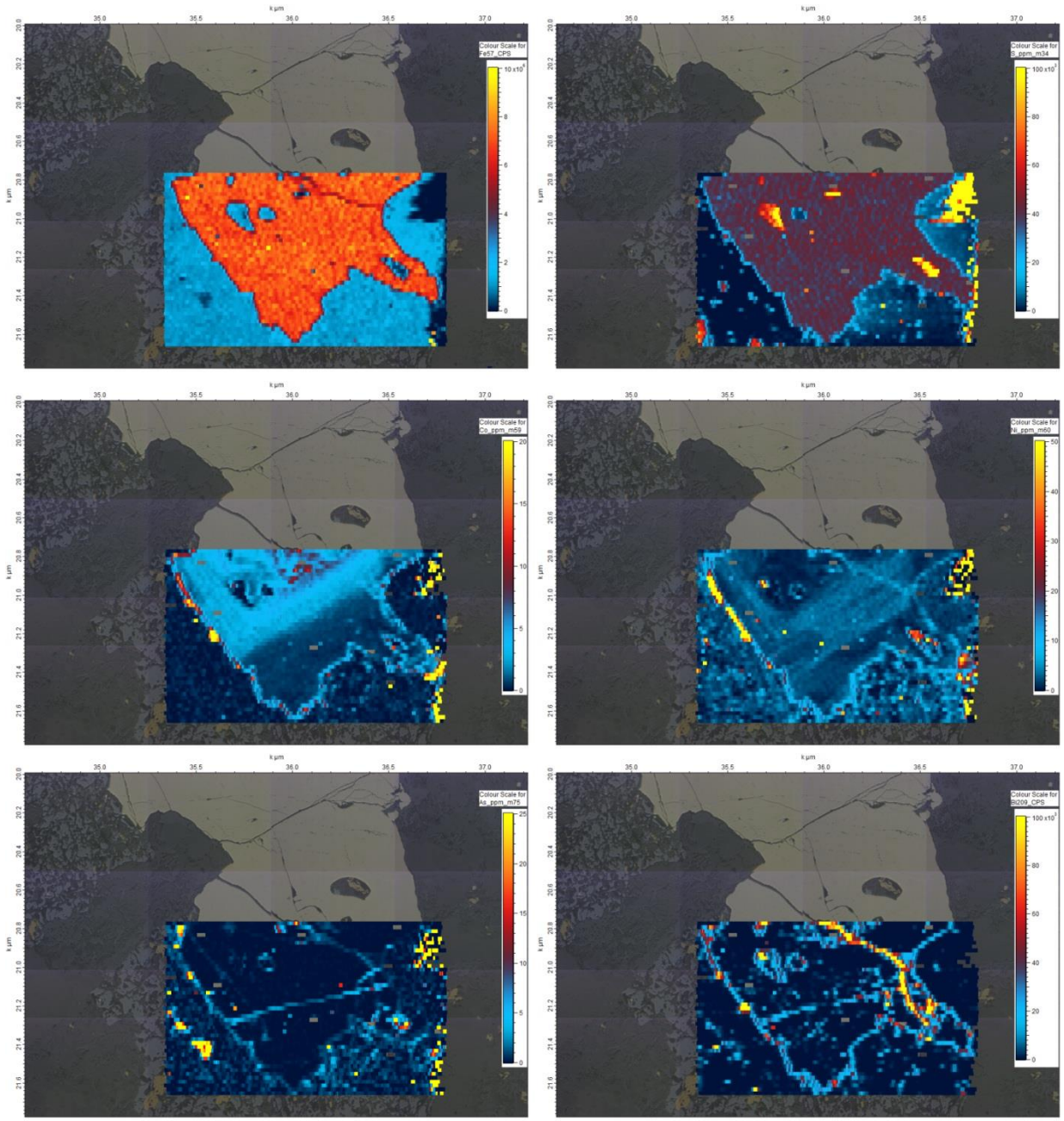

Figure 4-24 Evidence of multiple fluid phases from element maps of potassically altered sample 39209, where the initial sulphide growth (illustrated by Fe and S, top) shows zonation of Co & Ni (middle), with a later overprinting, crosscutting mineralising component (bottom – As & Bi used to illustrate)

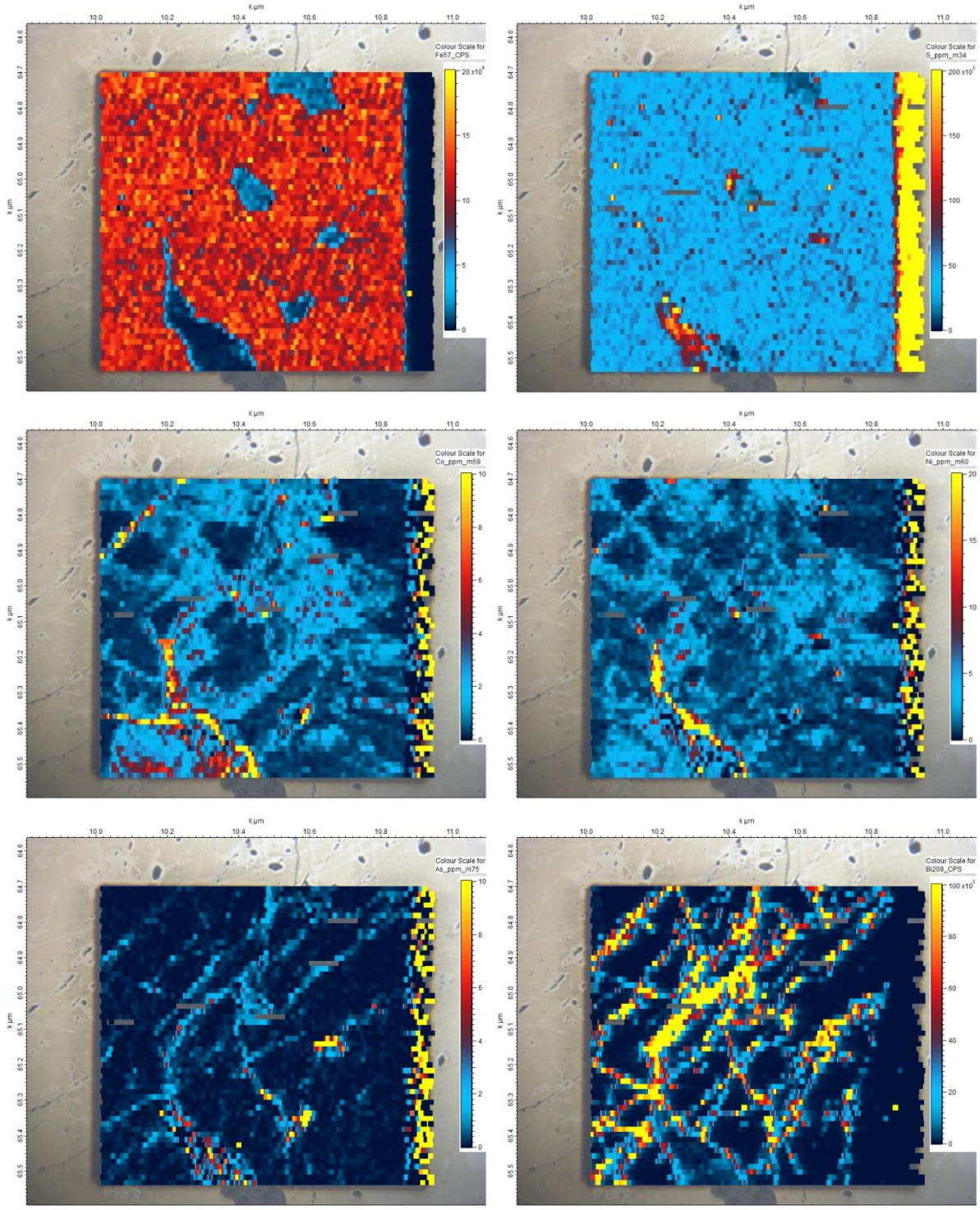

Figure 4-25 Evidence of multiple fluid phases from element maps of potassically altered sample 39219, where the initial sulphide growth (illustrated by Fe and S, top) shows zonation of Co & Ni (middle), with a later overprinting, crosscutting mineralising component as defined in statistical work earlier in this thesis (bottom – As & Bi used to illustrate)

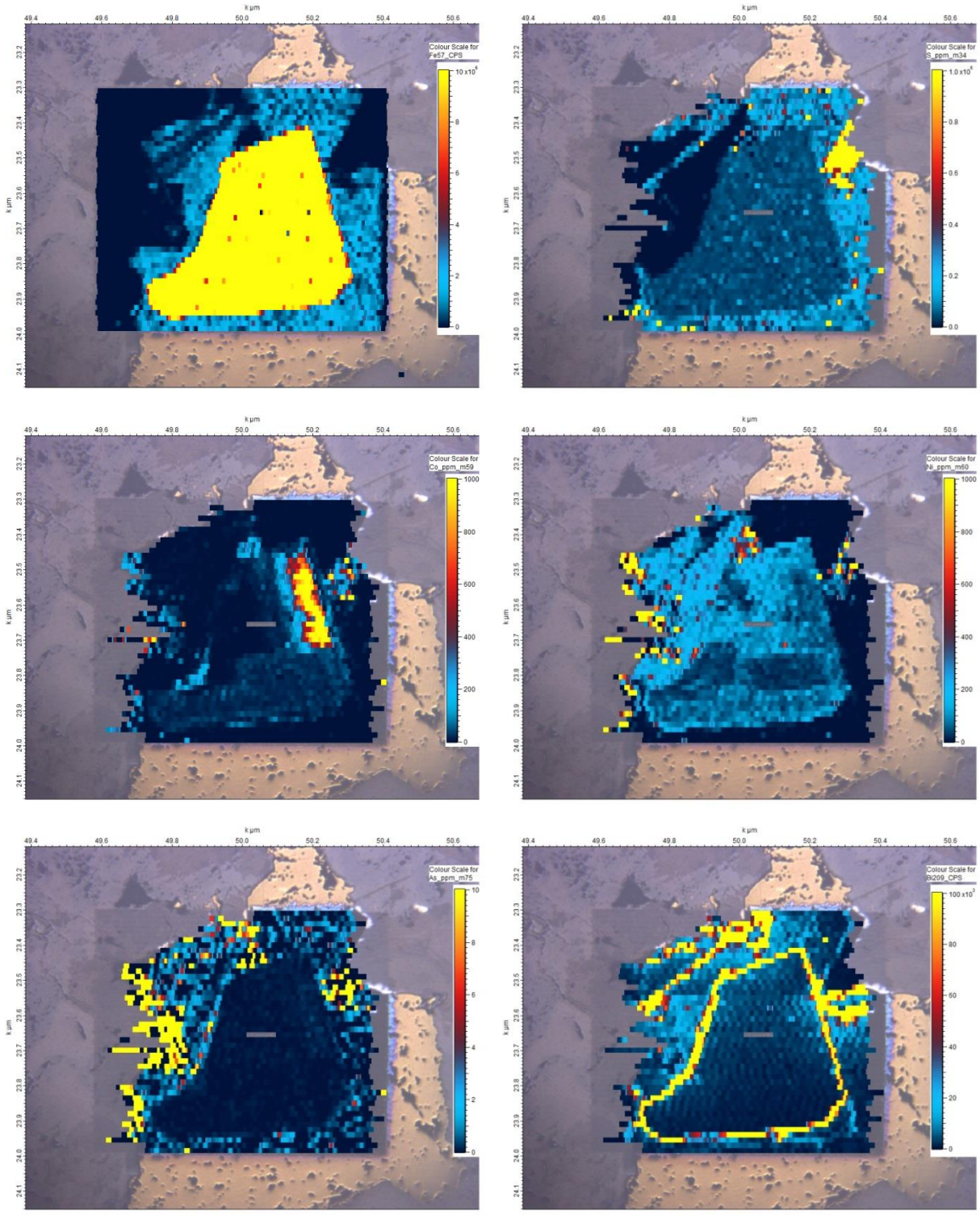

Figure 4-26 Evidence of multiple fluid phases from element maps of propylitically altered sample 39207, where the initial sulphide growth (illustrated by Fe and S, top) shows zonation of Co & Ni (middle), and relative absence of later overprinting by the mineralising component (bottom – As & Bi used to illustrate)

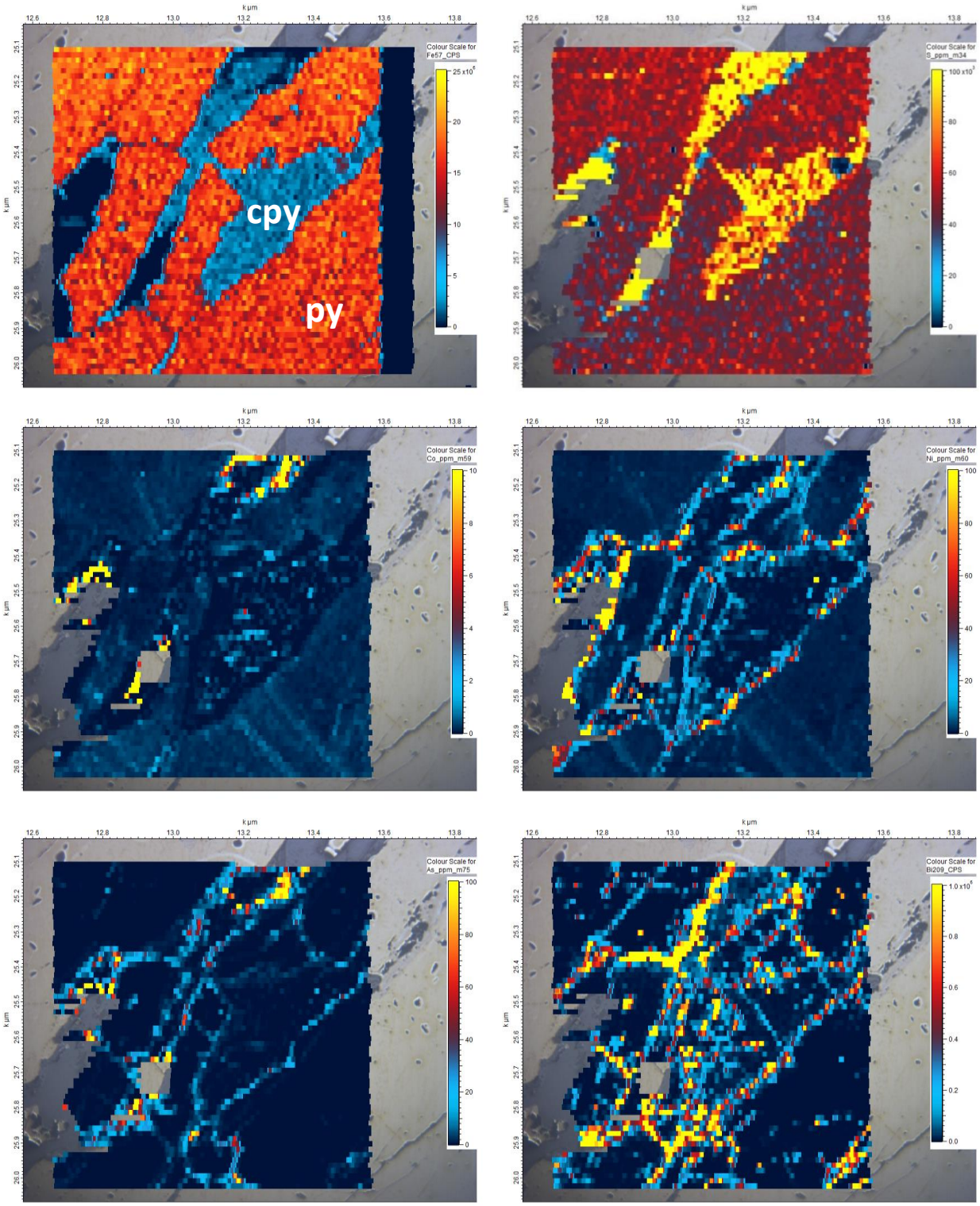

Figure 4-27 Chalcopyrite intergrowth within fractures of a large pyrite grain. Note the zonation pattern of Co and Ni developed prior to overprinting of chalcopyrite, while erratic veining and grain boundaries of the chalcopyrite are similar in pattern and extent to the overprinting of the mineralising component.

4.3 References

Baxter, S., Graham, N. T., Feely, M., Reavy, R. J., & Dewey, J. F., (2005), A microstructural and fabric study of the Galway Granite, Connemara, Western Ireland. Geological Magazine 142, 1–15

Crowley, Q. & Feely, M., (1997), New perspectives on the order and style of granite emplacement in the Galway Batholith, western Ireland. Geological Magazine 134, 539–48

El-Desouky, M., Feely, M. & Mohr, P., (1996), Diorite–granite magma mingling and mixing along the axis of the Galway Granite batholith, Ireland. Journal of the Geological Society, London 153, 361–74

Feely, M., Leake, B. E., Baxter, S., Hunt, J. & Mohr, P., (2006), A geological guide to the Granites of the Galway Batholith, Connemara, western Ireland. Geological Survey of Ireland, 62 pp. ISBN 1-899702-56-3

Feely, M., Selby, D., Hunt, J., & Conliffe, J. (2010) Long-lived granite-related molybdenite mineralisation at Connemara, western Irish Caledonides. Geological Magazine 147, 886-894

Leake, B. E., (2006), Mechanism of emplacement and crystallisation history of the northern margin and centre of the Galway Granite, western Ireland. Transactions of the Royal Society of Edinburgh, Earth Sciences 97, 1–23

Onuk, P., Melcher, F., Mertz-Kraus, R., Gäbler, H-E., Goldmann, S., (2016), Development of a Matrix-Matched Sphalerite Reference Material (MUL-ZnS-1) for Calibration of In Situ Trace Element Measurements by Laser Ablation-Inductively Coupled Plasma-Mass Spectrometry, Geostandards and Geoanalytical Research, 41, 263–272

Paton, C., Hellstrom, J., Paul, B., Woodhead, J., and Hergt, J., (2011), Iolite, a freeware for the visualisation and processing of mass spectrometer data, Journal of Analytical Spectrometry, vol. 26 pp. 2508-2518

RStudio Team, (2015), RStudio: Integrated Development for R. RStudio, Inc., Boston, MA URL http://www.rstudio.com/

Ubide, T., McKenna, C. A., Chew, D. M., Kamber, B. S., (2015), High-resolution LA-ICP-MS trace element mapping of igneous minerals: In search of magma histories, Chemical Geology, 409 pp. 157-168

Wagstaff, K., Cardie, C., Rogers, S., Schroedl, S., (2001), Constrained K-means Clustering with Background Knowledge, Proceedings of the Eighteenth International Conference on Machine Learning, p. 577–584

Wilson, S.A., *(1997),* The collection, preparation, and testing of USGS reference material BCR-2, Columbia River, Basalt: U.S. Geological Survey Open-File Report 98-xxx

Wilson S.A., Koenig A.E., Ridley W.I., (2002), Development of sulphide calibration standards for the laser ablation inductively-coupled plasma mass spectrometry, Journal of Analytical Atomic Spectrometry, 17, 406-409

Woodhead, J., Hellstrom, J., Hergt, J., Greig, A. and Maas, R., (2007), Isotopic and elemental imaging of geological materials by laser ablation Inductively Coupled Plasma mass spectrometry. Journal of Geostandards and Geoanalytical Research, 31(4), p. 33.

5.0 CHAPTER 5 DISCUSSION AND CONCLUSIONS

5.1 Introduction

Presented earlier in this study are petrographic, statistical and laboratory analyses of mineralisation and alteration textures at the Mace Mo-Cu deposit. Mineralisation at Mace Head is generally considered to form part of the uppermost portion of a porphyry type molybdenite-copper system, with Bergey (2008) drawing similarities to the Highmont deposit in the Highland Valley of British Columbia, and SLR's (2016) reporting suggesting that the Mace Mo-Cu deposit is situated at the upper-middle level of a larger porphyry type deposit. As porphyry systems are not common in Irish granites, the Mace deposit provides an interesting case study for exploration in Ireland. Previous research on the Mace deposit has focussed on structural controls for mineralisation. Early exploration drilling resulted in significant loss of molybdenum in quartz veins (Burns 1970), resulting in under-reporting of grades, until recent exploration drilling by SLR. The vein types and alteration sequences outlined during previous work on the Mace deposit suggest a multiphase mineralisation model, however vein paragenesis has been poorly understood up until now. Conventional treatment of commercial whole rock assays is not intended, or capable of defining a detailed paragenesis from drill core logging, however the geostatistical approach used here adds value to bulk rock assays in helping to target specific vectors for mineralisation, which are then further investigated using micro-beam techniques.

Structural controls on the Mace deposit are relatively well understood, with a strong south-southwest to east-northeast trending control constraining mineralisation within faults containing disseminated chalcopyrite and pyrite, and chalcopyrite and molybdenite concentrations in a quartz vein stockwork and disseminated in the host rock (Derham and Feely 1988). Post-mineralisation east-southeast to west-northwest trending faults have dextrally offset parts of the deposit from adjacent zones, and there are structural targets in the area that as-yet are untested by exploration.

Elsewhere in Galway, disseminated and quartz vein-hosted molybdenite mineralisation occurs throughout the granite and its satellite plutons (O'Raghallaigh et al. 1997). Fluid

inclusion work carried out by O'Reilly et al. (1997) concluded that three generations of fluids affected the Galway Granite. The earliest was a magmatic fluid derived from the granite during solidification, with molybdenite mineralisation attributed to this phase. Such a scenario is consistent with orthomagmatic porphyry emplacement and fractionation of mineralising fluids from parent magma, however in detail at Mace there may be a temporal difference between disseminated molybdenite in the host granitoids and in veins. The second was attributed to mixing of magmatic and meteoric fluids responsible for retrograde alteration in the area, which may help explain some of the proposed lower temperature propylitic and retrograde phyllic alteration seen at Mace. Remobilised molybdenite in the margins of larger quartz veins and breccias with quartz and granite clasts indicate reactivation of vein conduits in the system. The last fluid is associated with the observed late stage calcite-fluorite veins that have been shown to form a late overprinting of the deposit area after cooling of the granite and porphyry system veins. These late stage veins are observed by O'Reilly et al. (1997) to crosscut dolerite dykes dated by O'Connor et al. (1993) to 231±4 Ma, significantly younger than the 407±1.5 Ma (Feely et al. 2010) molybdenite at Mace Head.

O'Reilly et al. (1997) divide vein types in the Galway Granite into three types:

- V_1 veins are associated with molybdenite mineralisation and appear to be localised to small areas, occurring in stockworks, with wallrock that is generally neither brecciated nor sheared, and with a weak alteration halo.

- V_2 veins occur throughout the batholith and infill steeply dipping faults and fractures, typically parallel to the Shannawona fault or in an east-west orientation. O'Reilly et al. do not genetically associate sulphides with this vein type, but note that shearing and brecciation of wallrock and veins is evident.

- V_3 veins are mostly east-west trending, vertical to steeply dipping veins filling late fractures and strike-slip faults throughout the granite, with sericitisation of wallrock common.

The approach of O'Reilly et al. does not further distinguish vein types outside of these three broad categories, and V_1 vein types in their work most likely encompasses early

and molybdenite-bearing V1, V2, V3 and V4 veins using the SLR (2016) classification. These vein types range from orthomagmatic extensional veins (V1), through to porphyry related chalcopyrite and molybdenite bearing quartz veins (V2), fracture fill and slickensides (V3), and quartz stringers and veinlets (V4). Shearing and brecciation seen in V_2 veins of O'Reilly et al. may suggest a link with remobilised molybdenite associated with phyllic alteration and molybdenite fracture fill and slickensides at Mace.

These observations broadly concur with the observations of this thesis and the development of a paragenetic model for molybdenum-copper mineralisation at Mace Head. O'Reilly et al. (1997) conclude that the Galway Granite was a locus for repeated fluid alteration and mineralisation ranging in age from late-magmatic to post-orogenic. A similar range of fluid influx has been shown in this thesis. O'Reilly et al. suggest that the latest in the sequence of fluid events may be as a result of the granite forming a permeable block adjacent to sedimentary basins from which mineralising solutions can be expelled by tectonic activity related to collisional granite bodies, and while most porphyry systems are generated mainly in magmatic arc environments subjected to regional-scale stress regimes (Sillitoe 2010), a minority occupy post-collisional and other tectonic settings that develop after subduction ceases (Richards 2009). Leake (2011) attributes emplacement of the Galway batholith to a releasing bend along a major sinistral strike-slip fault that progressively opened extensional spaces towards the granite margin for granite magma to fill. McCarthy et al. (2015) show that two sets of shear zones (NNW–SSE and ENE–WSW) cross-cut the concentric foliation of the Galway Granite complex, meaning that these structures were active during the construction of the pluton, with sinistral transpression causing dilation along the intersection of the two fault sets, facilitating centralised magma ascent consistent with Leake's suggestion.

Sinclair (2007) suggests a close temporal relationship between magmatic activity and hydrothermal mineralisation in porphyry deposits, indicated by the presence of inter-mineral intrusions and breccias that were emplaced between or during periods of mineralisation. This fits the concentric emplacement model of McCarthy et al. (2015) and with the early molybdenite intrusion of O'Reilly et al. (1997), and is consistent with the multi-phase mineralisation and fluid intrusion history at Mace.

Although many of the observed quartz veins and stringers appear to be late and crosscut the granite host at Mace, molybdenite mineralisation has been dated (Re-Os) at 407.3±1.5 Ma (Feely et al. 2010), which is effectively coeval with granite emplacement.

Bergey's (2008) report concludes that the mineralisation at the Mace deposit shows similarities to the Highmont deposit in the Highland Valley of British Columbia in some respects, but with molybdenum more important relative to copper and a more obvious association with regional faulting. Structural controls on the Mace deposit are well understood, with ENE-trending faults clearly acting as a conduit for mineralisation (Leake 2011, Hutton 2015). Later, post-mineralisation, WNW faults have dextrally offset parts of the deposit from adjacent zones, which is consistent with observed trends at outcrop. Mapping by Hutton (2015) and others has indicated that there may be some as-yet untested structural targets in the area. Molybdenite at both Mace and at the Highmont Mine was emplaced predominantly in quartz veins and fracture fillings within a granodiorite intrusion that forms a part of a composite batholith. The Highmont deposit is part of the Highland Valley Cu-Mo porphyry district, within a composite zoned batholith with lithologies ranging from diorite and quartz diorite at the border to younger granodiorite in the centre. Similar to Highmont, Mace is hosted in granodioritic rocks, with several stages and styles of mineralisation and alteration identified. At Highmont, Bergey (2008) believed zones of mineralization along north-south faults within the batholith are unlikely to produce a mineable deposit, and deeper structural zones creating lines of weakness for mineralisation should be targeted.

5.2 Petrography

Presented earlier in this thesis is a petrographic study of representative thin sections from Mace drill core. The alteration and mineralisation styles observed are generally typical of a porphyry style mineralising system. At least three phases of mineralising fluid can be observed to have transported sulphide minerals through the host granite.

Alteration at Mace is primarily seen forming a halo around mineralised veins and it is believed that these veins originate from a deeper zone of more pervasive alteration and higher grade, consistent mineralisation (SLR 2015). This observation ties with Tellus

(2016) magnetic survey data showing a magnetic intensity low anomaly encompassing the deposit area and extending offshore to the south of Mace Head. Hydrothermal alteration is extensive and typically zoned on a deposit scale in porphyry systems (Lowell and Guilbert 1970) as well as around individual veins and fractures. In many porphyry deposits, alteration zones on a deposit scale consist of an inner potassic zone characterized by K-feldspar and/or biotite and an outer zone of propylitic alteration that consists of quartz, chlorite, epidote, calcite and, locally, albite associated with pyrite. Zones of phyllic alteration may be part of the zonal pattern between the potassic and propylitic zones, or can be irregular or tabular, younger zones superimposed on older alteration and sulphide assemblages (e.g. Moyle et al. 1990; Sillitoe 1993). Alteration mapping has not been carried out at Mace to date, however potassic, propylitic and phyllic alteration is encountered in all drill holes from the recent exploration campaign.

Alteration is observed to increase towards mineralised intervals, as is typical of many porphyry mineralisation systems. Increased quartz veining and partial brecciation is accompanied by strong but patchy propylitic-potassic alteration, which persists as a halo surrounding molybdenite-infilled, <40cm wide brecciated quartz veins. Although mineralised veins and fracture planes are observed throughout, a strong correlation between intense alteration and increased sulphide content, including chalcopyrite and pyrite, has been noted (SLR 2016).

Molybdenite at Mace occurs variably as patches, disseminations in quartz veins, striated and unstriated smears on slickensides, rosettes on partly recrystallized surfaces, and on open joint planes. Chalcopyrite occurs primarily as patches and disseminations within quartz veins and as disseminations within the granite. The ratio of copper to molybdenum has been observed to decrease away from mineralised veins, with copper disseminated more evenly through the deposit than molybdenum (SLR 2016). The results of SLR's block modelling and the Tellus magnetic survey data discussed earlier in the thesis highlight this observation

An early pyrite assemblage consists of quartz extension veins commonly containing large, euhedral pyrite crystals and disseminations. These vein lineaments appear to have been reactivated with further hydrothermal fluid intrusion carrying copper and

molybdenum sulphides. Reactivation of these early stage veins by chalcopyrite and molybdenite bearing fluids is evident under light microscopy. Pyrite in extensional quartz veins show clear oscillatory zonation of cobalt, nickel, and selenium, indicating that pyrite crystallisation is an early sulphide phase associated with emplacement of magmatic fluid related to granite emplacement. Crosscutting relationships with chalcopyrite and molybdenite bearing veins and overgrowth patterns of those elements further suggests that these quartz-pyrite veins were formed near-synchronous with granite emplacement.

A chalcopyrite assemblage occurs predominantly in areas of relatively strong potassic alteration, with chalcopyrite often seen throughout veins and groundmass as individual grains, clusters of grains, or disseminations. Disseminated chalcopyrite is most commonly associated with potassic alteration, with chalcopyrite commonly found within the groundmass of the host rock. This suggests that chalcopyrite was present in the host granite prior to full crystallisation, implying mineralising fluids capable of potassically altering the granite occurred in the early stages of mineralisation of the Carna granite at Mace.

A high Cu:Mo ratio is most commonly associated with strong potassic alteration in the Mace deposit, which is thought to be indicative of proximity to the source of mineralising fluids. Conventionally, potassic alteration forms the core of classic porphyry systems (Sillitoe 2010), with propylitic and phyllic alteration more distal to the centre of the deposit.

A molybdenite-chalcopyrite assemblage is generally hosted in quartz veins and is commonly seen as a second phase of mineralising fluid, reactivating older quartz vein conduits and overgrowing older pyrite within the veins. Molybdenite-rich veins and veinlets are also seen to crosscut older quartz veins and may often contain chalcopyrite. This assemblage comprises the bulk of Cu-Mo mineralisation at the Mace deposit.

Molybdenite is closely related to chalcopyrite in potassically altered zones. It is noteworthy that the proportion of molybdenite increases relative to chalcopyrite in zones of increased propylitic and phyllic alteration. Disseminated molybdenite and

narrow molybdenite-rich veins are observed to crosscut the potassic assemblage, with an overall molybdenum grade generally higher than in other mineralised vein styles in the deposit. This overprinting suggests that these vein types may post-date alteration. Larger quartz veins and associated breccias are strongly correlated with retrograde phyllic alteration, indicating a subsequent introduction of Mo-rich fluids, or alternatively remobilisation of pre-existing molybdenite within and through the deposit.

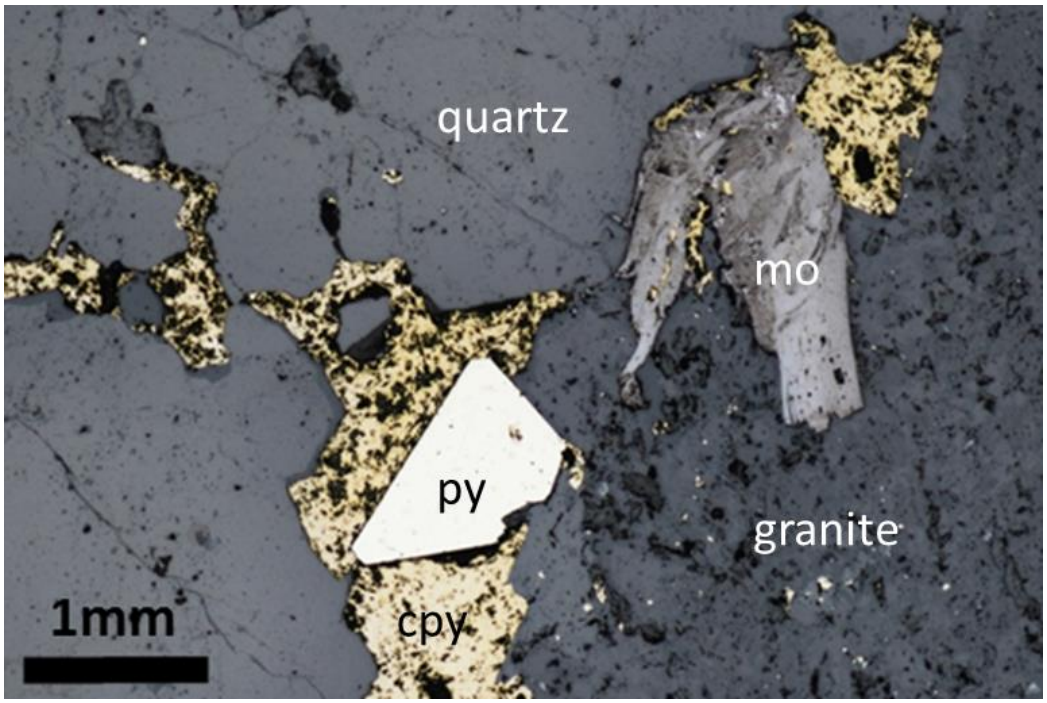

Figure 5-1 Clear secondary growth of euhedral pyrite (py) by chalcopyrite (cpy) and molybdenite (mo) at the boundary of a quartz vein

Petrography also allowed for some observations about the nature of phyllic alteration in the Mace deposit. McCarthy & Cloutier (2016) did not distinguish between propylitic and phyllic alteration, however they suggested that molybdenite mineralisation is most concentrated within discrete shear zones where phyllic alteration is recorded. Shear-zone hosted mineralisation suggests that molybdenite mineralisation here may have been a product of remobilisation of molybdenite during retrograde alteration to phyllic conditions. Infilling sericite growth around chalcopyrite and molybdenum has been observed during petrographic study of thin sections (see Figure 5-2), suggestive of a post-mineralisation phyllic alteration that concurs with McCarthy and Cloutier's shear zone observation. Sericite replacement of k-feldspar is pervasive in many samples

analysed under light microscope, with low magnetic susceptibility observed in sericite-enriched zones indicative of a magnetically destructive nature of the fluids responsible for the alteration. At the Henderson molybdenum porphyry deposit in Colorado, sericitic alteration is best developed above the orebody (Seedorf & Einaudi 2004), and indicates that potassic and sericitic alteration were not contemporaneous as sericitic alteration did not begin to form in the system until after intense potassic alteration had terminated. Yang et al. (2009) observed a similar alteration sequence at the Qulong porphyry Cu-Mo deposit in Tibet, where an outer halo of propylitic alteration (epidote–chlorite ± calcite) extends up to 2 km away from the deposit, and feldspar-destructive alteration (sericite–chlorite ± clay minerals) has overprinted most of the potassic and part of the propylitic alteration. At the MAX deposit in British Columbia, phyllic alteration (sericite) occurs predominately at shallower levels above the main potassic alteration zone (Lawley et al. 2010). These are consistent with the general interpretation at Mace that phyllic (sericite) alteration is a superimposed texture and a retrograde alteration style. At Endako in British Columbia, early stage K-feldspar and biotite alteration forms envelopes on veins and fractures, which is overprinted by a quartz-sericite- pyrite assemblage, with much of the molybdenite mineralisation related to the sericite alteration (Selby et al. 2000). Given the location of the existing drill holes at Mace north of the known magnetic low anomaly published by Tellus (2016) and the Cu:Mo ratio shown by SLR (2016) to increase towards that anomaly , it is not unreasonable to suggest that zones of strong sericitic alteration in Mace drill holes are indicative of a similar location above the porphyry centre.

A late stage calcite-fluorite-chlorite assemblage is obvious from drill core as an overprinting texture crosscutting the deposit. This vein assemblage may be related to interaction of meteoric fluids and country rocks to the granite batholith. Although many of the observed quartz veins and stringers appear to be late and crosscut the granite host, molybdenite mineralisation has been dated (Re-Os) at 407.3±1.5 Ma (Feely et al. 2010), which is effectively coeval with granite emplacement.

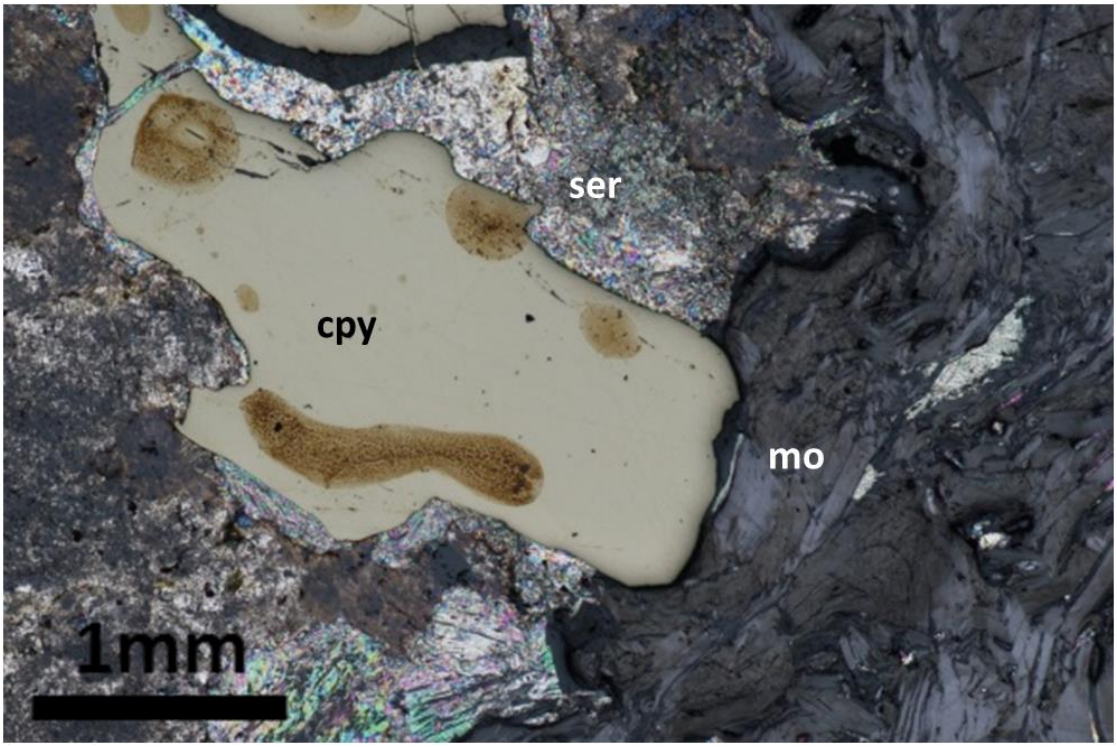

Figure 5-2 Sericite (ser) infill around chalcopyrite (cpy) and molybdenite (mo)

5.3 Statistical analysis

Statistical analysis of whole rock geochemistry assays classified the results into three distinct groups. The groups represent the hydrothermal fluids associated with mineralisation and alteration, the felsic host-rock component, and a mafic component of the host granite. Combined with petrographic and laboratory analyses, these statistical data enable differentiation of hydrothermal and magmatic phases according to their trace element signatures. Early pyrite in extensional quartz veins has been shown to be related to the mafic magmatic component of the host granite, with a strong zonation of cobalt, nickel and selenium. These three elements were identified as mafic magmatic components of the Mace host rock by PCA and k-means clustering.

PCA and k-means clustering identified 13 of the 33 assayed elements as related to or part of the mineralising component in the Mace deposit. These elements may be considered pathfinder elements for future assays for Mo-Cu mineralisation.

5.4 Laboratory analyses

Laboratory analyses of selected thin sections by light microscopy, SEM and LA-ICP-MS highlighted a number of features in pyrite grains that can be used to develop paragenetic sequences for hydrothermal activity in the Mace deposit. Pyrite was found to be a more successful sulphide for detecting zonation and variation within the grain than molybdenite and chalcopyrite.

Through LA-ICP-MS it was possible to define crystallisation of early pyrite as close to coeval with mafic magmatic emplacement. Cobalt-nickel-selenium zonation of pyrite in extensional quartz veins may be indicative of host-rock influence on early hydrothermal fluids forming these veins. Statistical work undertaken during this thesis identified Co-Ni-Se as part of the mafic magmatic component of the whole rock geochemical assays. The zonation pattern found in pyrite grains indicates that these sulphides formed at a time close to synchronous with initial granite emplacement at Mace Head, but that some pyrite grains were subject to later enrichment or depletion of magmatic elements. This zonation pattern may have been caused by changes in mobility of trace elements with changes in acidity and pressure caused by declining depths and temperatures of hydrothermal fluids (Sillitoe 2010, Figure 5-3).

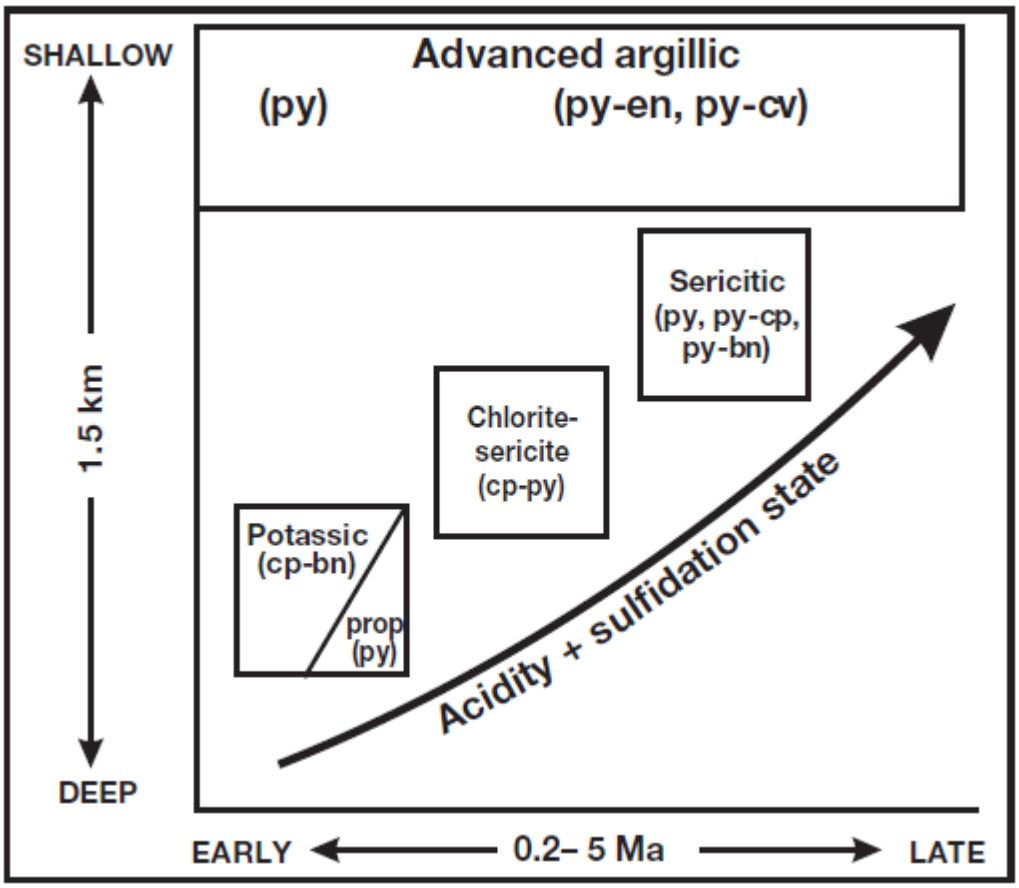

Figure 5-3 Schematic representation of generalized alteration-mineralisation sequence in porphyry Cu systems in relation to paleodepth and system life span (Sillitoe 2010)

A clear crosscutting and overgrowing by copper-molybdenite of early pyrite is visible under light microscopy and SEM in many of the pyrite grains analysed, showing that mineralising fluid intrusion occurred after crystallisation of the pyrite-quartz extension veins in the system (Figure 5-1).

The overgrowing pattern of chalcopyrite and molybdenite on pyrite grains appears through laser mapping to have a much stronger effect where potassic alteration is the dominant alteration type. The highest copper-molybdenite ratio is apparent where potassic alteration is strongest. Disseminated chalcopyrite in the granite host rock may elevate the ratio where chalcopyrite and molybdenite occur as part of the mineralising component. This suggests that the initial magmatic component contained a certain amount of Cu near the source of mineralisation, which was added to by the intrusion of

mineralising fluid. Increased Cu:Mo ratios inside pyrite grains in both potassic and propylitic/phyllic alteration zones further suggest that copper was present during crystallisation of pyrite early in the history of the deposit area (Figure 5-4).

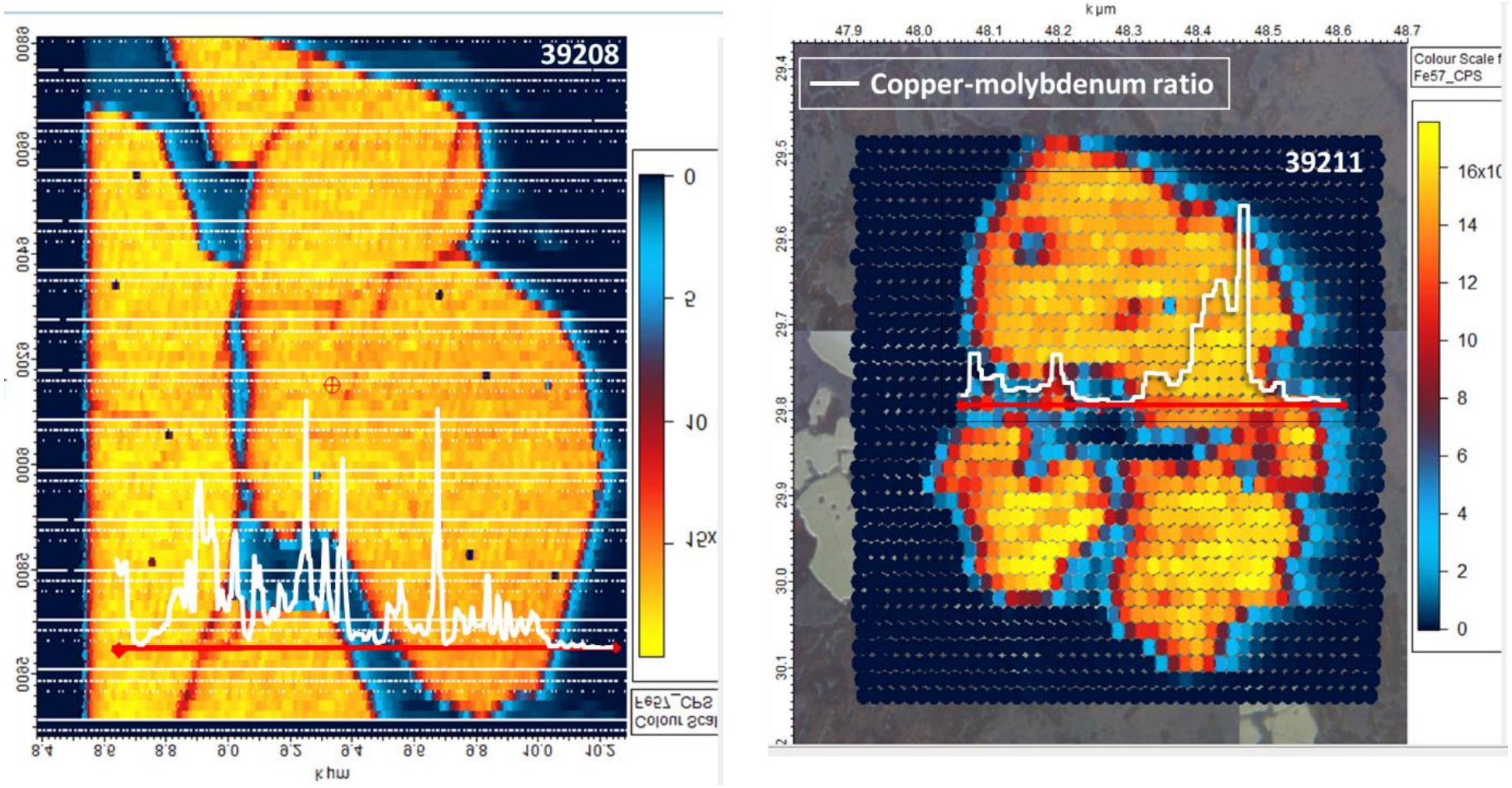

Figure 5-4 Examples from early pyrite grains in both potassic (left) and propylitic (right) alteration showing an increased Cu:Mo ratio inside the grain compared to grain margins and groundmass, suggestive of a copper component of magmatic vein fluids.

5.5 Economic implications of this research

The resource estimate undertaken for SLR Consulting on behalf of MOAG Copper Gold Resources Ltd. of between five and fifteen million tonnes, grading between 0.10% Mo and 0.15% Mo, 0.05% Cu and 0.10% Cu, and between 0.5 g/t Ag and 1 g/t Ag, indicates that the deposit is currently sub-economic when taking current molybdenum prices into account. Given the suggestion by Bergey (2008), Leake (2011) and SLR (2016) that the deposit is in the upper part of a larger porphyry system, it is clear that further definition of the location of the Mo-Cu prospect within the system and the vectors towards mineralisation are vital to future exploration on and around the deposit area.

The results of this research have economic ramifications both at the deposit scale at Mace Head as well as for the rest of the Connemara granite batholith. SLR's resource model and previous exploration targeting for Mace Head were based on grade models without paragenetic and alteration-system controls. Mineralisation was treated as vein-hosted and was envisaged to gradually decrease northwards from the southern coast of Mace Head. As such, prior models were not constrained by robust alteration and hydrothermal models.

Tellus (2016) magnetic survey data showing an approximately circular magnetic low encompassing the deposit area and extending offshore to the SSE, and SLR's (2016) Cu:Mo ratio voxel implying an increase in the Cu:Mo ratio in a SSE direction, suggests Mo-Cu mineralisation vectors towards the origin of mineralising fluids at depth off the south coast of Mace Head. Given the evidence from this thesis that the erosion level at the deposit is approximately at the upper-middle part of the system, significant mineralisation may exist below the levels drilled to date and south of the current target area.

A classic porphyry style stockwork has not been intersected at Mace, and there is potential to intersect such a system below the latest drilling depth of just over 200 vertical metres. Drilling has shown that mineralisation is more consistent towards the south of the exploration area.

Mineralised quartz veins are associated with higher temperature potassic alteration, while some of the largest quartz veins both in terms of thickness and molybdenum grade are associated with strong propylitic and phyllic alteration. Using Sillitoe's (2010) classifications, this may be indicative of a sequence from an initial high temperature fluid evidenced by potassic alteration, through progressively more distal and lower temperature propylitic-phyllic phases, and with a final, relatively cooler, non-economically mineralised calcite-fluorite-chlorite assemblage overprinting the deposit at a late stage in its history. This would suggest that increased potassic alteration may be expected with proximity to the centre of the porphyry system and therefore the source of mineralisation.

The intimate association between mineralisation and alteration suggests that mineralising fluid transport and alteration of the host granites was coeval and multi-stage. Mineralised quartz veins are associated with higher temperature potassic alteration, while some of the largest quartz veins both in terms of thickness and Mo grade are associated with strong propylitic alteration. Unaltered granite in the deposit area has been observed to contain "barren" quartz veins – those where the only sulphide present is pyrite – suggesting that the first phases of economic mineralising fluid entering the system were the same fluids responsible for alteration textures seen at Mace.

5.6 Correlation of alteration, mineralisation, and emplacement history

Through the techniques employed in this thesis it has been possible to correlate alteration textures with mineralised vein intrusion and the known emplacement history of the Galway Granite. Table 6 shows the broad relationships between alteration and mineralisation in the deposit, and suggests that mineralisation at Mace fits the alteration styles common in a classic porphyry system. The table provides an approximation of the spatial and temporal alteration-mineralisation sequence. This conceptual model for paragenesis will allow targeting of potassic alteration and later propylitic alteration, quartz veins and breccias to vector towards areas of strong potassic alteration at depth and target a quartz vein stockwork that may be expected in a classic porphyry deposit.

Table 6 Correlation between alteration textures, mineralogy, petrographic assemblages and emplacement history at the Mace Head Mo-Cu porphyry deposit

Alteration Texture	Dominant Mineralogy	Vein Type	Petrographic assemblage	Emplacement History
Pre-alteration	Magmatic (cobalt-nickel-selenium)	V1	Pyrite	Late pluton emplacement
	Pyrite			
Potassic	High copper-molybdenum ratio	V1, V2, V3, V4	Chalcopyrite	Early alteration phase
	Copper-molybdenum	V2, V3, V4	Chalcopyrite-molybdenite	Post-potassic alteration/ retrograde alteration
Propylitic/Phyllic	Molybdenum	V2, V3	Chalcopyrite-molybdenite	Post-potassic alteration: distal/ retrograde alteration
	Molybdenum	V2, V3	Sericite	Retrograde alteration
Post-alteration overprinting	Calcite-fluorite-chlorite	V7	Calcite-fluorite-chlorite	Post molybdenum-copper mineralisation

5.7 Discussion

Disseminated and quartz vein-hosted molybdenite mineralisation occurs throughout the Galway Granite and its satellite plutons (O'Raghallaigh et al. 1997). Feely et al. (2010) shows that episodic molybdenite mineralisation occurred across the Galway Granite for c. 40 m.y from c.423 Ma in the NW Omey pluton to c.383 Ma at Costelloe in the east (Figure 5-5).

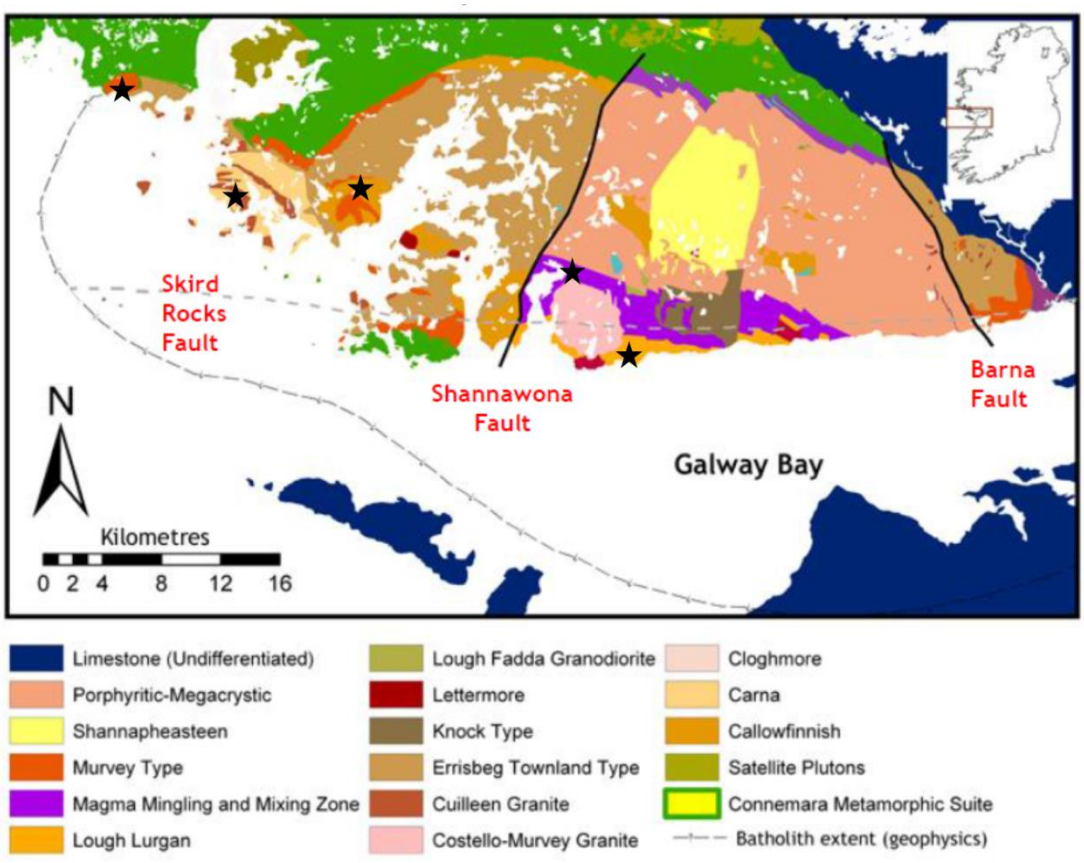

Figure 5-5 Black stars indicate significant molybdenite occurrences in the Galway Granite Batholith. Not shown is the molybdenite occurrence at Omey, northwest of the pictured area. Map modified from Crowley (1997)

Sinclair's (2007) classification of a porphyry Mo deposit lists principal ore minerals are molybdenite, scheelite, wolframite, cassiterite, bismuthinite, and native bismuth, while minor amounts of chalcopyrite may also be present. Bismuthinite (or aikinite) has been identified during petrographic and LA-ICP-MS studies of Mace granite, while tungsten is a common trace element throughout the deposit. Associated minerals listed by Sinclair

include pyrite, magnetite, quartz, K-feldspar, biotite, muscovite, clay minerals, fluorite, and topaz. Most of these minerals are seen at Mace with the exception of topaz, although fluorite is common. Sinclair's comments on general alteration zonation matches almost exactly with the observations at Mace; in a classic porphyry system, hydrothermal alteration is extensive and typically zoned on a deposit scale as well as around individual veins and fractures. In many porphyry deposits, these alteration zones consist of an inner potassic zone characterized by K-feldspar and/or biotite (± other elements) and an outer zone of propylitic alteration that consists of quartz, chlorite, epidote, calcite and, locally, albite associated with pyrite. These alteration zones are well developed at Mace. Phyllic alteration may be part of the zonal pattern between the potassic and propylitic zones, or can comprise younger zones superimposed on or above older alteration and sulphide assemblages. Evidence of a superimposed phyllic alteration texture along reactivated quartz veins, fractures, and breccia zones can be seen in drill core from Mace. Fluid inclusion studies by Suzuki et al (2000) indicate that molybdenite in the Galway Granite experienced hydrothermal alteration after deposition, suggesting that the molybdenite may show open-system behaviour during post-depositional exposure to hydrothermal fluids, with these fluids representing a hydrothermal event significantly younger than the age of molybdenite deposition. This is consistent with the suggestion in this thesis and by McCarthy and Cloutier (2016) of a retrograde phase of phyllic alteration remobilising molybdenite in the porphyry system at Mace, and with the second phase of fluid suggested by O'Reilly et al. (1997) attributed to mixing of magmatic and meteoric fluids also associated with retrograde alteration.

Sillitoe's (2010) stylised porphyry system model (Figure 5-6) shows potassic alteration closest to the core of the system, which concurs with the observations of this thesis that the highest Cu-Mo values are found where potassic alteration is strongest. Propylitic alteration is postulated by Sillitoe to be a more distal alteration texture, while phyllic (chlorite-sericite) alteration occurs above the potassically altered core of the system.

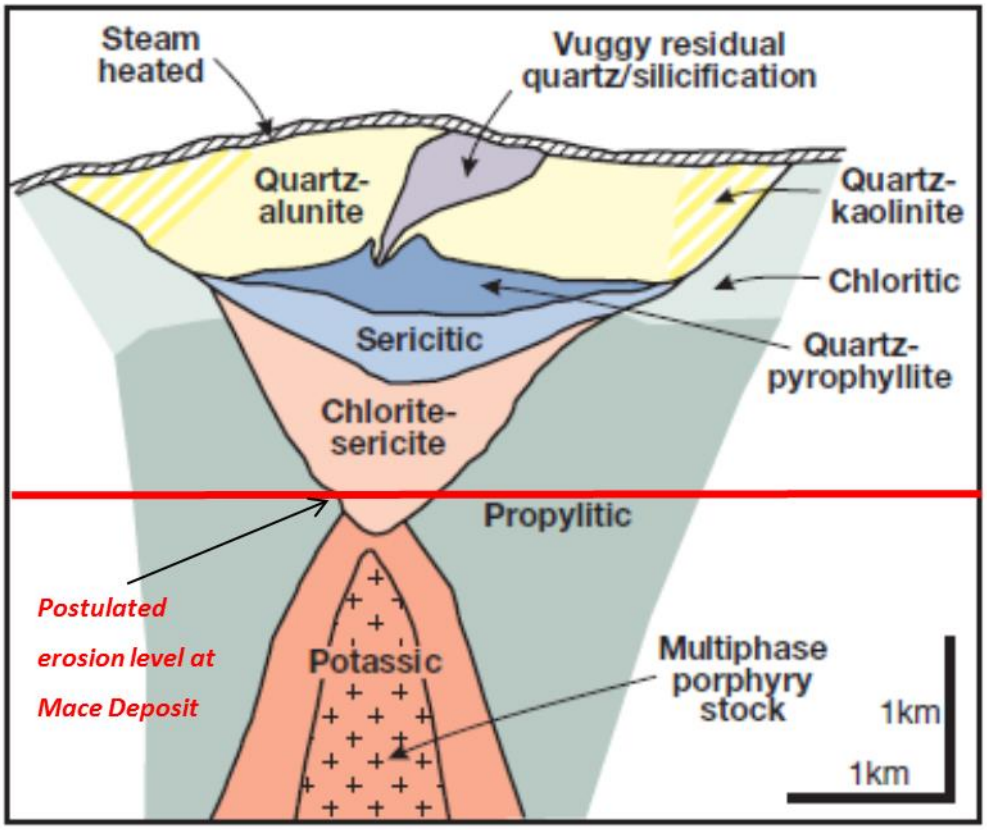

Figure 5-6 Sillitoe's (2010) generalised alteration-mineralisation zoning pattern for a non-telescoped porphyry Cu system. The work of this thesis indicates an erosion level near the upper centre of a porphyry deposit.

This suggests that the source of mineralising fluids is more closely related to potassic alteration than to other alteration styles observed in the Mace deposit. SLR's (2016) suggestion that the deposit is located near the upper middle of a porphyry-type deposit (see Figure 5-6) implies that increased potassic alteration may be expected at depth nearer the heart of the system. This leads to the assumption that potassic alteration may be a reliable vector towards mineralisation within the Mace deposit. Propylitic alteration is therefore expected to occur as a more distal alteration texture within a porphyry deposit, which is supported by the higher Cu:Mo ratio reported in the south-east of the area explored by drilling, indicative of higher Cu as a result of proximity to the source of mineralisation.

These observations tie well with work contained in this thesis suggesting that potassic alteration may act as a vector towards the source of mineralisation, with increasing

propylitic alteration with distance from the mineralising source and phyllic alteration less well developed but visible in patches across the deposit. The main sulphide minerals and alteration patterns observed in core samples can be used to generate a chronology of mineralisation at Mace.

5.8 A paragenetic sequence for the development of mineralisation and alteration textures at Mace Head

The Mace Mo-Cu porphyry deposit contains many classic porphyry features and textures such as alteration zonation centred on a potassic core, multiphase mineralising veins, and mineralisation styles similar to other known porphyry examples. Applying statistical and laboratory analytical techniques, petrography, and modern porphyry knowledge has increased the understanding of the paragenesis of alteration and mineralisation of the Mace porphyry system, and allowed a generalised paragenetic sequence for mineralisation at Mace in the context of a classic porphyry deposit, as shown in Figure 5-7

Emplacement of the Galway plutons was controlled by the WNW-ESE Skird Rocks Fault, the NNE-trending Shannawona Fault, and the NNW-trending Barna Fault (Hunt et al. 2006). Leake (2011) and McCarthy et al. (2015) attribute emplacement of the batholith to fault movement that progressively opened extensional spaces towards the granite margin for granite magma to fill. The first phase of mineralisation can be attributed to a magmatic-derived fluid during final stages of granite crystallisation (O'Reilly et al. 1997), with minor molybdenite mineralisation formed from this fluid. O'Reilly et al. (1997) attributed retrograde alteration to a second, mixed magmatic and meteoric fluid drawn into the granite in a meteoric convection system driven by magmatic heat soon after intrusion. The need to explain alteration of Upper Carboniferous dolerite dykes means that this fluid may in fact be younger, although it has been shown that dyke emplacement was an ongoing process throughout the evolution of the Mace system.

Potassic alteration linked with groundmass-hosted chalcopyrite when occurring together with a high assay copper-molybdenum ratio suggests a proximal fluid source for copper mineralisation. Potassic alteration is therefore likely to be associated with

primary mineralisation. A mixture of primary and remobilised mineralisation in propylitic and phyllic retrograde alteration zones is a result of overprinting and replacing pre-existing alteration textures. Large quartz vein breccias indicate a reactivation of existing vein conduits by later hydrothermal fluids and remobilisation of mineralising elements related to phyllic alteration as defined by development of sericitic haloes. These veins and breccias may be related to the influence of meteoric fluids on magmatic fluids (O'Reilly et al. 1997).

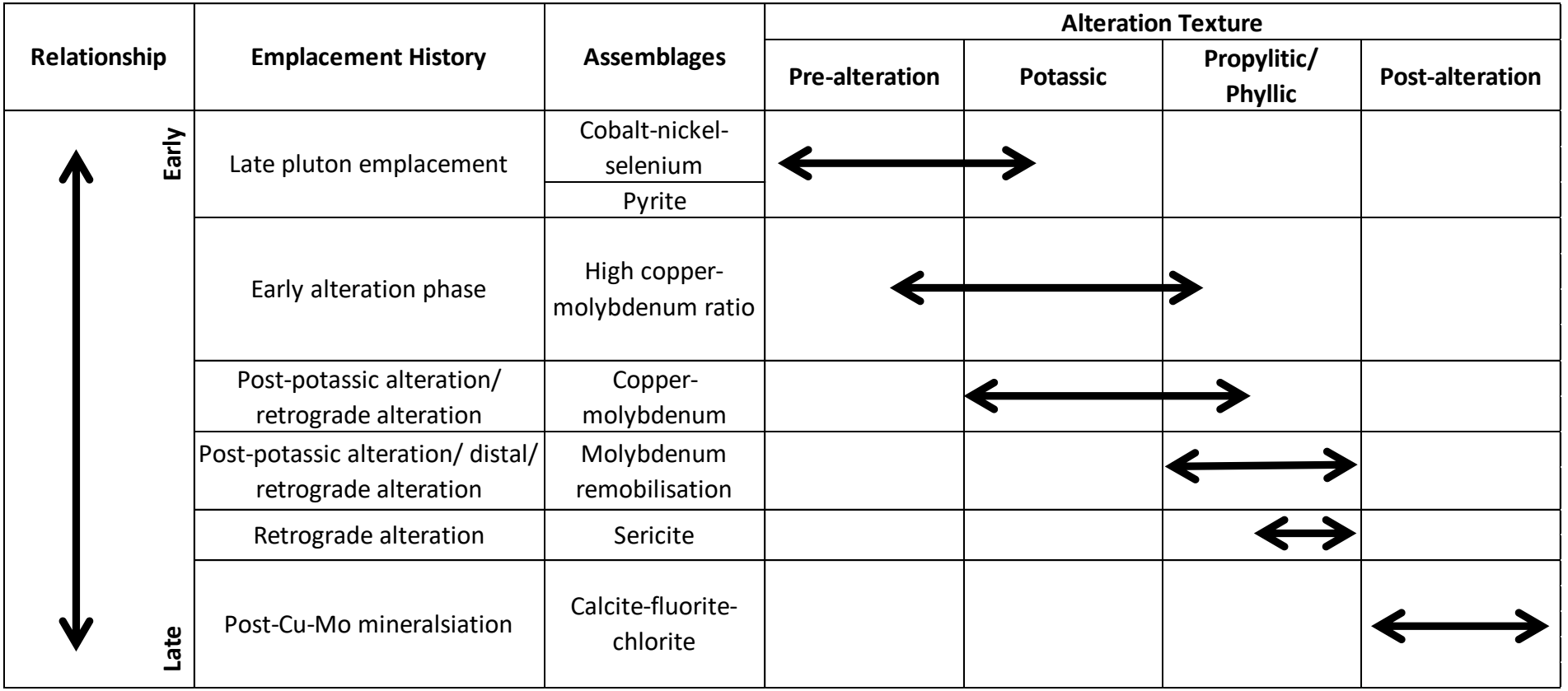

Figure 5-7 A paragenetic sequence for development of mineralisation and alteration textures at Mace Head

5.9 Conclusions

Given that the evidence from previous reports, the latest exploration drilling, and this thesis suggests that current work at Mace has not encountered the highest grade of the deposit, it is reasonable to suggest that current resource estimates are not comparable to those of other deposits of a similar size and scale. Deep drilling below the level currently investigated should be strongly recommended in order to confirm the presence of a classic porphyry deposit, with evidence so far suggesting that a larger Cu-Mo deposit may be encountered at depth.

Alteration zones typical of classic porphyry style deposits may correlate with mineralised grades encountered at greater depths. Potassic alteration is generally more prevalent nearest the source of mineralisation, having developed shortly after crystallisation of the granite magma and associated with early quartz-chalcopyrite-molybdenite veins. Propylitic alteration is a spatially or temporally distal texture after potassic alteration, also having associated molybdenite and chalcopyrite. Phyllic alteration is seen as a superimposed sericitic texture above the deposit, or as a retrograde imprint on potassic or propylitic alteration indicative of cooling of the hydrothermal system, possibly influenced by the introduction of meteoric fluids. This event is associated with some of the largest quartz veins and breccias in the deposit and with high molybdenum grades in drill core through remobilisation or introduction of molybdenite along these conduits.

Late stage unmineralised calcite-fluorite-chlorite veining acts as a useful marker of the end of the mineralisation sequence, where a much later, cooler fluid phase is introduced well after deposit related alteration and mineralisation.

Despite the advances in compiling a paragenetic sequence for the Mace porphyry Mo-Cu deposit, a number of areas remain where further work would be useful and are beyond the scope of this study. As a quartz vein stockwork, generally expected in a porphyry deposit, has not been encountered through drilling at Mace up to now, it may be expected that targeting exploration towards zones of highest potassic alteration and Cu:Mo ratio will result in intersecting higher grades of molybdenum and copper, and

that the highest grades may be expected to the south of previous drilling locations and at a depth below approximately 200m where drilling has so far tested. The Tellus (2016) magnetic low anomaly and SLR (2016) Cu:Mo voxel model strongly suggests that increased mineralisation may be encountered just south of Mace pier at the southern tip of Mace Head. Further work on structural controls at Mace may identify deep-seated structures similar to the Highmont deposit (Bergey 2008) responsible for early emplacement and creating lines of weakness for later faulting, remobilisation of mineralisation and introduction of new mineralising fluids.

5.10 References

Bergey, W. R. (2008), Geological Report on The Mace Molybdenum-Copper Prospect Connemara, County Galway, Ireland

Burns, D.J., (1970), Drilling on Licence 934, Mace, Co. Galway: West Galway Joint Project: Anglo United Trust Private Report

Derham, J.M., and Feely, M., (1988), A K-feldspar breccia from the Mo-Cu stock work deposit in the Galway Granite, west of Ireland: Journal of the Geological Society, v. 145, p. 661-667

Feely, M., Selby, D., Hunt, J., & Conliffe, J. (2010) Long-lived granite-related molybdenite mineralisation at Connemara, western Irish Caledonides. Geological Magazine 147, 886-894

Hunt, J., Feely, M. Yates, M. Selby, D. Creaser, R. Leake, B. (2006). *Deconstructing the late-Caledonian Galway Batholith: P-T-t perspectives of granite magmatism in Connemara, western Ireland*. Paper presented at Harrisburg symposium, New Brunswick (2006)

Hutton, D. H. W., (2015), Report on the Mace Granite Prospect - June 2015: Internal Report to MOAG Copper Gold Resources

Lawley, C. J. M., Richards, J. P., Anderson, R. G., Creaser, R. A., & Heaman, L. M., (2010), Geochronology and Geochemistry of the MAX Porphyry Mo Deposit and its Relationship to Pb-Zn-Ag Mineralisation, Kootenay Arc, Southeastern British Columbia, Canada. Economic Geology, v. 105, pp. 1113–1142

Leake, B., (2011), Stoping and the mechanisms of emplacement of the granites in the Western Ring Complex of the Galway granite batholith, western Ireland. Earth and Environmental Science Transactions of the Royal Society of Edinburgh, v. 102, p. 1-16

Lowell, J.D., & Guilbert, J.M., (1970), Lateral and vertical alteration-mineralisation zoning in porphyry ore deposits: Economic Geology, v. 65, p. 373-408

McCarthy, W. & Cloutier, J. (2016), *Hyperspectral reflectance and magnetic alteration of the Mace Mo-Cu deposit, Co Galway*. Report to MOAG. University of St. Andrews

McCarthy, W., Reavy, R. J., Stevenson C. T., & Petronis, M. S., (2015), Late Caledonian transpression and the structural controls on pluton construction; new insights from the Omey Pluton, western Ireland. Earth and Environmental Science Transactions of the Royal Society of Edinburgh, 1–18

Moyle, A.J., Doyle, B.J., Hoogvliet, H., & Ware, A.R., (1990), Ladolam gold deposit, Lihir Island, in Hughes, F.E., ed., Geology of the Mineral Deposits of Australia and Papua New Guinea: The Australasian Institute of Mining and Metallurgy, Melbourne, p. 1793-1805

O'Raghallaigh, C., Feely, M., McArdle, P., MacDermott, C., Geoghegan, M. & Keary, R., (1997), Mineral localities in the Galway Bay Area: Geological Survey of Ireland, Report Series, RS97/1 (Mineral Resources), 70 pp

O'Reilly C., Jenkin, G. R. T., Feely, M., Alderton, D. H. M, & Fallick, A. E., (1997), A fluid inclusion and stable isotope study of 200 Ma of fluid evolution in the Galway Granite, Connemara, Ireland, Contrib Mineral Petrol. 129: 120-142

Richards, J. P., (2009), Postsubduction porphyry Cu-Au and epithermal Au deposits: Products of remelting of subduction-modified lithosphere: Geology, v. 37, p. 247−250

Seedorff, E. & Einaudi, M. T., (2004), Henderson Porphyry Molybdenum System, Colorado: I. Sequence and Abundance of Hydrothermal Mineral Assemblages, Flow Paths of Evolving Fluids, and Evolutionary Style, Economic Geology, Vol. 99, pp. 3–37

Selby, D., Nesbitt, B. E., & Muehlenbachs, K., (2000), Hydrothermal Alteration and Fluid Chemistry of the Endako Porphyry Molybdenum Deposit, British Columbia, Economic Geology Vol. 95, pp. 183–202

Sillitoe, R. H., (1993), Gold-rich porphyry copper deposits: geological model and exploration implications, in Kirkham, R.V., Sinclair, W.D., Thorpe, R.I., and Duke, J.M., eds., Mineral Deposit Modeling: Geological Association of Canada, Special Paper 40, p. 465-478.

Sillitoe, R. H., (2010), Porphyry copper systems: Economic Geology, v. 105, p. 3–41

Sinclair, W.D., (2007), Porphyry deposits, *in* Goodfellow, W.D., ed., Mineral Deposits of Canada: A Synthesis of Major Deposit-Types, District Metallogeny, the Evolution of Geological Provinces, and Exploration Methods: Geological Association of Canada, Mineral Deposits Division, Special Publication No. 5, p. 223-243

SLR Environmental Consulting (Ireland) Ltd, Internal Exploration Reports to MOAG Copper Gold Resources, 2015-2016

Tellus Programme of the Geological Survey of Ireland, accessed 15th March 2017, www.tellus.ie

Yang, Z., Hou, Z., White, N. C., Chang, Z., Li, Z., & Song, Y., (2009), Geology of the post-collisional porphyry copper–molybdenum deposit at Qulong, Tibet, Ore Geology Reviews, 36, 133–159

Appendices

A Study of Alteration and Mineralisation at the Mace Mo-Cu Porphyry, Ireland

Submitted in support of the degree of Master of Science in Geology

By

Shane Lavery

Table of Contents

Appendix 1 Sample Descriptions

Sample Number	Hole Number	From (m)	To (m)	Drill Log Lithology	Polished Core Photo Description
39207	16-934-36	118.61	118.7	Granite	Epidote alteration. Med-Coarse granite. Ksp between epidote grains. Qtz ext veins w/ some Mo stringers. Py in qtz.
39208	16-934-36	110.69	110.8	Granite	Strong potassic alteration with common dark Mo veins/stringers and large pyrite crystals. Some stringers through. Large milky qtz vein w some Mo and rare chlorite.
39209	14-934-05	151.09	151.3	Weak-Moderately Altered Granite	Pale aplite vein with smaller minor aplite vein surrounding by pale blue-grey med granite. Some minor epidote-chlorite alteration. Pyrite common in granite.
39210	14-934-05	141.63	141.8	Strongly-Very Strongly Altered Granite	Qtz breccia. At least 2-3 phases of hydrothermal fluid. Central portion composed of relatively unbrecciated qtz (c.7cm) with possible minor fluorite. Outer section of vein (c.4-6cm each side) strongly brecciated. Dark muddy matrix - possibly pyrolusite w/ some Mo. Some pyrite in breccia matrix. Chlorite-epidote alteration in interclastic parts of breccia, often altering into clasts.
39211	15-934-12	154.4	154.6	Quartz Breccia	Granite breccia. Highly brecciated with sharply angular clasts of pale yellow altered granite. Matrix composed almost entirely of greenish epidote-chlorite. Common ksp in granite.
39212	15-934-12	165.09	165.3	Granite	

39213	15-934-12	174	174.4	Granite	Ksp altered granite with Mo in vuggy veinlets. Progressively more epidote-rich down(?)hole
39214	15-934-12	182.79	182.9	Granite	Med coarse granite with some epidote-chlorite alteration. Py and cpy in groundmass/stringers. Qtz veins altered
39215	15-934-12	197.12	197.3	Granite	Epidote-chlorite altered granite with med-strong bleached alteration haloes with ksp near stringer veins. One large pegmatitic ksp/qtz vein.
39216	16-934-36	103	103.2	Felsite Porphyry	"Unmineralised" porphyry with stringers and veinlets surrounded by med-strong epidote-chlorite alteration haloes. Some light brecciation. Possibly some calcite fracture coatings.
39217	15-934-18	27.75	28.05	Porphyry	Felsite porphyry with clear qtz/granitic stockwork veins containing py and other sulphides. Veins commonly have epidote alteration halo. Mo present in veins.
39218	15-934-18	72.18	72.4	Granite	Porphyry similar to 39217 but with fewer veins and with a sharp contact with med-coarse granite.
39219	15-934-18	122.8	123.1	n/a	Pink ksp pegmatite/aplite zone between less altered granite edges. Mo and sulphides visible in vein stockwork and in groundmass. Large (3cm) central vein with abundant sulphides ad Mo.
39220	15-934-18	123.21	123.4	n/a	Med granite with mild epidote alteration and sericitic alteration. Qtz vein with abundant py and other sulphides inc. cpy.

Appendix 2 SEM Image Descriptions

Sample ID	SEM Image No.	Description
39207	T52797	Py & cpy in vein
39207	T52798	Cpy, Mo
39207	T52799	Mo + Cpy (?) intergrowth
39207	T52800/ T52801	Mo veinlet crosscutting
39208(1)	T52802/T52803	Uneven vein contact w/ brecciation & some stringers
39208(1)	T52804	Some possible. Cpy
39208(1)	T52805/06	wavy vein pattern T52805 = SE Detector, T52806 = BSE Detector
39208(2)	T52808	Py grain against Mo minerals.
39208(2)	T52809	close up on fracture-Mo relationship
39208(2)	T52810	fractured Mo vein
39208(2)	T52811	textured grains in groundmass w/sulphides
39208(2)	T52812	dark grain w/alteration, near Mo patch
39208(2)	T52813	close up of dark grain
39208(2)	T52814	Fracturing within sulphides
39208(2)	T52815	close up of fracturing
39209	T52816	Brecciated crystals relationship
39209	T52817	Mo and possible Tourmaline at interface of central aplite vein
39209	T52818	Cluster of grains
39209	T52819	inter-sulphide grains
39210	T52821	Narrow fracture through altered remains of vein (?)
39210	T52822	Contact between crystals
39211	T52823	Margin - very faint
39213(1)	T52824/25	Contact between dark (epidote?) with texture/striations, and light vein qtz(?)
39213(1)	T52826	Mix of epidote and other minerals at vein contact
39213(1)	T52827	Boundary of vein w/ ?cpy grain
39213(3)	T52828	stringer/fracture
39213(3)	T52829	Fracture with Mo close by
39213(3)	T52830	Mo and alteration at cavity/vug margin
39213(3)	T52831	close up of Mo
39213(3)	T52832	possible fracture/cavity crosscutting vein, also possible crosscutting vein on other side
39214	T52833	vein contact w/sulphide grain (+T52834 = zoomed out)
39214	T52835	sulphides/Mo in vein zoomed out. T52836 - close up inc intergrowth?
39214	T52837	Sulphides in vein
39214	T52838	Sulphides in vein
39214	T52839	More sulphides in vein
39214	T52840	close up sulphides in vein
39215(1)	T52900	Vein contact against large sulphide grain.

39215(1)	T52901	Close up of vein contact with groundmass and sulphide grain
39215(1)	T52902	Vein with small sulphide grains, alteration halo OR 2 fluid phases T52903 - Close up
39215(1)	T52904/05	narrow stringer w/ sulphides
39215(2)	T52906	Large grain w/ Mo and sulphides
39215(2)	T52907	displacement and crosscutting of grain in corner
39215(2)	T52907	middle section with highly included grain
39215(2)	T52909	Grain interactions in groundmass
39216	T52910	Fracture/vein
39216	T52911	close up of contact
39216	T52912/13	Fracture zone (unclear) w/ close up
39217	T52914/15	contact of vein
39217	T52916/17	vein contact w/ sulphides - NB Mo in groundmass not vein??
39217	T52918/19	Cpy/Py in vein next to contact
39218	T52954/55	granite-porphyry contact with vein crosscutting
39218	T52956	2x veins at contact between granite and porphyry
39218	T52957	Sulphide in stringer
39218	T52958/59	close up of centre of grain
39219(2)	T52960/61/62	Sulphide in vein plus close ups. 62 = possible alteration of sulphide w/ granite alteration?
39219(2)	T52963	Mo + Sulphides intergrowth in groundmass
39219(2)	T52964/65	Alteration of sulphides in veinlet - py, cpy, titanite (?)
39220	T52966	Crystal contact - NB Large void/chip in grain
39220	T52967/68	Sulphides + sphalerite (?) (Zn, Na, S) near void/sulphide mass + 68 = close up
39220	T52969	Galena in Pyrite 70 - dextral offset at fracture?? Coeval with fracturing?
39220	T52971	Galena with FeAsSb and FeAs minerals - NB - late stage in pyrite
39220	T52972/73	fracturing and veining cpy and py etc. 73 - close up w/ galena etc.
39220	T52974	Galena to left of fracture in Py
39220	T52975	lots of intergrowing elements, Cpy

Appendix 3 Light Microscope Imagery

Reflected light (left) and transmitted light (right) microscope photographs

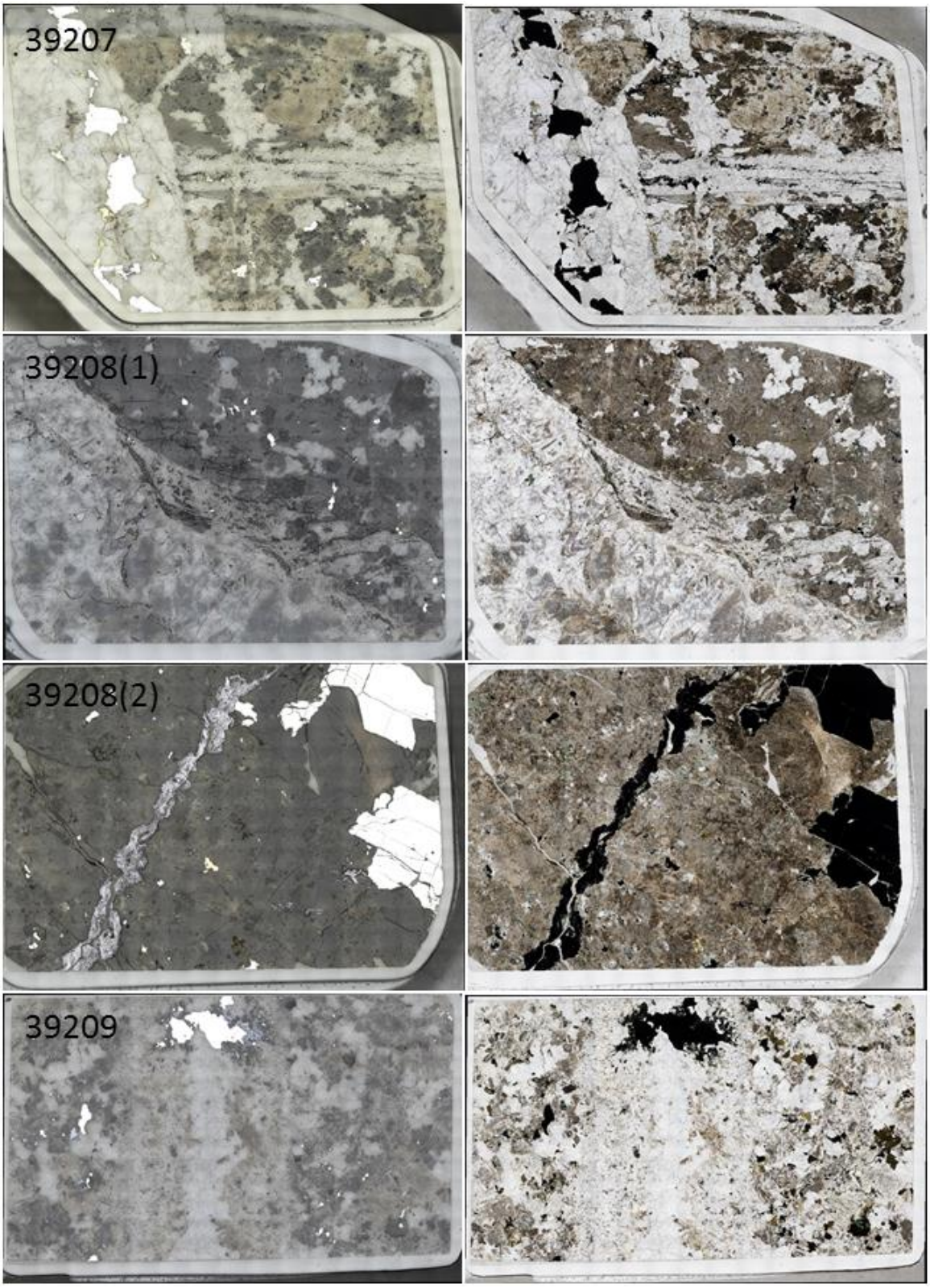

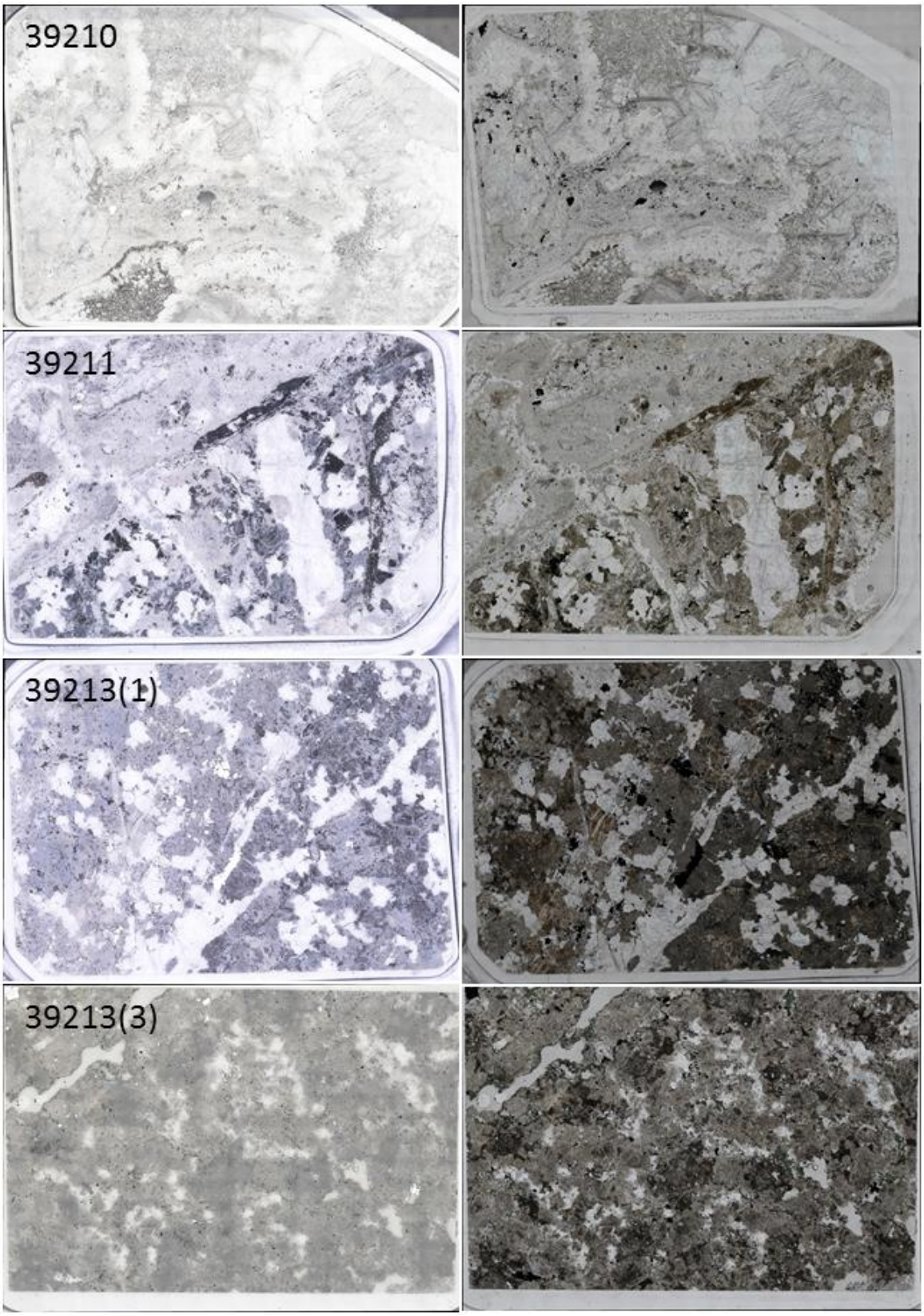
39210
39211
39213(1)
39213(3)

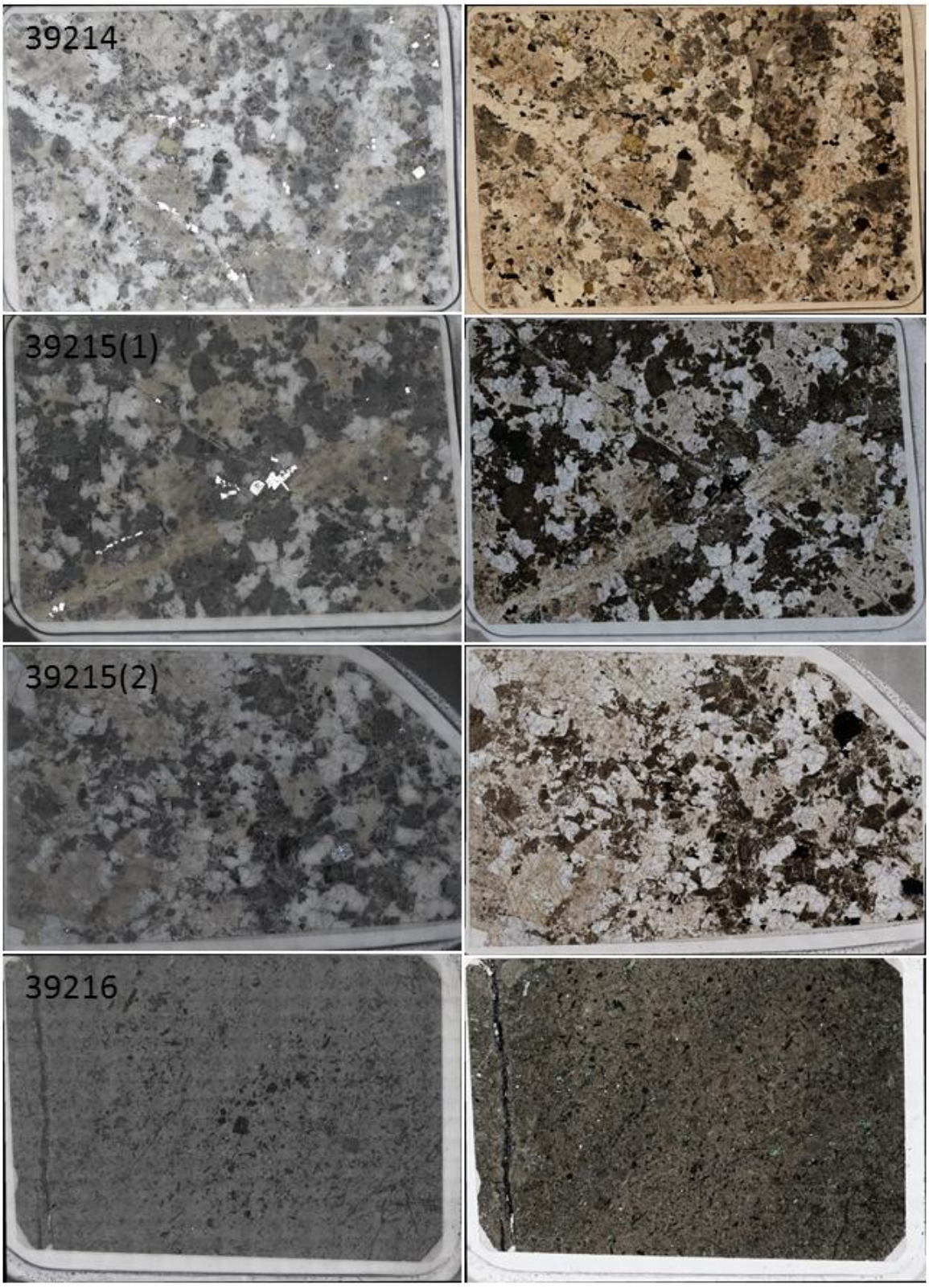
39214
39215(1)
39215(2)
39216

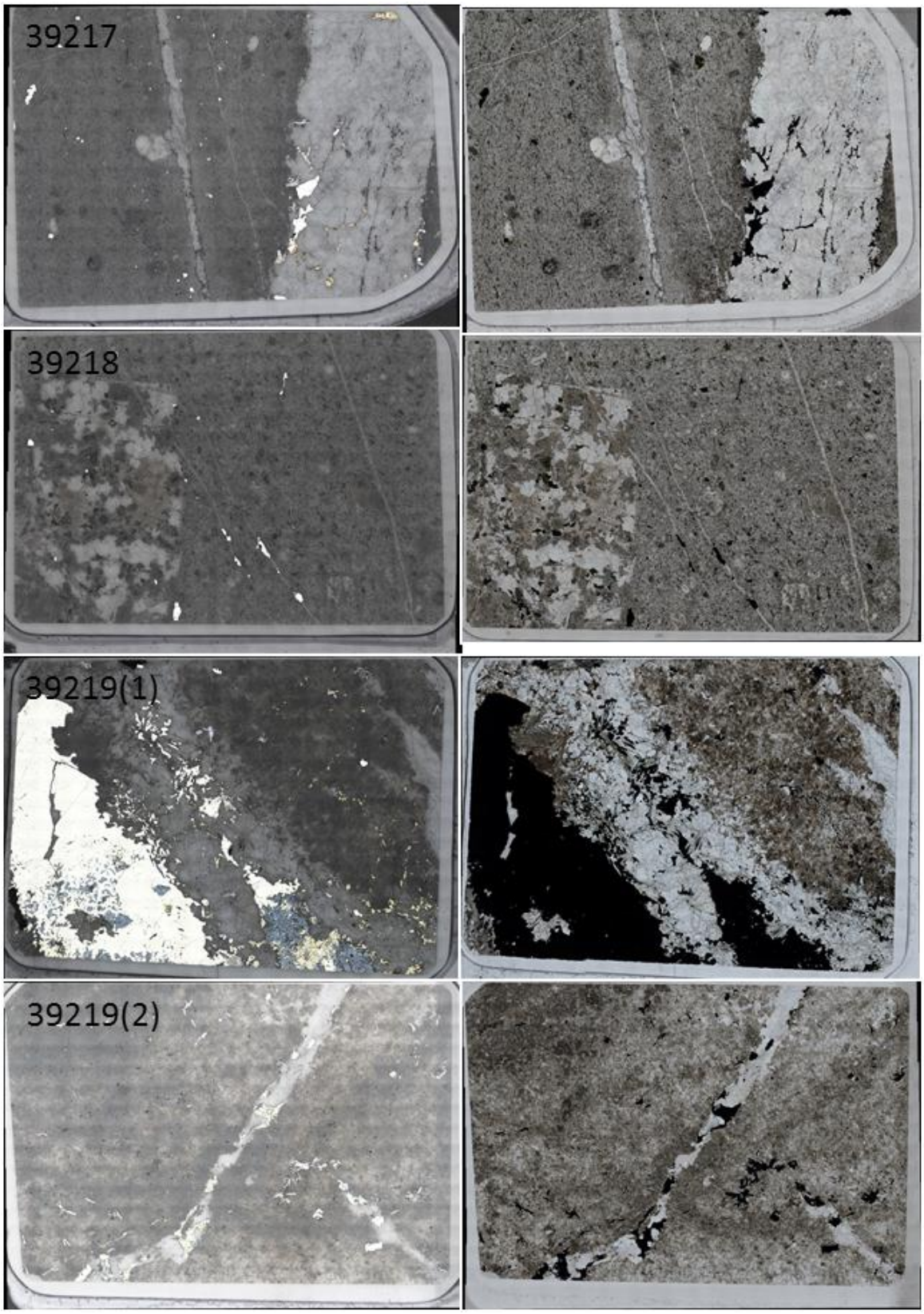
39217
39218
39219(1)
39219(2)

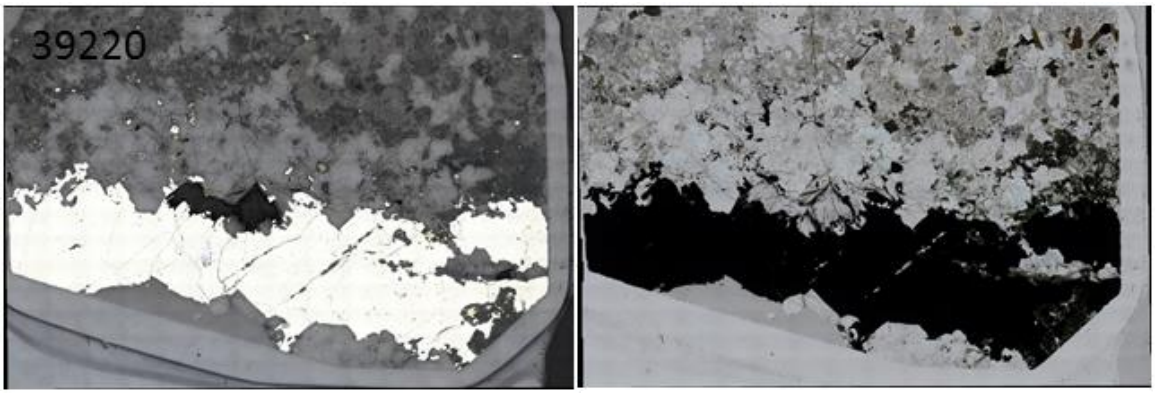
39220

Appendix 4 SEM Images

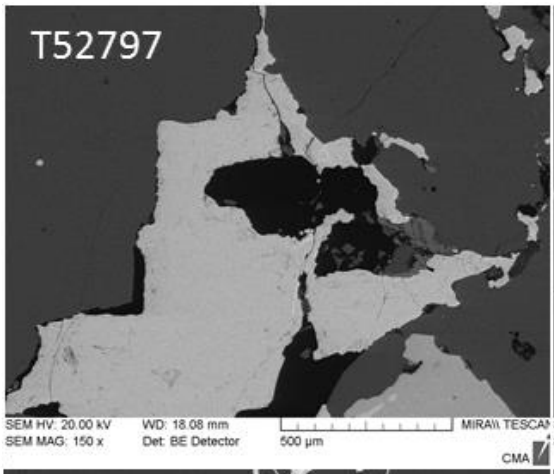
T52797
SEM HV: 20.00 kV
SEM MAG: 150 x
WD: 18.08 mm
Det: BE Detector
500 µm
MIRA\\ TESCAN
CMA

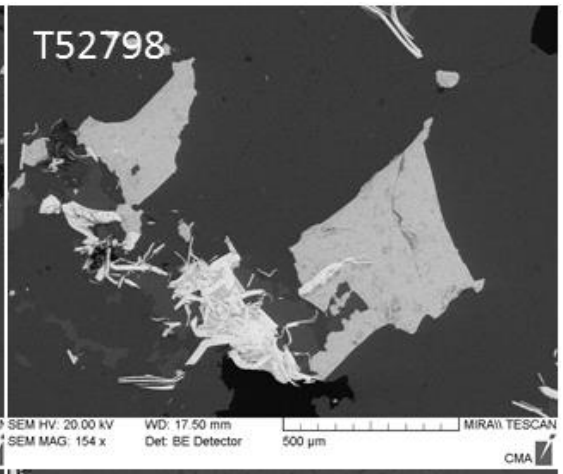
T52798
SEM HV: 20.00 kV
SEM MAG: 154 x
WD: 17.50 mm
Det: BE Detector
500 µm
MIRA\\ TESCAN
CMA

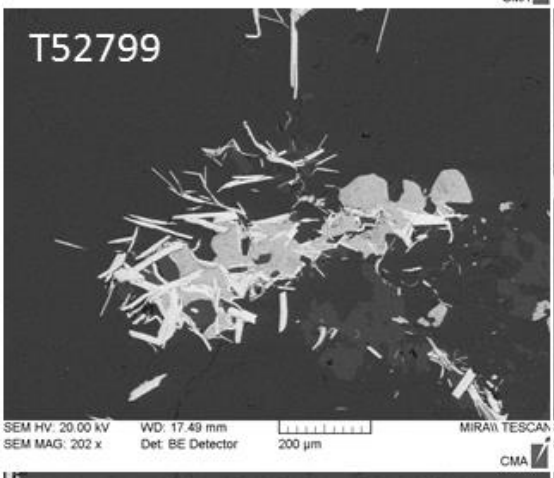
T52799
SEM HV: 20.00 kV
SEM MAG: 202 x
WD: 17.49 mm
Det: BE Detector
200 µm
MIRA\\ TESCAN
CMA

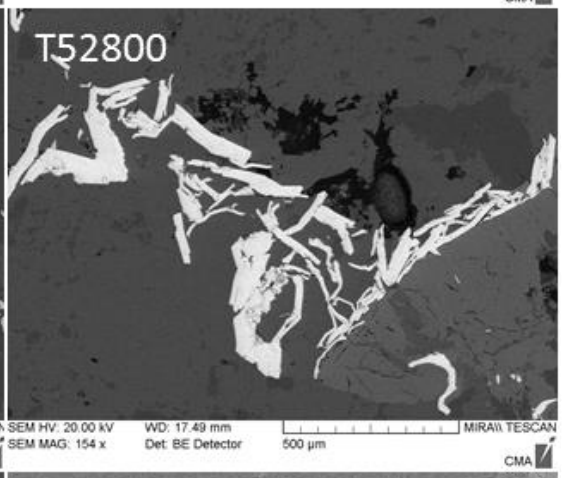
T52800
SEM HV: 20.00 kV
SEM MAG: 154 x
WD: 17.49 mm
Det: BE Detector
500 µm
MIRA\\ TESCAN
CMA

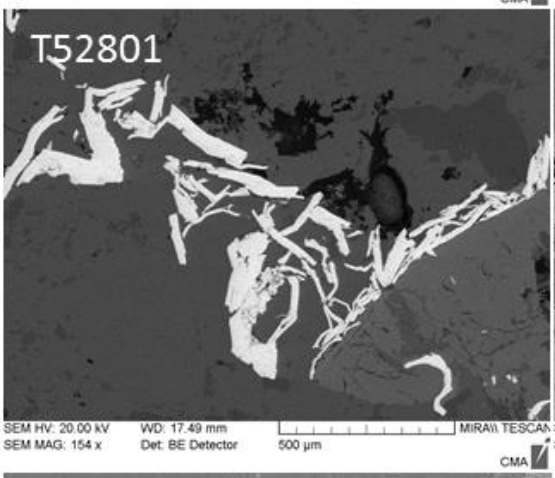
T52801
SEM HV: 20.00 kV
SEM MAG: 154 x
WD: 17.49 mm
Det: BE Detector
500 µm
MIRA\\ TESCAN
CMA

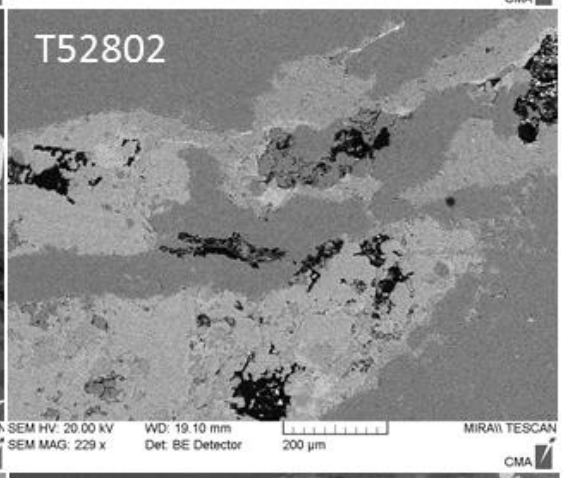
T52802
SEM HV: 20.00 kV
SEM MAG: 229 x
WD: 19.10 mm
Det: BE Detector
200 µm
MIRA\\ TESCAN
CMA

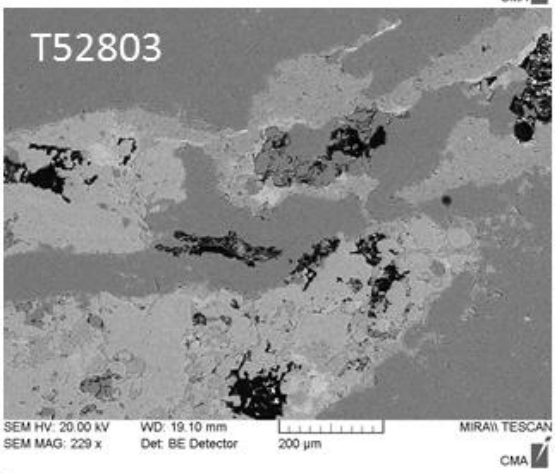
T52803
SEM HV: 20.00 kV
SEM MAG: 229 x
WD: 19.10 mm
Det: BE Detector
200 µm
MIRA\\ TESCAN
CMA

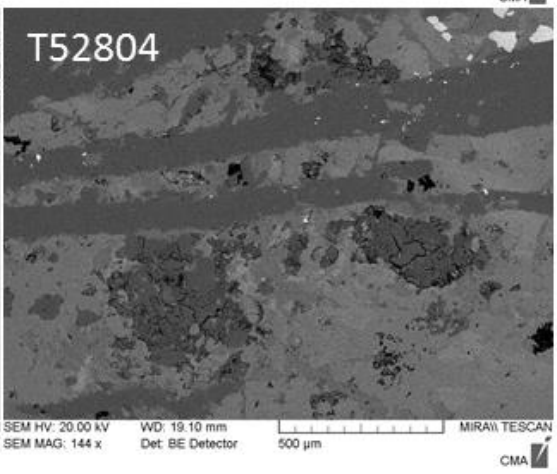
T52804
SEM HV: 20.00 kV
SEM MAG: 144 x
WD: 19.10 mm
Det: BE Detector
500 µm
MIRA\\ TESCAN
CMA

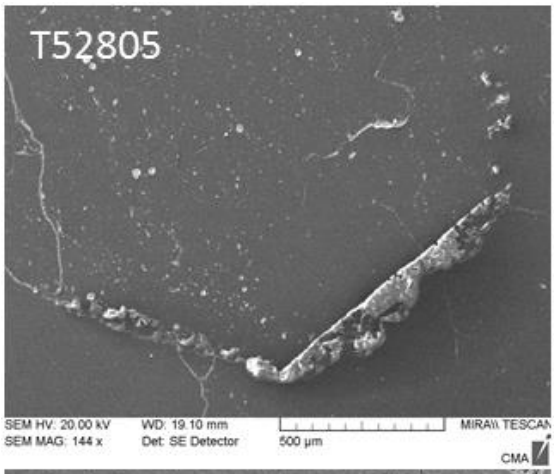
T52805
SEM HV: 20.00 kV
SEM MAG: 144 x
WD: 19.10 mm
Det: SE Detector
500 µm
MIRA\\ TESCAN
CMA

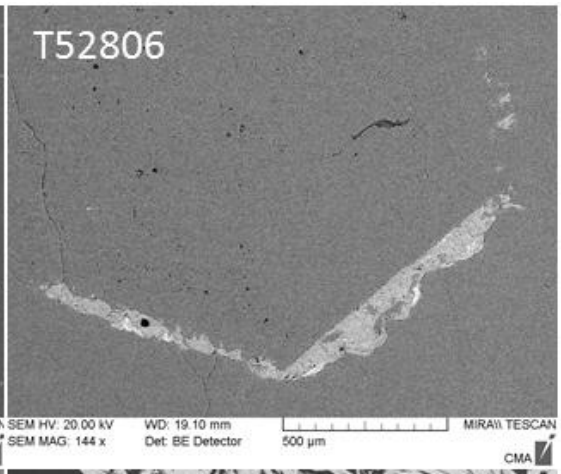
T52806
SEM HV: 20.00 kV
SEM MAG: 144 x
WD: 19.10 mm
Det: BE Detector
500 µm
MIRA\\ TESCAN
CMA

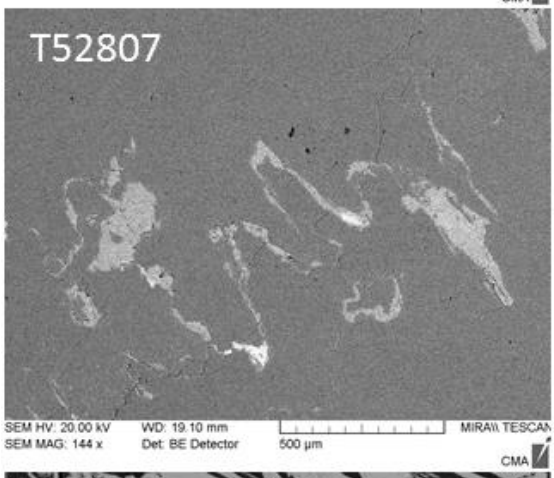
T52807
SEM HV: 20.00 kV
SEM MAG: 144 x
WD: 19.10 mm
Det: BE Detector
500 µm
MIRA\\ TESCAN
CMA

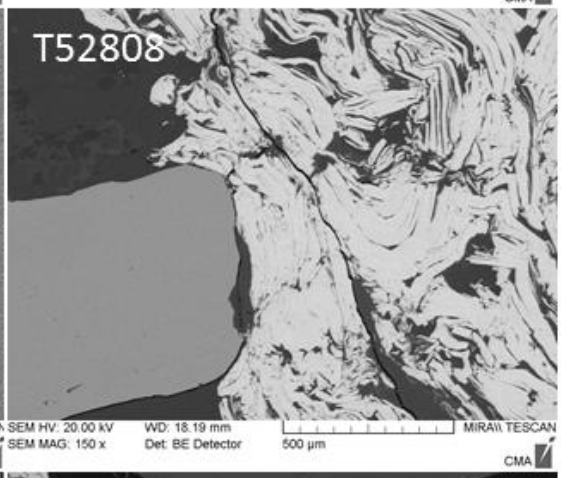
T52808
SEM HV: 20.00 kV
SEM MAG: 150 x
WD: 18.19 mm
Det: BE Detector
500 µm
MIRA\\ TESCAN
CMA

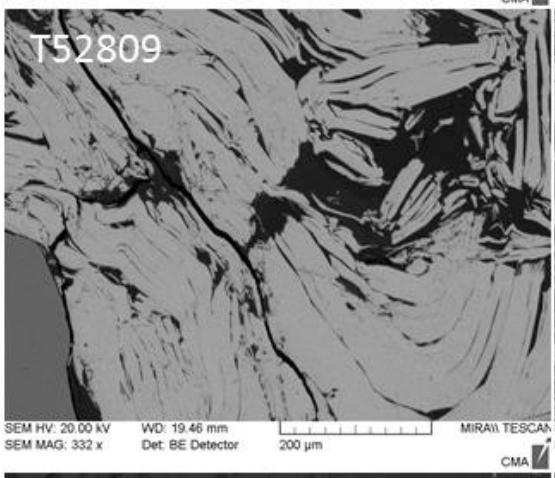
T52809
SEM HV: 20.00 kV
SEM MAG: 332 x
WD: 19.46 mm
Det: BE Detector
200 µm
MIRA\\ TESCAN
CMA

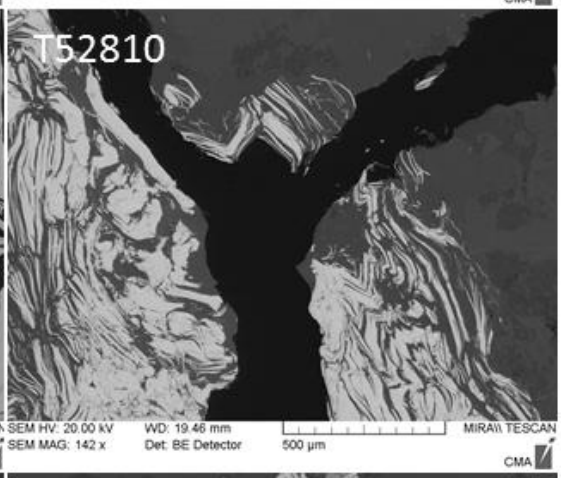
T52810
SEM HV: 20.00 kV
SEM MAG: 142 x
WD: 19.46 mm
Det: BE Detector
500 µm
MIRA\\ TESCAN
CMA

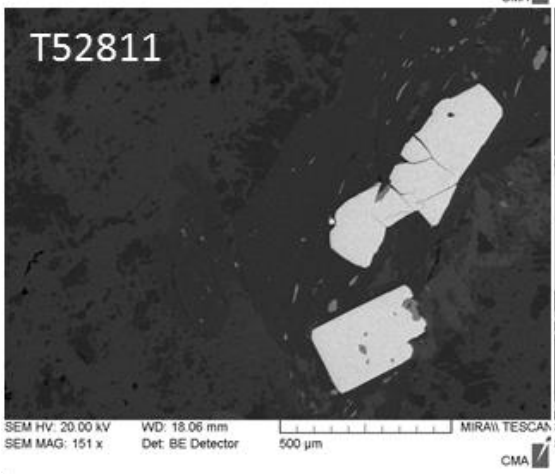
T52811
SEM HV: 20.00 kV
SEM MAG: 151 x
WD: 18.06 mm
Det: BE Detector
500 µm
MIRA\\ TESCAN
CMA

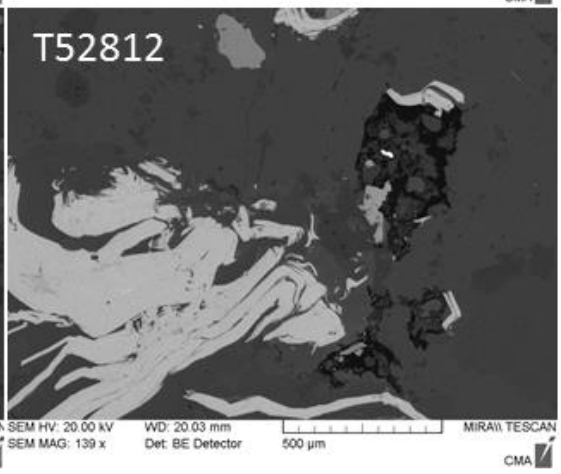
T52812
SEM HV: 20.00 kV
SEM MAG: 139 x
WD: 20.03 mm
Det: BE Detector
500 µm
MIRA\\ TESCAN
CMA

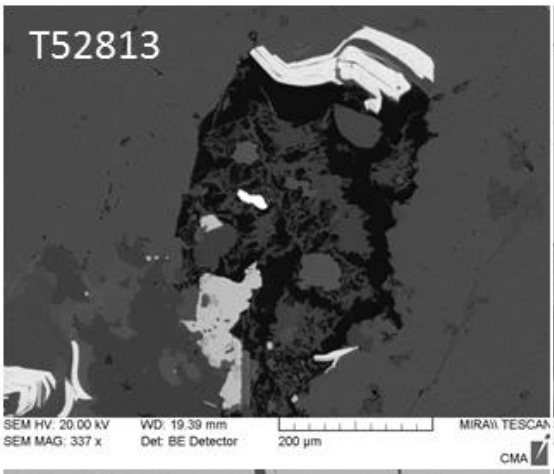
T52813
SEM HV: 20.00 kV
SEM MAG: 337 x
WD: 19.39 mm
Det: BE Detector
200 µm
MIRA\\ TESCAN
CMA

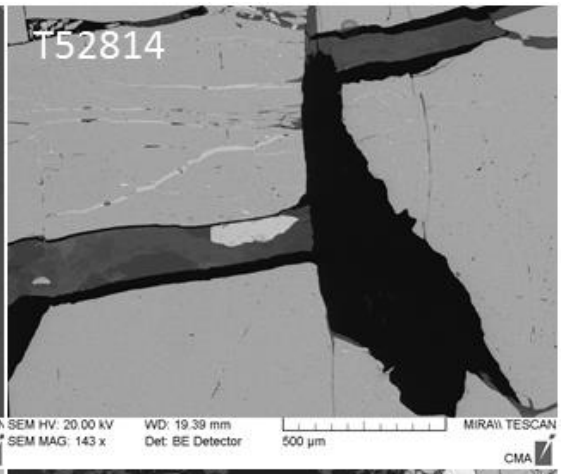
T52814
SEM HV: 20.00 kV
SEM MAG: 143 x
WD: 19.39 mm
Det: BE Detector
500 µm
MIRA\\ TESCAN
CMA

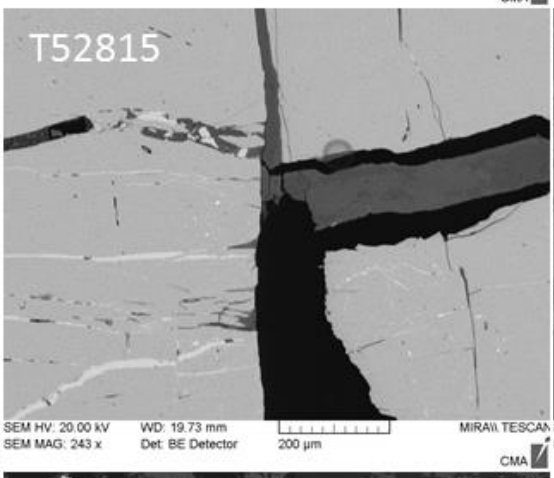
T52815
SEM HV: 20.00 kV
SEM MAG: 243 x
WD: 19.73 mm
Det: BE Detector
200 µm
MIRA\\ TESCAN
CMA

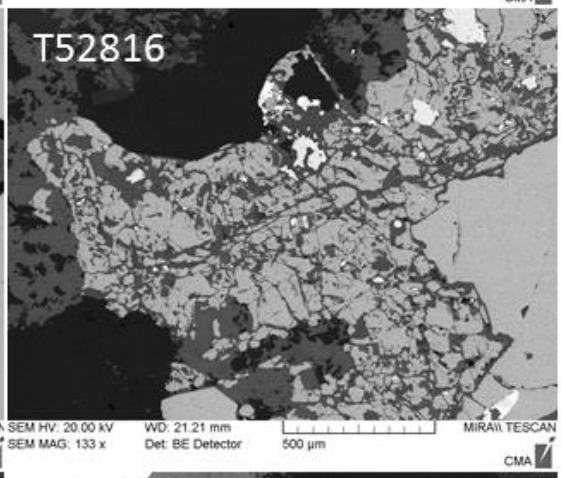
T52816
SEM HV: 20.00 kV
SEM MAG: 133 x
WD: 21.21 mm
Det: BE Detector
500 µm
MIRA\\ TESCAN
CMA

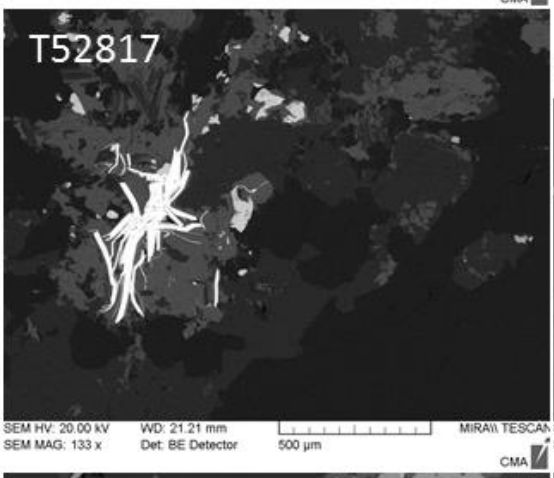
T52817
SEM HV: 20.00 kV
SEM MAG: 133 x
WD: 21.21 mm
Det: BE Detector
500 µm
MIRA\\ TESCAN
CMA

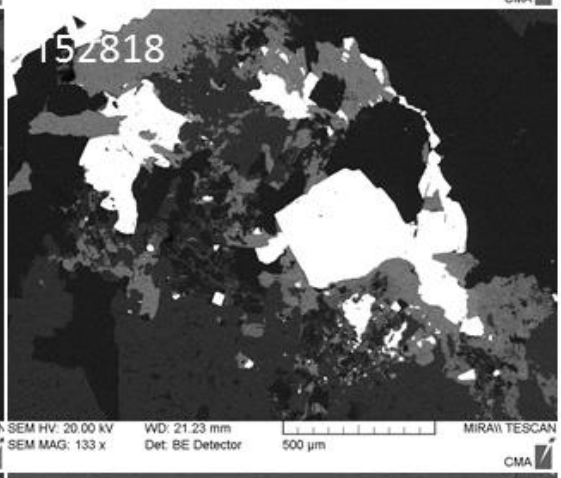
T52818
SEM HV: 20.00 kV
SEM MAG: 133 x
WD: 21.23 mm
Det: BE Detector
500 µm
MIRA\\ TESCAN
CMA

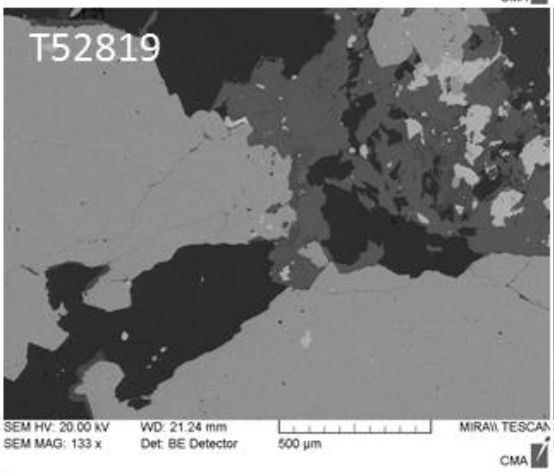
T52819
SEM HV: 20.00 kV
SEM MAG: 133 x
WD: 21.24 mm
Det: BE Detector
500 µm
MIRA\\ TESCAN
CMA

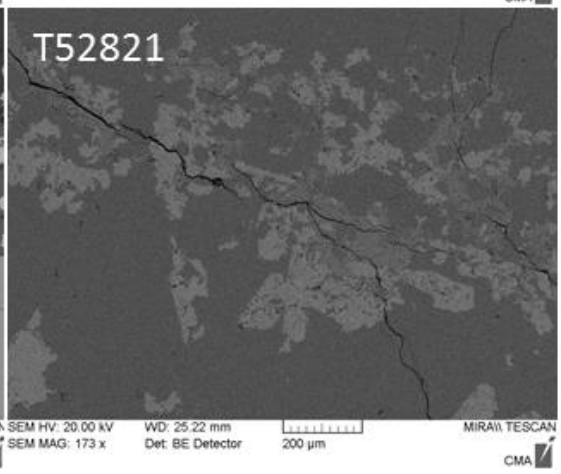
T52821
SEM HV: 20.00 kV
SEM MAG: 173 x
WD: 25.22 mm
Det: BE Detector
200 µm
MIRA\\ TESCAN
CMA

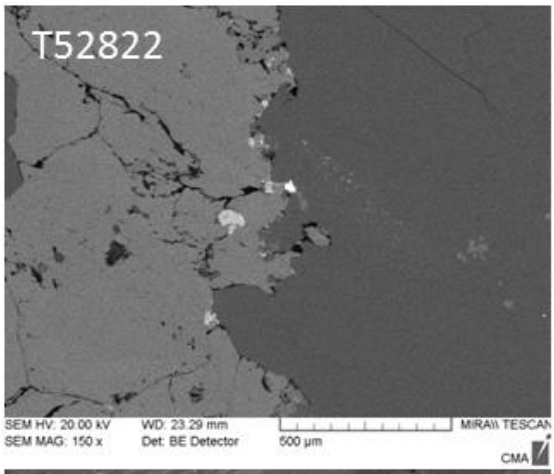
T52822
SEM HV: 20.00 kV
SEM MAG: 150 x
WD: 23.29 mm
Det: BE Detector
500 µm
MIRA\\ TESCAN
CMA

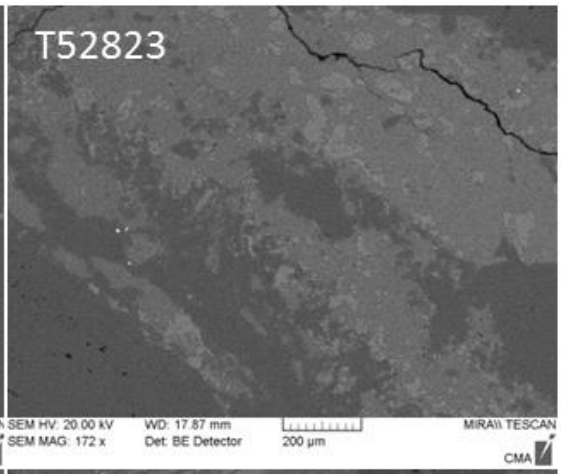
T52823
SEM HV: 20.00 kV
SEM MAG: 172 x
WD: 17.87 mm
Det: BE Detector
200 µm
MIRA\\ TESCAN
CMA

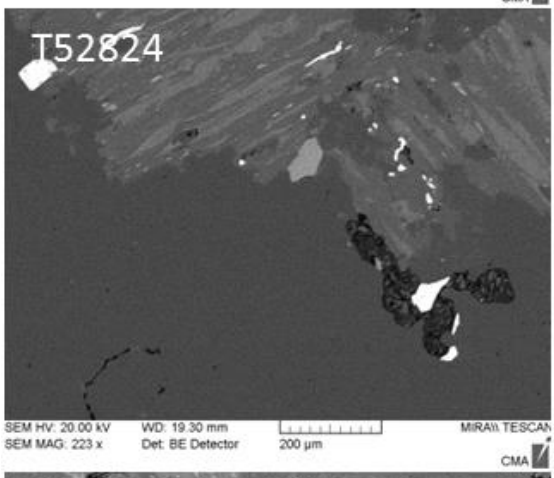
T52824
SEM HV: 20.00 kV
SEM MAG: 223 x
WD: 19.30 mm
Det: BE Detector
200 µm
MIRA\\ TESCAN
CMA

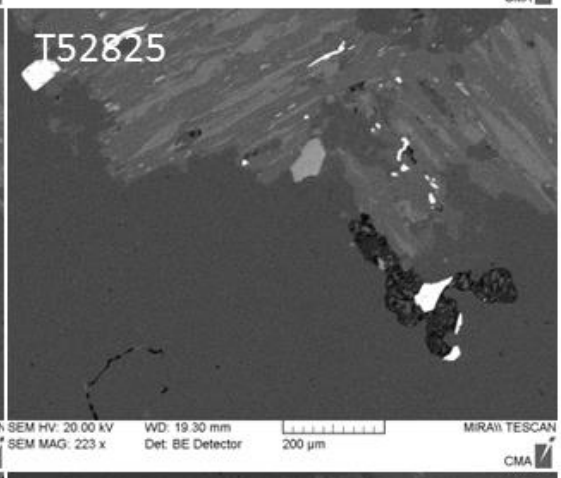
T52825
SEM HV: 20.00 kV
SEM MAG: 223 x
WD: 19.30 mm
Det: BE Detector
200 µm
MIRA\\ TESCAN
CMA

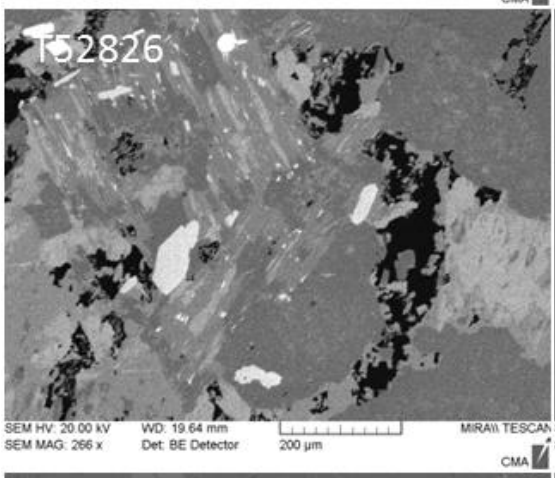
T52826
SEM HV: 20.00 kV
SEM MAG: 266 x
WD: 19.64 mm
Det: BE Detector
200 µm
MIRA\\ TESCAN
CMA

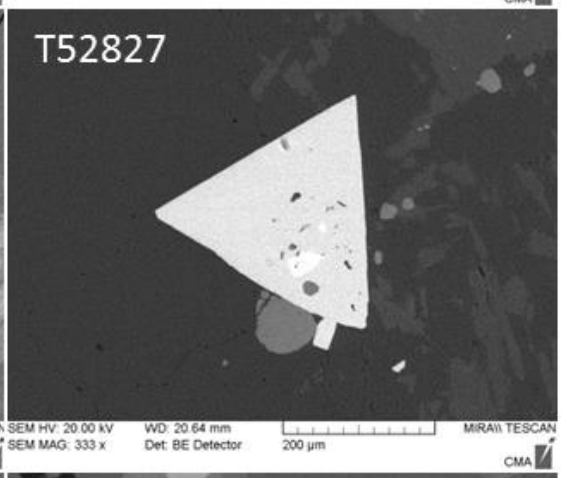
T52827
SEM HV: 20.00 kV
SEM MAG: 333 x
WD: 20.64 mm
Det: BE Detector
200 µm
MIRA\\ TESCAN
CMA

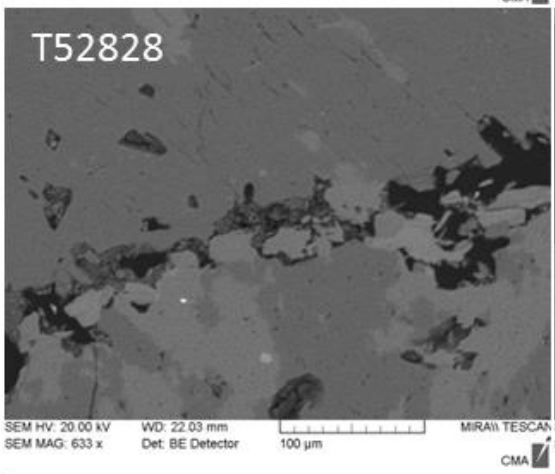
T52828
SEM HV: 20.00 kV
SEM MAG: 633 x
WD: 22.03 mm
Det: BE Detector
100 µm
MIRA\\ TESCAN
CMA

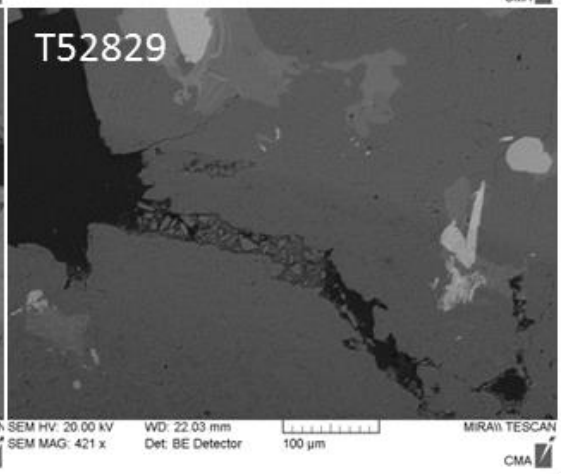
T52829
SEM HV: 20.00 kV
SEM MAG: 421 x
WD: 22.03 mm
Det: BE Detector
100 µm
MIRA\\ TESCAN
CMA

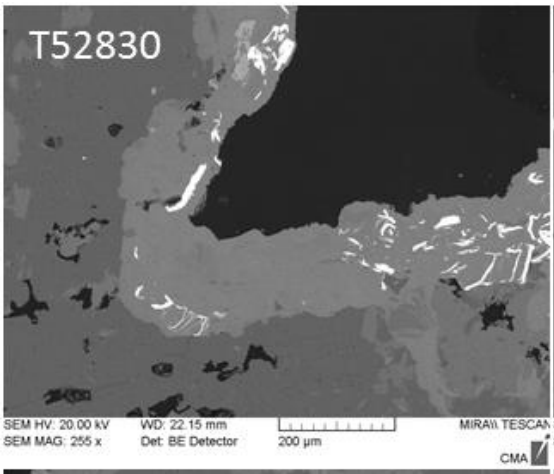
T52830
SEM HV: 20.00 kV
SEM MAG: 255 x
WD: 22.15 mm
Det: BE Detector
200 µm
MIRA\\ TESCAN
CMA

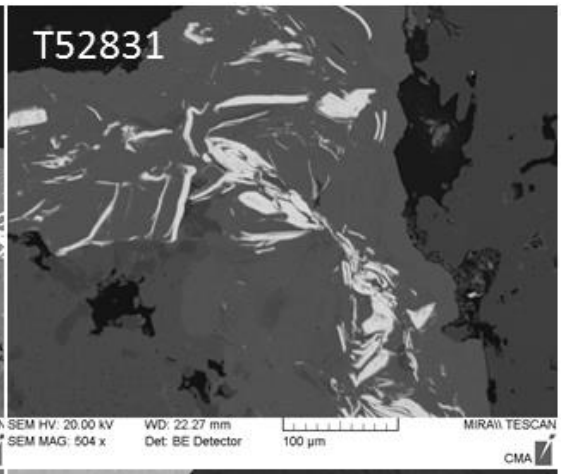
T52831
SEM HV: 20.00 kV
SEM MAG: 504 x
WD: 22.27 mm
Det: BE Detector
100 µm
MIRA\\ TESCAN
CMA

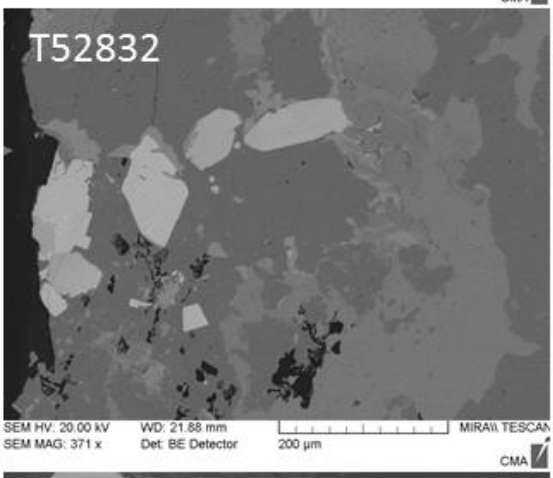
T52832
SEM HV: 20.00 kV
SEM MAG: 371 x
WD: 21.88 mm
Det: BE Detector
200 µm
MIRA\\ TESCAN
CMA

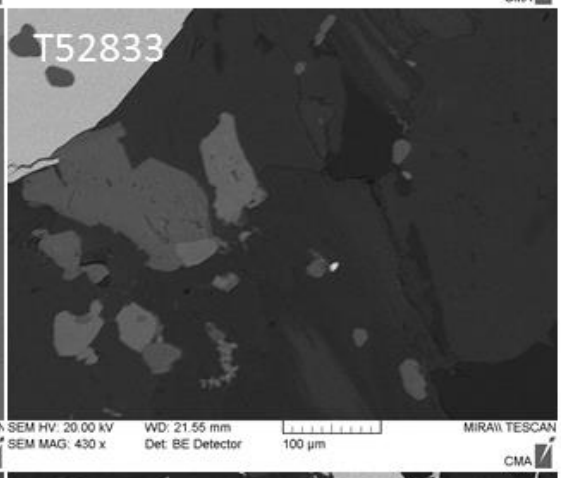
T52833
SEM HV: 20.00 kV
SEM MAG: 430 x
WD: 21.55 mm
Det: BE Detector
100 µm
MIRA\\ TESCAN
CMA

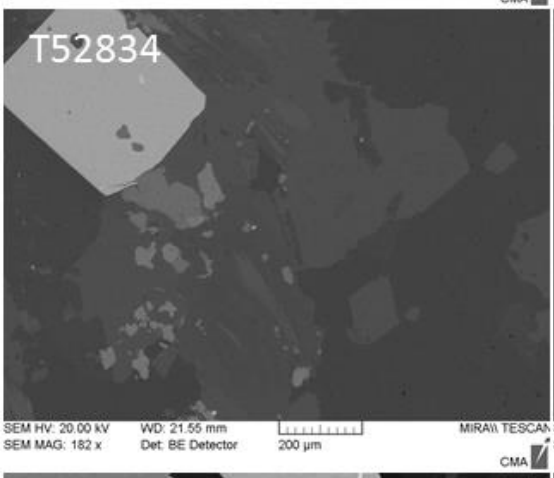
T52834
SEM HV: 20.00 kV
SEM MAG: 182 x
WD: 21.55 mm
Det: BE Detector
200 µm
MIRA\\ TESCAN
CMA

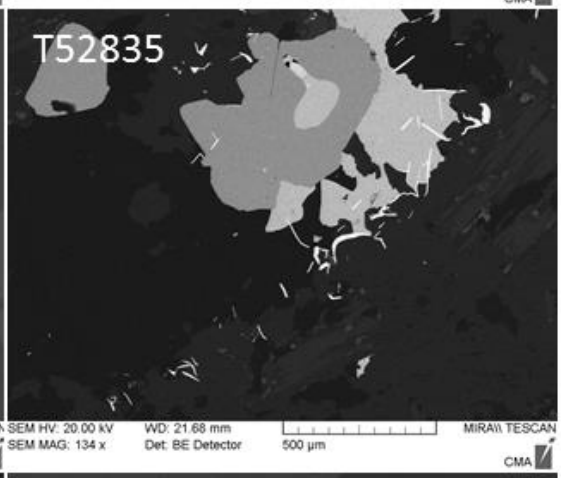
T52835
SEM HV: 20.00 kV
SEM MAG: 134 x
WD: 21.68 mm
Det: BE Detector
500 µm
MIRA\\ TESCAN
CMA

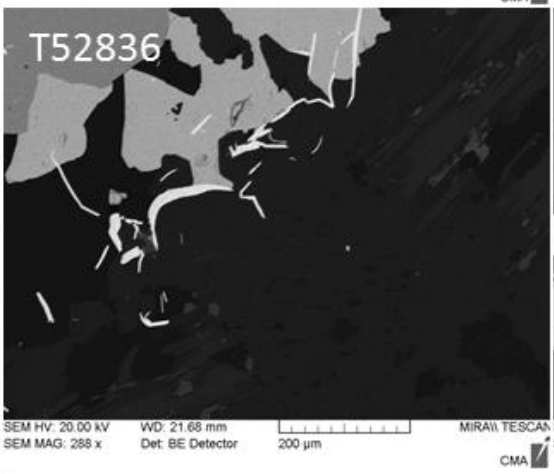
T52836
SEM HV: 20.00 kV
SEM MAG: 288 x
WD: 21.68 mm
Det: BE Detector
200 µm
MIRA\\ TESCAN
CMA

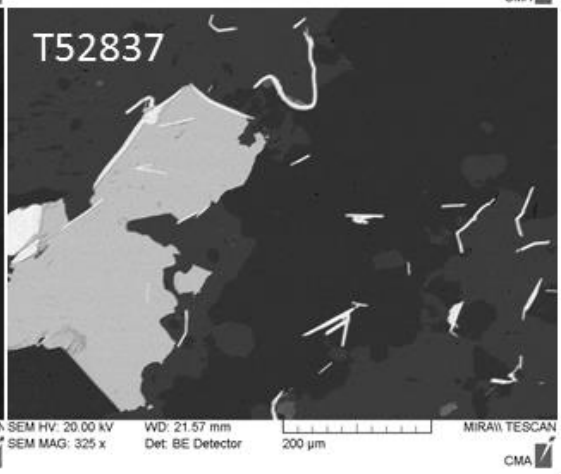
T52837
SEM HV: 20.00 kV
SEM MAG: 325 x
WD: 21.57 mm
Det: BE Detector
200 µm
MIRA\\ TESCAN
CMA

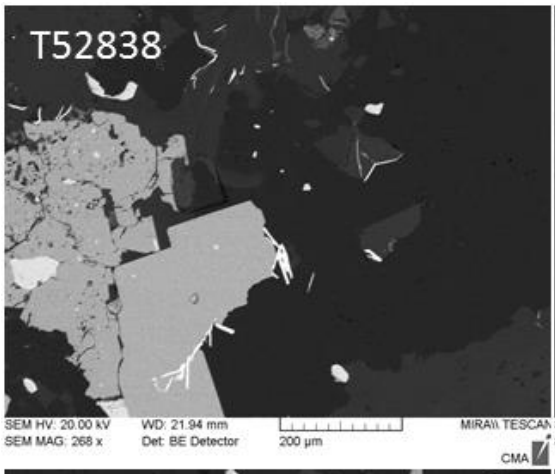
T52838
SEM HV: 20.00 kV
SEM MAG: 268 x
WD: 21.94 mm
Det: BE Detector
200 µm
MIRA\\ TESCAN
CMA

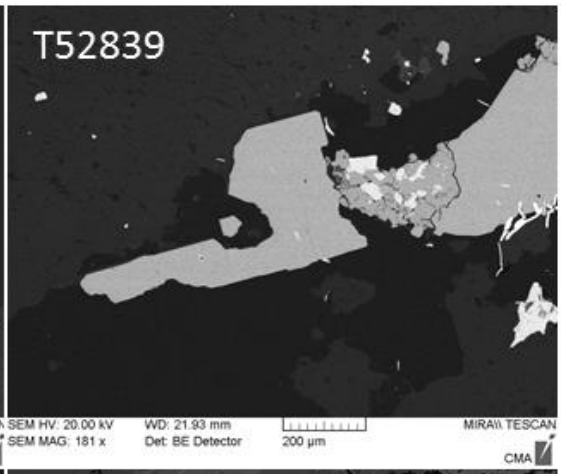
T52839
SEM HV: 20.00 kV
SEM MAG: 181 x
WD: 21.93 mm
Det: BE Detector
200 µm
MIRA\\ TESCAN
CMA

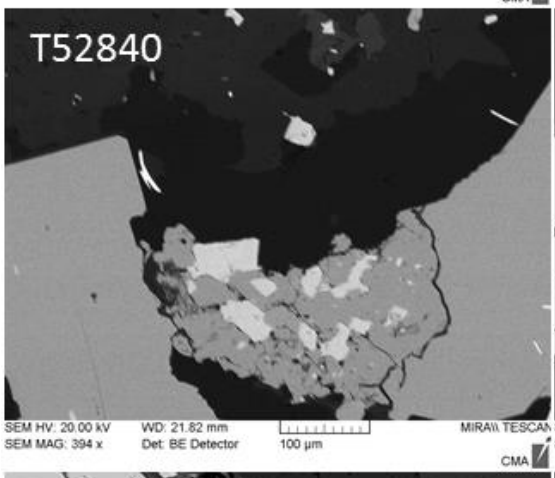
T52840
SEM HV: 20.00 kV
SEM MAG: 394 x
WD: 21.82 mm
Det: BE Detector
100 µm
MIRA\\ TESCAN
CMA

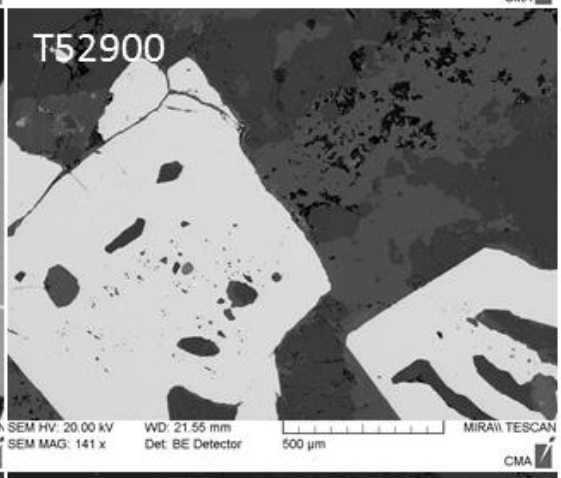
T52900
SEM HV: 20.00 kV
SEM MAG: 141 x
WD: 21.55 mm
Det: BE Detector
500 µm
MIRA\\ TESCAN
CMA

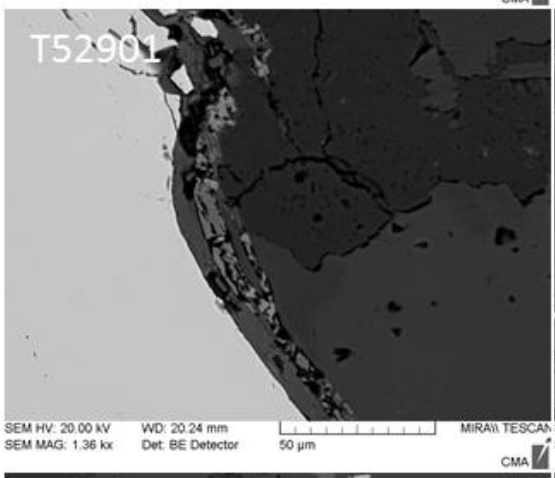
T52901
SEM HV: 20.00 kV
SEM MAG: 1.36 kx
WD: 20.24 mm
Det: BE Detector
50 µm
MIRA\\ TESCAN
CMA

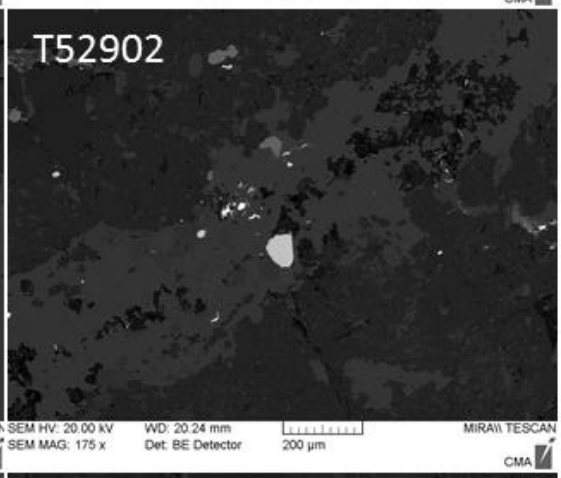
T52902
SEM HV: 20.00 kV
SEM MAG: 175 x
WD: 20.24 mm
Det: BE Detector
200 µm
MIRA\\ TESCAN
CMA

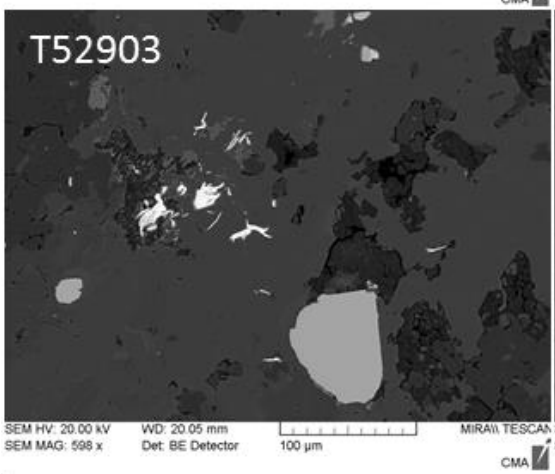
T52903
SEM HV: 20.00 kV
SEM MAG: 598 x
WD: 20.05 mm
Det: BE Detector
100 µm
MIRA\\ TESCAN
CMA

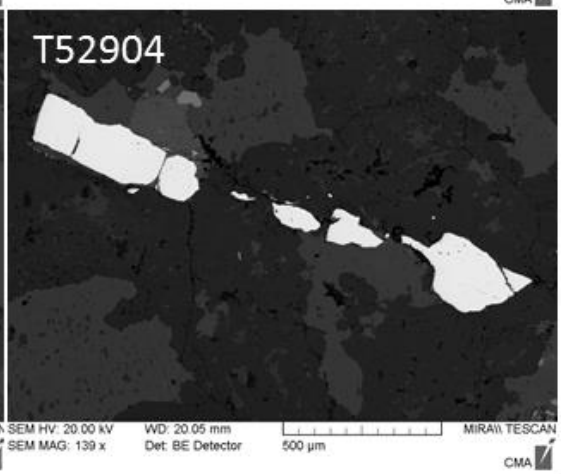
T52904
SEM HV: 20.00 kV
SEM MAG: 139 x
WD: 20.05 mm
Det: BE Detector
500 µm
MIRA\\ TESCAN
CMA

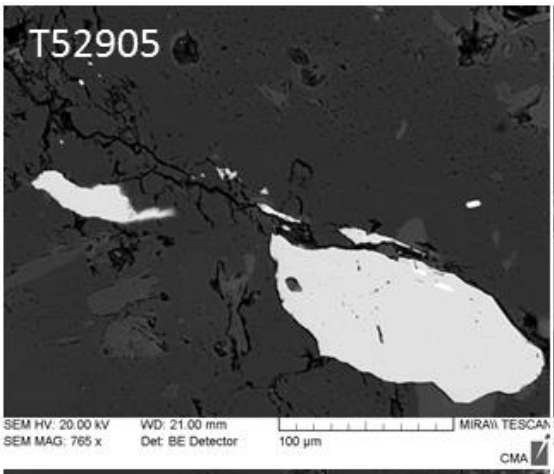
T52905
SEM HV: 20.00 kV
SEM MAG: 765 x
WD: 21.00 mm
Det: BE Detector
100 µm
MIRA\\ TESCAN
CMA

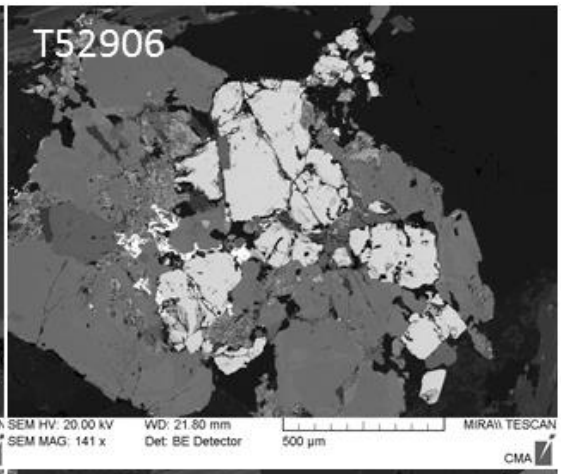
T52906
SEM HV: 20.00 kV
SEM MAG: 141 x
WD: 21.80 mm
Det: BE Detector
500 µm
MIRA\\ TESCAN
CMA

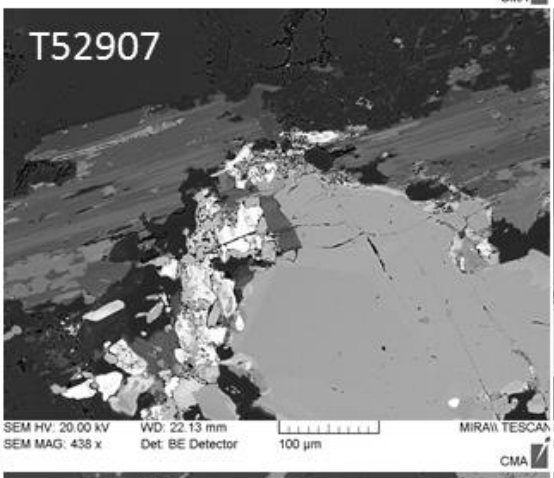
T52907
SEM HV: 20.00 kV
SEM MAG: 438 x
WD: 22.13 mm
Det: BE Detector
100 µm
MIRA\\ TESCAN
CMA

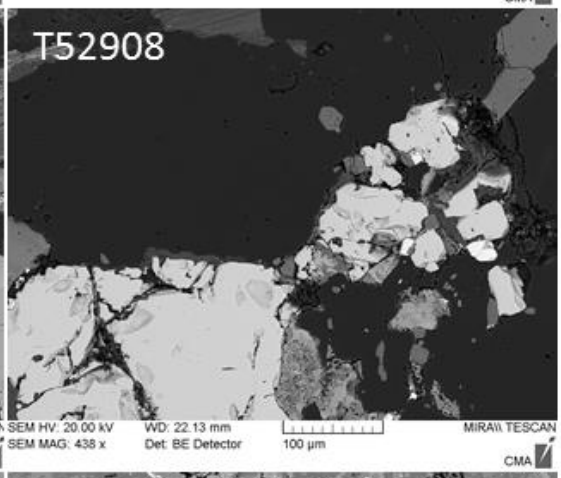
T52908
SEM HV: 20.00 kV
SEM MAG: 438 x
WD: 22.13 mm
Det: BE Detector
100 µm
MIRA\\ TESCAN
CMA

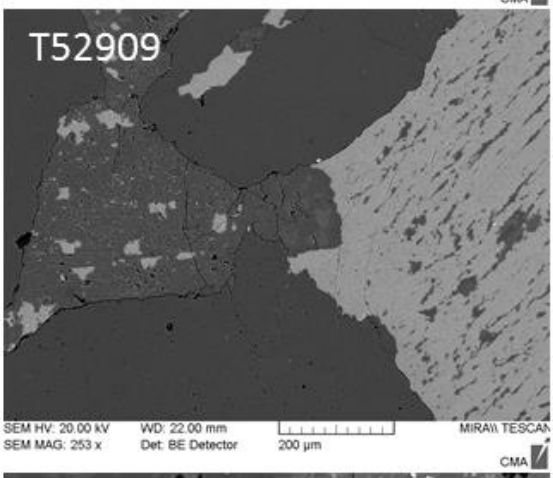
T52909
SEM HV: 20.00 kV
SEM MAG: 253 x
WD: 22.00 mm
Det: BE Detector
200 µm
MIRA\\ TESCAN
CMA

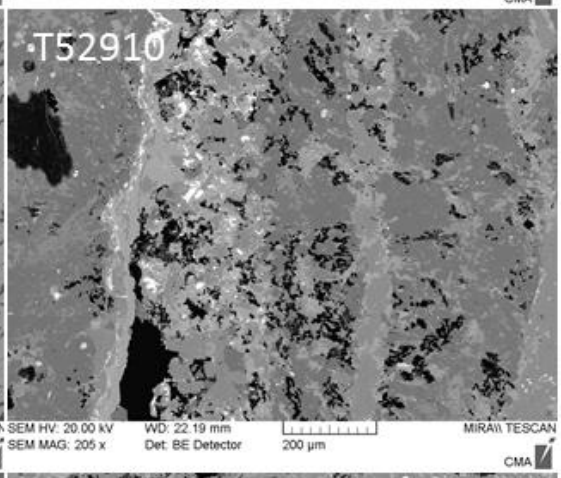
T52910
SEM HV: 20.00 kV
SEM MAG: 205 x
WD: 22.19 mm
Det: BE Detector
200 µm
MIRA\\ TESCAN
CMA

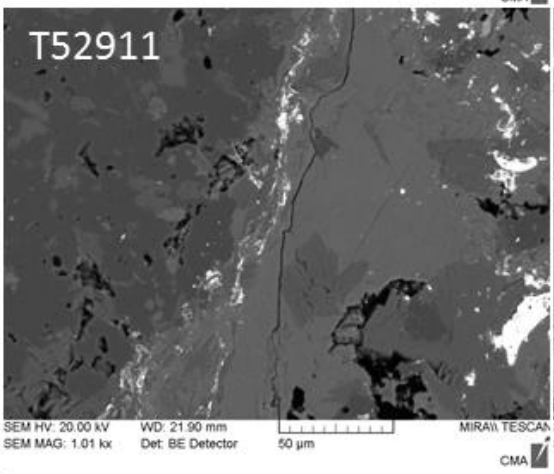
T52911
SEM HV: 20.00 kV
SEM MAG: 1.01 kx
WD: 21.90 mm
Det: BE Detector
50 µm
MIRA\\ TESCAN
CMA

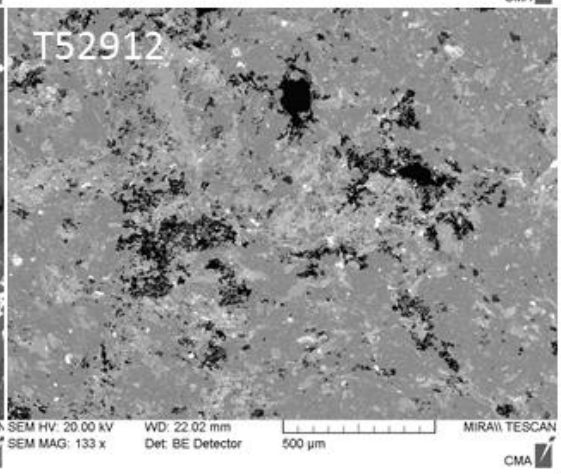
T52912
SEM HV: 20.00 kV
SEM MAG: 133 x
WD: 22.02 mm
Det: BE Detector
500 µm
MIRA\\ TESCAN
CMA

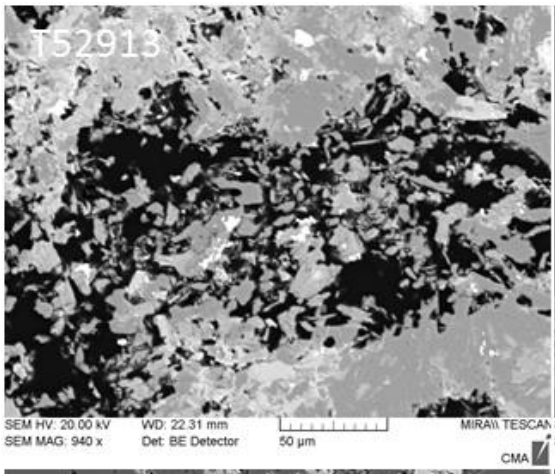
T52913
SEM HV: 20.00 kV
SEM MAG: 940 x
WD: 22.31 mm
Det: BE Detector
50 µm
MIRA\\ TESCAN
CMA

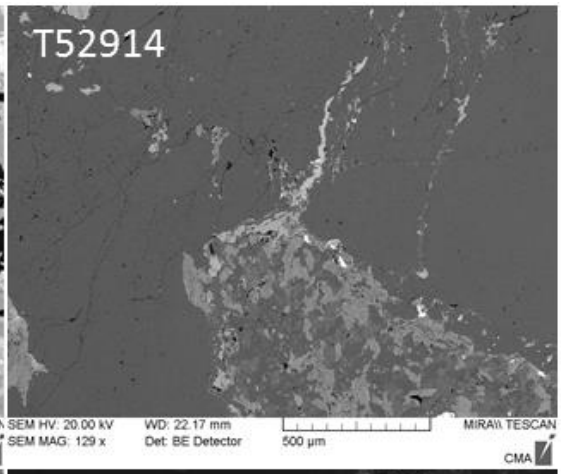
T52914
SEM HV: 20.00 kV
SEM MAG: 129 x
WD: 22.17 mm
Det: BE Detector
500 µm
MIRA\\ TESCAN
CMA

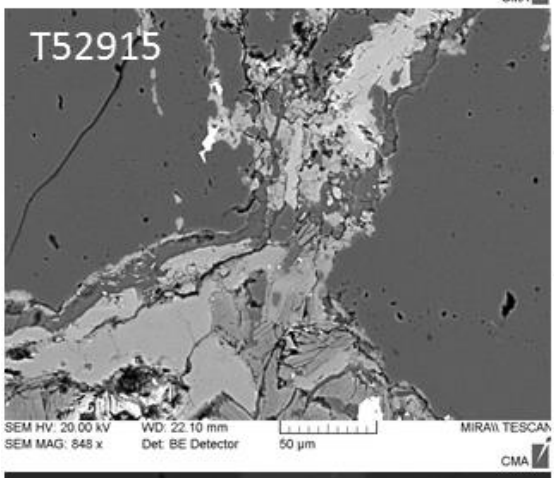
T52915
SEM HV: 20.00 kV
SEM MAG: 848 x
WD: 22.10 mm
Det: BE Detector
50 µm
MIRA\\ TESCAN
CMA

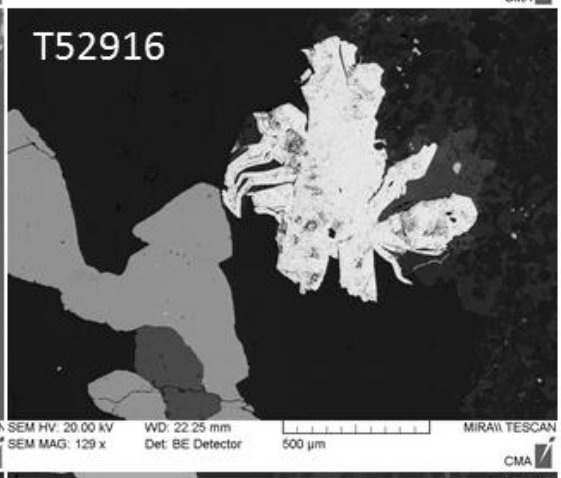
T52916
SEM HV: 20.00 kV
SEM MAG: 129 x
WD: 22.25 mm
Det: BE Detector
500 µm
MIRA\\ TESCAN
CMA

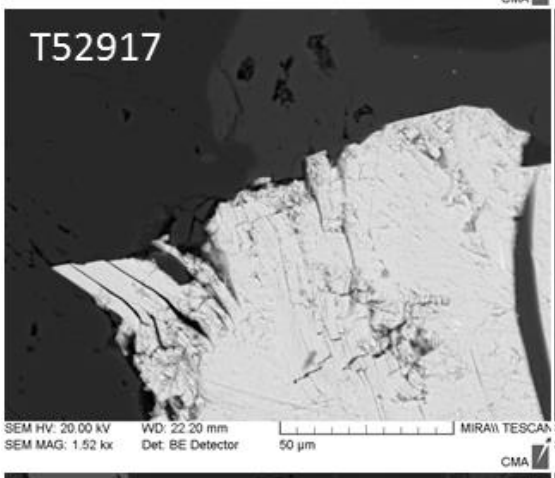
T52917
SEM HV: 20.00 kV
SEM MAG: 1.52 kx
WD: 22.20 mm
Det: BE Detector
50 µm
MIRA\\ TESCAN
CMA

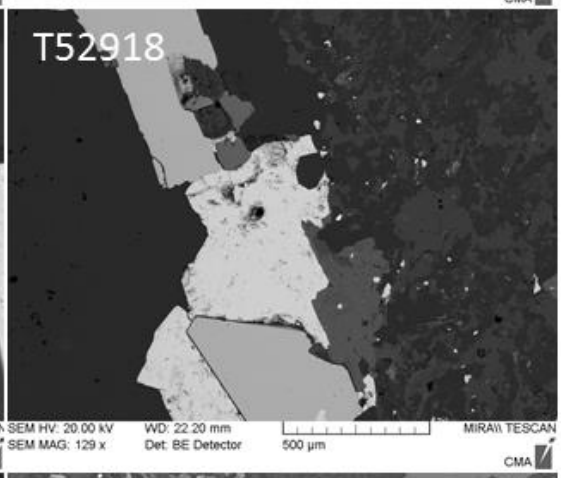
T52918
SEM HV: 20.00 kV
SEM MAG: 129 x
WD: 22.20 mm
Det: BE Detector
500 µm
MIRA\\ TESCAN
CMA

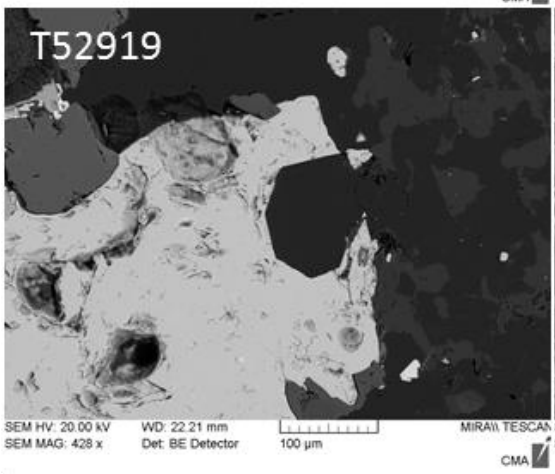
T52919
SEM HV: 20.00 kV
SEM MAG: 428 x
WD: 22.21 mm
Det: BE Detector
100 µm
MIRA\\ TESCAN
CMA

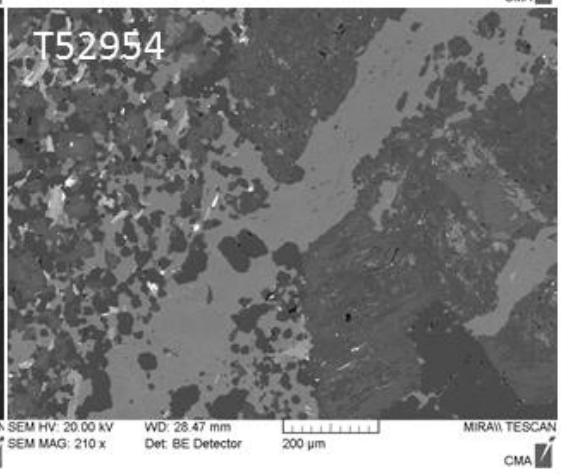
T52954
SEM HV: 20.00 kV
SEM MAG: 210 x
WD: 28.47 mm
Det: BE Detector
200 µm
MIRA\\ TESCAN
CMA

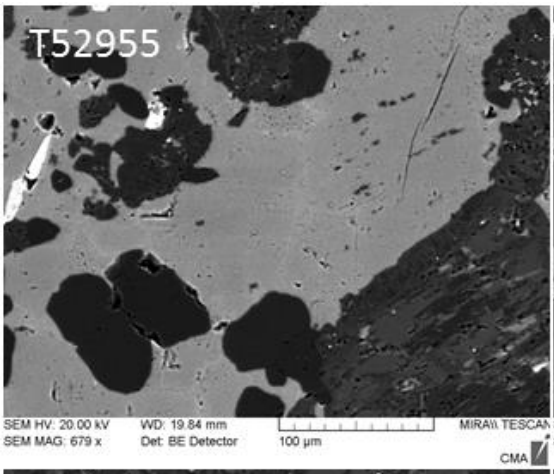
T52955
SEM HV: 20.00 kV
SEM MAG: 679 x
WD: 19.84 mm
Det: BE Detector
100 µm
MIRA\\ TESCAN
CMA

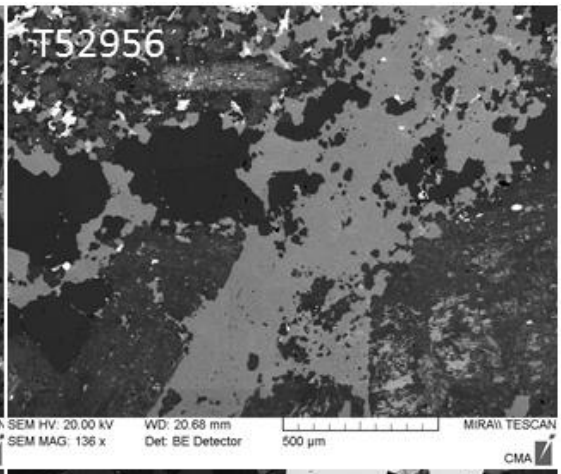
T52956
SEM HV: 20.00 kV
SEM MAG: 136 x
WD: 20.68 mm
Det: BE Detector
500 µm
MIRA\\ TESCAN
CMA

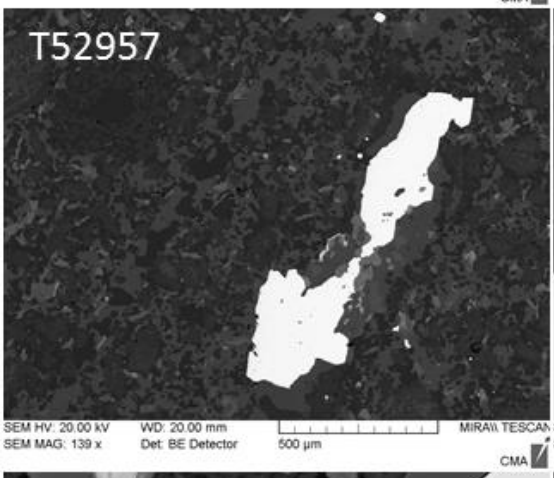
T52957
SEM HV: 20.00 kV
SEM MAG: 139 x
WD: 20.00 mm
Det: BE Detector
500 µm
MIRA\\ TESCAN
CMA

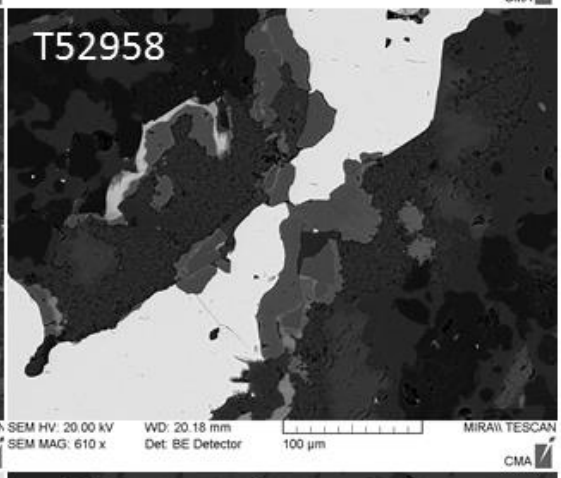
T52958
SEM HV: 20.00 kV
SEM MAG: 610 x
WD: 20.18 mm
Det: BE Detector
100 µm
MIRA\\ TESCAN
CMA

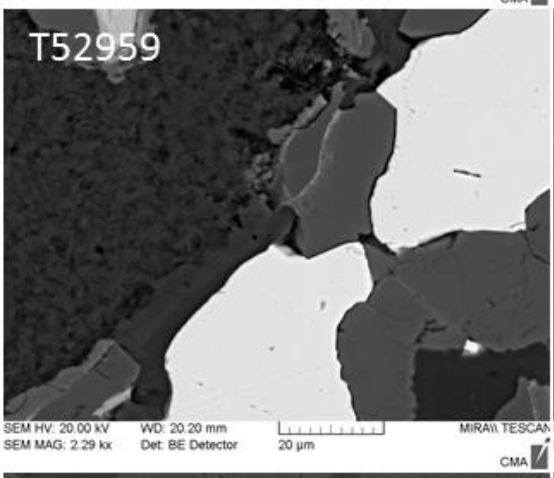
T52959
SEM HV: 20.00 kV
SEM MAG: 2.29 kx
WD: 20.20 mm
Det: BE Detector
20 µm
MIRA\\ TESCAN
CMA

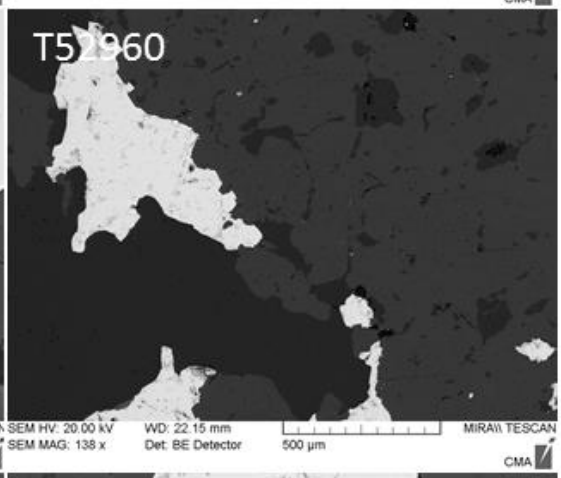
T52960
SEM HV: 20.00 kV
SEM MAG: 138 x
WD: 22.15 mm
Det: BE Detector
500 µm
MIRA\\ TESCAN
CMA

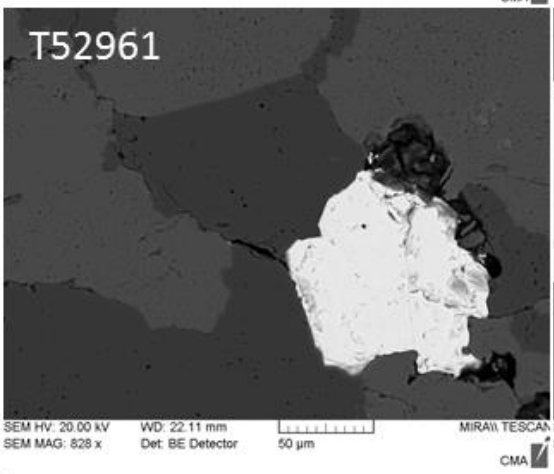
T52961
SEM HV: 20.00 kV
SEM MAG: 828 x
WD: 22.11 mm
Det: BE Detector
50 µm
MIRA\\ TESCAN
CMA

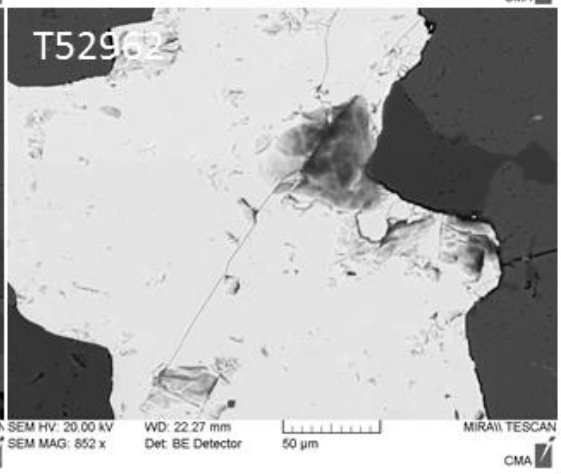
T529
SEM HV: 20.00 kV
SEM MAG: 852 x
WD: 22.27 mm
Det: BE Detector
50 µm
MIRA\\ TESCAN
CMA

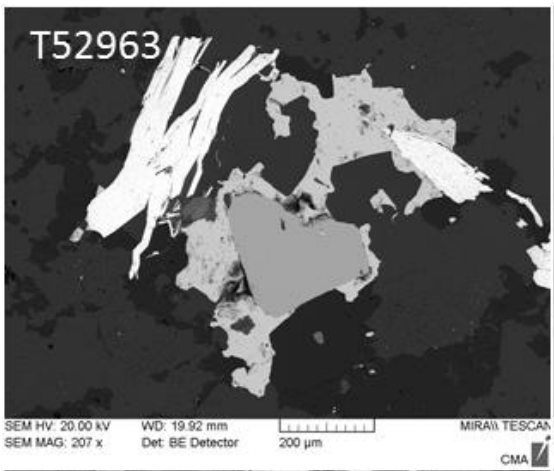
T52963
SEM HV: 20.00 kV
SEM MAG: 207 x
WD: 19.92 mm
Det: BE Detector
200 µm
MIRA\\ TESCAN
CMA

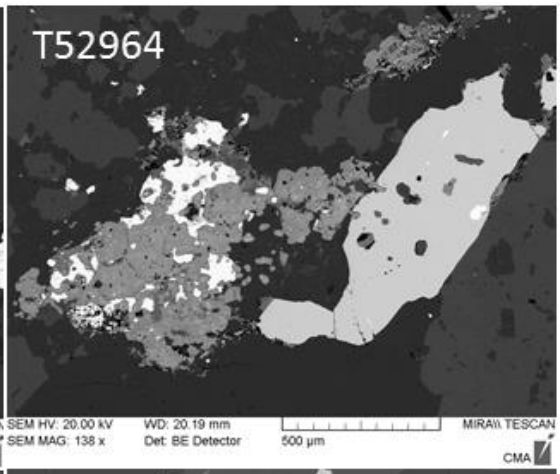
T52964
SEM HV: 20.00 kV
SEM MAG: 138 x
WD: 20.19 mm
Det: BE Detector
500 µm
MIRA\\ TESCAN
CMA

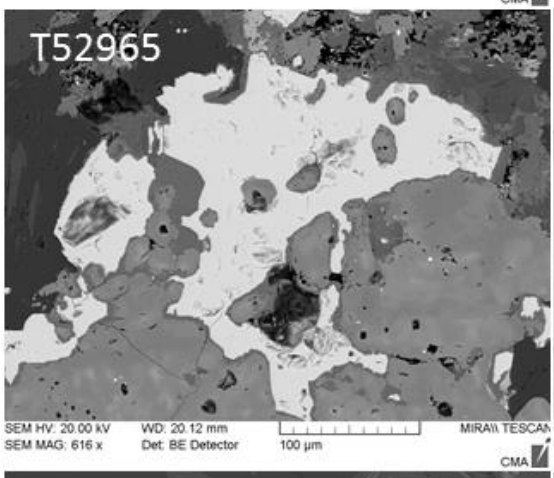
T52965
SEM HV: 20.00 kV
SEM MAG: 616 x
WD: 20.12 mm
Det: BE Detector
100 µm
MIRA\\ TESCAN
CMA

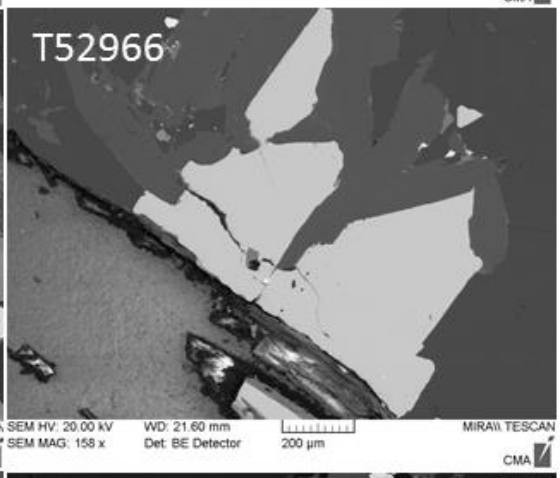
T52966
SEM HV: 20.00 kV
SEM MAG: 158 x
WD: 21.60 mm
Det: BE Detector
200 µm
MIRA\\ TESCAN
CMA

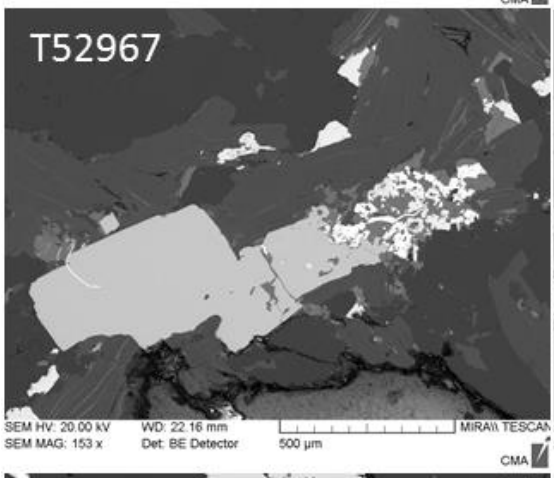
T52967
SEM HV: 20.00 kV
SEM MAG: 153 x
WD: 22.16 mm
Det: BE Detector
500 µm
MIRA\\ TESCAN
CMA

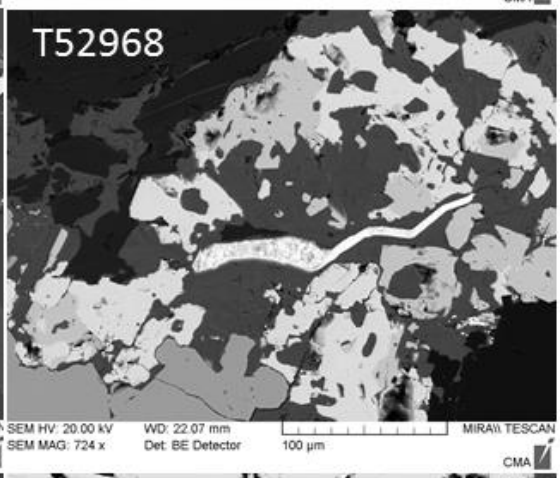
T52968
SEM HV: 20.00 kV
SEM MAG: 724 x
WD: 22.07 mm
Det: BE Detector
100 µm
MIRA\\ TESCAN
CMA

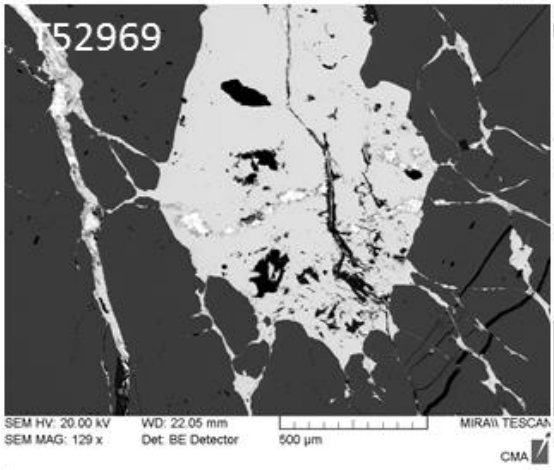
T52969
SEM HV: 20.00 kV
SEM MAG: 129 x
WD: 22.05 mm
Det: BE Detector
500 µm
MIRA\\ TESCAN
CMA

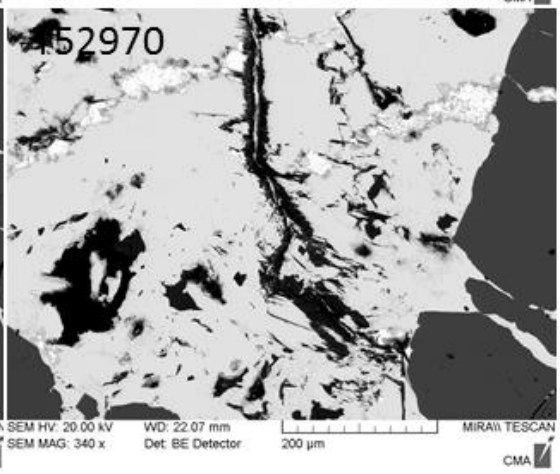
T52970
SEM HV: 20.00 kV
SEM MAG: 340 x
WD: 22.07 mm
Det: BE Detector
200 µm
MIRA\\ TESCAN
CMA

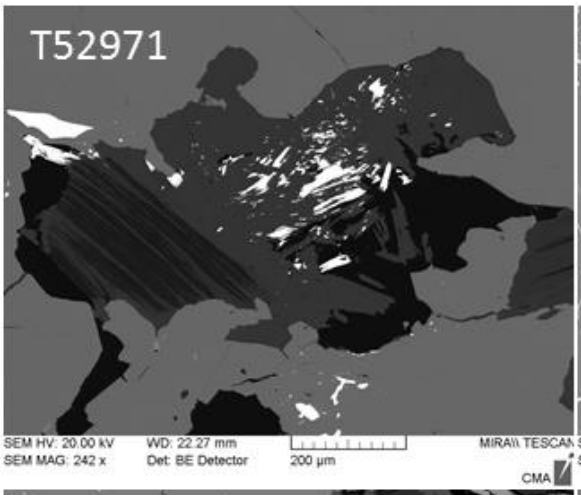
T52971
SEM HV: 20.00 kV
SEM MAG: 242 x
WD: 22.27 mm
Det: BE Detector
200 µm
MIRA\\ TESCAN
CMA

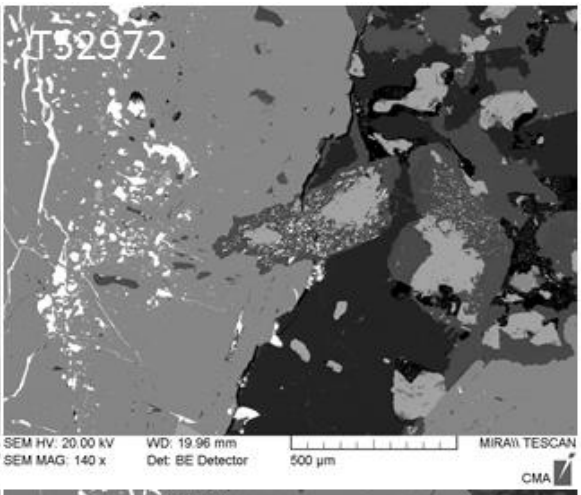
T52972
SEM HV: 20.00 kV
SEM MAG: 140 x
WD: 19.96 mm
Det: BE Detector
500 µm
MIRA\\ TESCAN
CMA

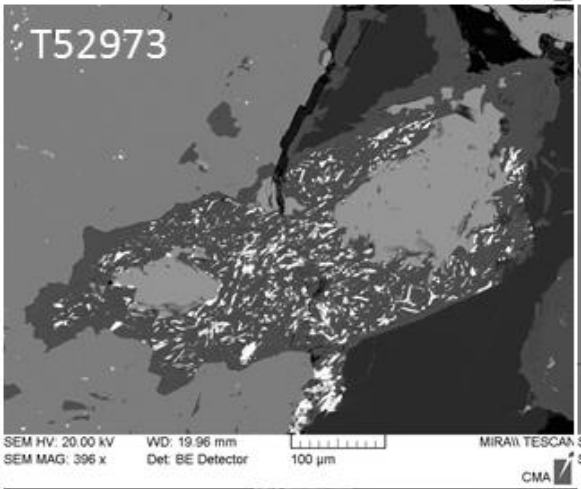
T52973
SEM HV: 20.00 kV
SEM MAG: 396 x
WD: 19.96 mm
Det: BE Detector
100 µm
MIRA\\ TESCAN
CMA

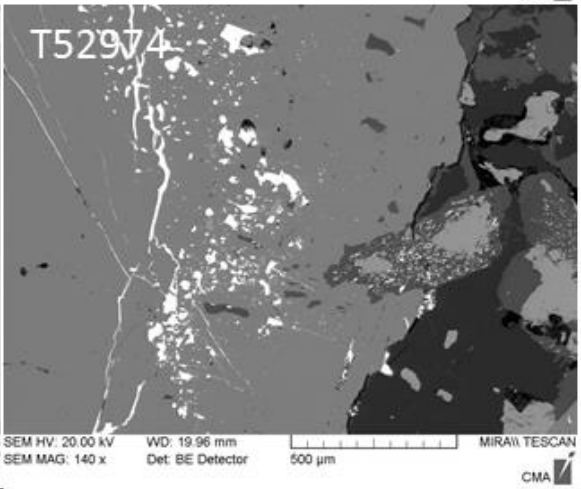
T52974
SEM HV: 20.00 kV
SEM MAG: 140 x
WD: 19.96 mm
Det: BE Detector
500 µm
MIRA\\ TESCAN
CMA

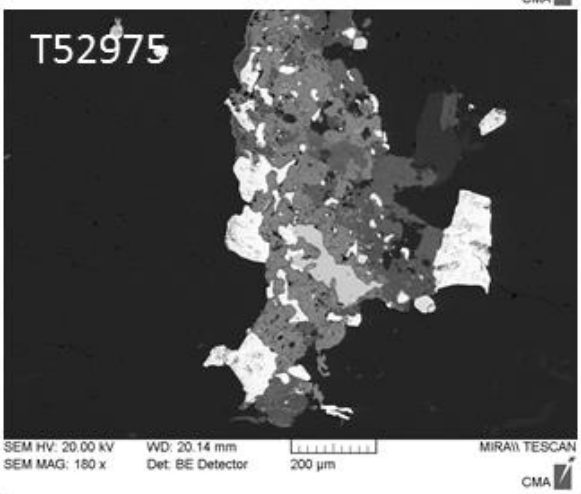
T52975
SEM HV: 20.00 kV
SEM MAG: 180 x
WD: 20.14 mm
Det: BE Detector
200 µm
MIRA\\ TESCAN
CMA

I declare that this thesis has not been submitted as an exercise for a degree at this or any other university and it is entirely my own work.

I agree to deposit this thesis in the university's open access institutional repository or allow the library to do so on my behalf

Electronically signed by Shane Lavery

19111515003169009590904425 1